UNIVERSITA' DEGLI STUDI DI VERONA

School of Life and Health Sciences

Ph.D. in Cardiovascular Science

XXXI Cycle

The relevance of L-type calcium channel gating properties to cardiac arrhythmia and differential modulation of L-type Ca_V channels by the $\alpha_2\delta$-1 auxiliary subunit

PhD Candidate: **Federica Steccanella**

VR398693

Mentor:

Prof. Giovanni Battista Luciani, University of Verona

Co-mentor:

Prof. Luca Giacomello, University of Verona

Prof. Riccardo Olcese, University of California Los Angeles

Academic Year 2018-2019

Table of Contents

ACKNOWLEDGEMENTS

Firstly, I would like to express my sincere gratitude to my advisor Prof. Giovanni Battista Luciani for the opportunity he gave me more than three years ago to join such a special Ph.D. program and for allowing me to develop and expand my scientific skills and interests. Without his precious support it would not be possible to conduct this research and cut the finishing line.

A very special gratitude goes to Prof. Luca Giacomello who has been a unique mentor since I joined his team for my Bachelor's degree program. He supported me greatly and was always willing to help me with insightful comments and encouragement.

My sincere thanks also go to Prof. Riccardo Olcese for his patience, encouragement, and immense knowledge. His guidance helped me in all the time of my research and beyond. I could not have imagined having better guide for my Ph.D study. Without his precious teaching and his inspirational mentoring, it would not be possible to accomplish this important goal.

I would like to truthfully thank Prof. Anna Moroni and Prof. Michela Ottolia for accepting to being part of my Doctoral Committee and for their valuable and indispensable suggestions that contribute to perfectionate my research project.

I would particularly thank Dr. Marina Angelini who patiently taught me how to patch myocytes and analyse data. She had always time to help me and answer my infinite silly questions (that's why she has so frequent migraine attacks now). I extremely thank also Dr. Nicoletta Savalli that guided me from DNA manipulation to oocyte voltage clamp, towards protein molecular rearrangements and amazing fluorescence signals.

A very special thank goes Drs. Hrayr Karagueuzian and Arash Pezhouman who have been incredible teachers directing me towards the complexity of heart anatomy and rhythmicity and the perfused heart Langendorff experiments.

I also thank all the members of the "Olcese Lab weekly meeting" for the time they have spent to help me, for the stimulating discussions, for the sleepless nights we were working together before deadlines, and for all the fun we have had in the last months performing experiments to the beat of music.

I sincerely thank Dr. Giulio Innamorati who has been the first to believe in me and never stopped to be supportive. He played a fundamental role in my scientific training and in the achievement of my carrier goals.

Finally, I would like to thank my parents and my friends who have provided me through moral and emotional support throughout my research, especially during my staying at UCLA. Words cannot express how grateful I am to them for all the encouragement they have given me.

ABSTRACT

Voltage-gated calcium (Ca^{2+}) channels are transmembrane proteins that transduce membrane potential changes into intracellular Ca^{2+} fluxes to initiate cell contraction, synaptic transmission, enzyme regulation, gene expression just to mention a few. Accordingly, many pathological conditions depend on the altered activity of these proteins and it remains of primary importance understanding their mechanisms of action in both the physiological and pathological contexts. The present thesis embraces two projects involving two different L-type Ca^{2+} channels: the cardiac voltage-gated Ca^{2+} channel $Ca_V1.2$ and the skeletal $Ca_V1.1$. The long-term goals of these two projects is to investigate how these proteins control cardiac and skeletal muscle function. This information may help developing new therapeutic approaches.

The goal of the first project aimed to investigate a novel antiarrhythmic strategy that targets the non-inactivating population of cardiac Cav1.2 channels.

Cardiovascular disease is the leading cause of mortality in developed countries. In cardiac patients, about 50% of deaths are sudden, and typically caused by fatal tachyarrhythmia such as ventricular fibrillation (Priori et al., 2015; Al-Khatib et al., 2018). Current therapeutic strategies include antiarrhythmic drugs and implantable cardioverter defibrillators, but their efficacy remains limited by proarrhythmic side effects (1989; Waldo et al., 1996), and costs and patient eligibility, respectively. Thus, a widely applicable, cost-effective strategy, able to avoid the negative inotropic effect of current antiarrhythmics, is strongly needed.

Malfunction of L-type Ca^{2+} channel has been linked to numerous cardiac diseases. Particularly, Early Afterdepolarizations (EADs) which are trigger of *Torsades de pointes*, polymorphic ventricular tachycardia as well as some re-entrant tachyarrhythmias, are defined as transient membrane potential oscillations during the plateau phase of the cardiac action potential (AP), (Antzelevitch and Burashnikov, 2011). EADs formation is attributed to the L-type calcium channel (LTCC) current ($I_{Ca,L}$), as it is the main regenerative current during this phase of the action potential (January et al., 1988; January and Riddle, 1989; Xie et al., 2009; Madhvani et al., 2011; Madhvani et al., 2015). Rapid activation of LTCC produces a peak $I_{Ca,L}$ that is essential for excitation-contraction coupling. However, some of these channels remain active producing a late Ca^{2+} current (late $I_{Ca,L}$) that persists towards the end of the AP plateau. In conditions of reduced repolarization reserve, this non-inactivating component of $I_{Ca,L}$ prevails on K^+ conductances, resulting in in an abnormal membrane potential depolarization from which EADs arise (Xie et al., 2009; Qu and Chung, 2012). As demonstrated by dynamic clamp analysis, a small reduction of this late current can potently suppress EAD occurrence (Madhvani et al., 2015). Thus, a drug that selectively targets the late $I_{Ca,L,}$ should efficiently suppress EADs with minimal effect on contractility, overcoming the negative inotropic effect typical of class IV antiarrhythmics. Interestingly, roscovitine (Seliciclib, R-roscovitine), a purine analog, which is in phase II clinical trials as an anticancer agent, possesses also the ability to

accelerate the voltage-dependent inactivation of $Ca_V1.2$ LTCCs, preferentially reducing "late $I_{Ca,L}$" (non-inactivating component) over "peak" (Yarotskyy and Elmslie, 2007; Yarotskyy et al., 2010). In this work, we applied electrophysiological techniques to demonstrate that reduction of late $I_{Ca,L}$ by roscovitine, verified both in native and cloned $Ca_V1.2$ channels, abolished EADs in rabbit ventricular myocytes without compromising contraction efficiency. Furthermore, this reduction suppressed and/or prevented EAD-mediated ventricular fibrillation in rabbit and rat hearts. In both isolated myocyte and heart experiments, roscovitine effect was independent from the mechanism chosen to induce EADs (hypokalemia and/or oxidative stress). These results suggest that 1) limiting sustained/anomalous Ca^{2+} channels function during the plateau phase is an effective and safe antiarrhythmic strategy and that 2) roscovitine can be considered as a potential pilot compound for a new class of antiarrhythmics that likely would not compromise heart contractility.

In the second project I have investigated the molecular mechanisms by which the $\alpha_2\delta$-1 auxiliary subunit differently modulates the L-type Ca^{2+} $Ca_V1.1$ channels compared to their close relative $Ca_V1.2$ isoform.

In striated muscle, the voltage-gated Ca^{2+} channels $Ca_V1.1$ and $Ca_V1.2$ are the sensors that convert the electrical impulse into increases in intracellular Ca^{2+} levels that allow muscle contraction. Both channels possess four positively charged modules, called voltage-sensing domains (VSD I-IV), that undergo a conformational change upon membrane depolarization. VSD either open the channel pore ($Ca_V1.2$) or activate Ca^{2+} release through the ryanodine receptors from the sarcoplasmic reticulum ($Ca_V1.1$). Both $Ca_V1.1$ and $Ca_V1.2$ channels are expressed in the plasma membrane as protein complexes formed by the co-assembly of a pore forming subunit (α_1) and several modulatory subunits ($\alpha_2\delta$, β and γ) which modify their voltage dependent properties (Catterall, 2011; Bannister and Beam, 2013). In $Ca_V1.2$ isoform, the association of $\alpha_2\delta$-1 subunit significantly facilitates channel activation by remodelling the voltage-dependent properties of three out of four cardiac VSDs, allowing the channels to operate at physiological membrane potentials (Savalli et al., 2016). In addition, $\alpha_2\delta$-1 subunit accelerates activation kinetics of $Ca_V1.2$ channels (Platano et al., 2000; Savalli et al., 2016), producing the typical fast Ca^{2+} current observed during a ventricular action potential. Interestingly, the same regulatory subunit has opposite effects on the $Ca_V1.1$ channels, as it slows down their activation kinetics and leaves almost unperturbed the voltage-dependent activation of the pore. However, the molecular mechanism by which this auxiliary subunit modulates the properties of $Ca_V1.1$ VSDs is still unknow.

To gain a mechanistic insight on this modulation, we overexpressed in *Xenopus* oocytes, channels containing the human pore-forming subunit α_{1S} and the auxiliary subunit β_{1a} in absence or presence of $\alpha_2\delta$-1. Using the voltage clamp fluorometry technique, we simultaneously recorded the ionic current flowing through the pore and the movement of each voltage sensor over a wide range of membrane potential to derive both pore and VSDs voltage-dependent relationships. We observed that the four $Ca_V1.1$ VSDs possess unique properties in terms of kinetics, voltage dependence and

sensitivity that might reveal different functional roles. Specifically, the voltage dependence of VSD III was compatible with that of Ca^{2+} release during the skeletal AP, indicating that VSD III might be the key VSD that opens the ryanodine receptors. As opposite to $Ca_V1.2$, we found that the presence of $\alpha_2\delta$-1 slowed down the activation kinetics of the human $Ca_V1.1$ channels and accelerated the rate of channel closure, contributing to reduce Ca^{2+} influx during depolarization. This auxiliary subunit facilitated channel opening by ~ 10 mV shift toward hyperpolarizing membrane potentials, an effect that might be assigned to the remodelling of VSD I properties, as VSD I voltage-dependent activation shifted ~ 20 mV to more negative membrane potentials. Instead, in the presence of $\alpha_2\delta$-1 VSDs II-IV remain unaffected, suggesting that VSD I could play a major role in channel opening.

Project 1

Roscovitine as a Prototypical Member of a Novel Class of Antiarrhythmics that Modify L-type Calcium Channel Gating Properties

1. INTRODUCTION

1.1 The electrical activity of the heart

The heart is a hollow muscular organ that functions as an electromechanical two-sided pump. The right side comprises the right atrium (RA) and ventricle (RV) and is a low-pression system that pumps blood to the lungs. The left side, that includes the left atrium (LA) and ventricle (LV), works against high pressure to supply the systemic circulation with oxygenated blood. The two sides are separated by muscular septa. The unidirectionality of the blood flow (from the atria to the ventricles) is ensured by the atrioventricular valves.

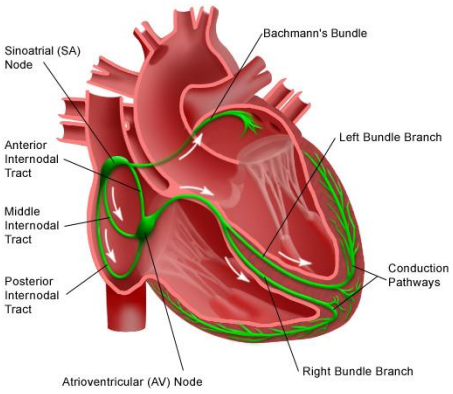

Figure 1 – The conduction system of the heart.

The electrical impulse is spontaneously generated by specialized cells forming the sinoatrial (SA) node in the right atrium (Fig. 1). These cells function as a pacemaker, and set the sinus rhythm, firing an electrical stimulus that enables the atrial myocardium to contract. The electrical impulse travels from the SA node to the atrioventricular (AV) node, where it slows down. This short delay (20 milliseconds) ensure the complete contraction of the atria ahead of the ventricles. The atrial and ventricular tissues are also electrically isolated from one another by a plane of connective tissue that prevents the impulse from spreading directly to the ventricles without passing through the AV node. From the AV node the electrical signal is passed to the bundle of His and allows for ventricular contraction. The impulse propagates down the conduction pathway that divides into the left and right bundle branches before splitting into the Purkinje fibres, to stimulate the right and left ventricles (van Weerd and Christoffels, 2016). The depolarization wave, initiated by the SA node and terminated in the Purkinje fibres, creates an electrical current that can be recorded using surface electrodes and displayed as an electrocardiogram (Fig. 2).

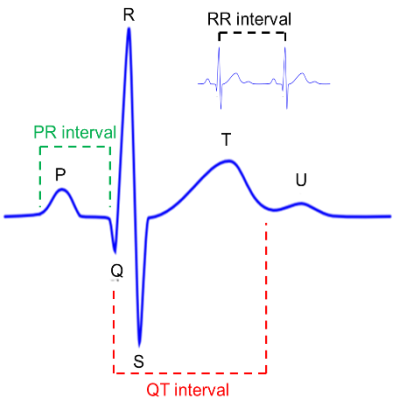

Figure 2 - The electrocardiogram. Representation of the electrical activity of the heart as four prominent points (the P wave, the QRS complex, the T and U waves) together with the major intervals (indicated as dashed lines).

A normal electrocardiogram (ECG) exhibits seven prominent points and intervals. **1**) The small P wave represents the depolarization of the atria. The atria begin contracting approximately 25 ms after the start of the P wave. **2**) The large QRS complex represents the depolarization of the ventricles, which begin to contract at the peak of the R wave. The QRS complex masks atria repolarization. **3**) The T wave represents the repolarization of the ventricles. **4**) The U wave is not always visible, and it might represent the last phase of ventricular or

Purkinje fibers repolarization. **5**) The PR interval measures the time from the beginning of atrial depolarization to the initiation of the QRS complex and informs about the electrical delay between the SA node and the AV node. **6**) The QT interval quantifies the time for ventricular activation and recovery. **7**) The RR interval indicates the heart rate. Deviations from normal ECG intervals, e.g. an increased heart rate and prolongation of the QT interval and QRS duration, are therefore indicative of conduction dysfunction and are associated with cardiac arrhythmias.

At the cellular level, the depolarization opens the voltage-dependent Ca^{2+} channels leading to an influx of Ca^{2+} and contraction after a few milliseconds (Bers, 2002; Ashikaga et al., 2007). This delay is instrumental for the Ca^{2+} to enter the cell and induce the release of Ca^{2+} from the sarcoplasmic reticulum (SR) (Fig. 3). The raise in intracellular Ca^{2+} concentration engages the sarcomeres which shorten myocytes. This event takes places in millions of cells at the same time, ultimately propelling blood out of the chambers. Contraction (systole) is followed by muscle relaxation (diastole) to refill the heart of blood for the next beat. For diastole to happen, the intracellular Ca^{2+} concentration must decrease. Ca^{2+} is therefore recycled back by the sarcoplasmic reticulum (SR) through the sarco-endoplasmic reticulum Ca^{2+}-ATPase (SERCA) pump or extruded outside the cell via Na/Ca-

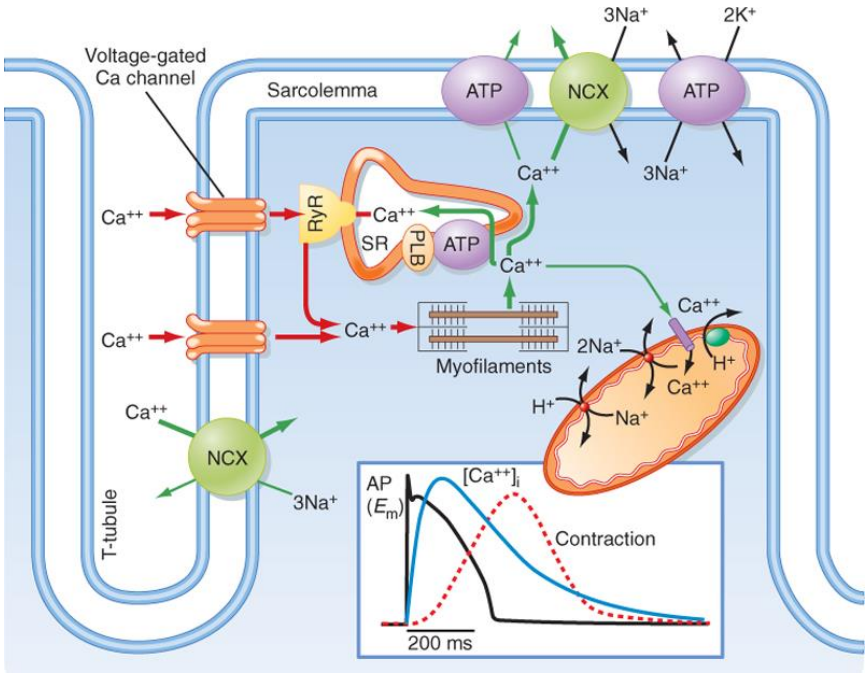

Figure 3 – Calcium cycling in cardiac myocytes. Schematic representation of the calcium pathways that allow for cell contraction (red arrows) and relaxation (green arrows). After membrane depolarization, Ca^{2+} enters cardiomyocytes through voltage-gated calcium channels (orange) and Na^+/Ca^{2+} exchanger (NCX, green). The local increase of calcium activates the ryanodyne receptors (RyR, yellow) located on the SR, producing a massive extrusion of calcium in the cytoplasm. Here, calcium binds to and remodels contractile myofilaments (troponin C, myosin and actin), resulting in cell shortening. To achieve cell relaxation, resting calcium concentration is restored by SR Ca^{2+}-ATPase pump (SERCA, purple) and NCX, with a small contribution of the sarcolemmal Ca^{2+}-ATPase and mitochondrial Ca^{2+} uniporter. The inset highlights the differences in time between action potential (black line), Ca^{2+} transient (blue line) and contraction (red dotted line) measured in a rabbit ventricular myocyte at 37°C. From (Bers, 2002).

exchanger (NCX). In this context, the cell repolarizes before the following stimulus triggers another contraction.

1.2 Ventricular action potential

All cardiac muscle cells are electrically coupled to one another by structures known as gap junctions which allow the action potential (AP) to propagate from one cell to the next. By this mean, the spontaneous AP generated by cardiac conductive cells is spread directly to the contractile cells.
The AP is a transient modification in transmembrane voltage that results from the orchestrated activity of multiple voltage-gated ion channels and transporters. In the cardiac tissue, AP shape and duration vary from region to region due to different type and density of ion channels and transporters expressed.
In a human ventricular myocyte, the AP lasts ~300 ms and includes **5 phases** (indicated by the numbers 0 through 4). Its configuration is determined by the balance between the inward (depolarizing) and outward (repolarizing) ionic currents schematically sketched in Figure 4.

During **phase 0**, the activation of voltage-gated sodium channels produces a massive influx of sodium (Na^+) ions that depolarizes the membrane potential from its resting level (~-80 mV) towards Na^+ electro-chemical equilibrium potential (~40 mV) contributing to the upstroke of the AP. The inward Na^+ current (I_{Na}) is very rapid and transient, as the most Na^+ channels inactivate within one millisecond, thus terminating phase 0. Sub-sequent activation of the transient outward K^+ current (I_{to}), by membrane depolarization, contributes to a brief repolarization (**phase 1**) rapidly interrupted by **phase 2**. This phase is also known as the "plateau" phase due to the membrane potential remaining almost constant, as the membrane very slowly begins to repolarize. This phase is responsible for the large duration of the action potential and is essential for **1**) the engagement of the contraction machinery and **2**) the prevention of electrical re-excitation and tetanic contraction in the heart, which could inhibit relaxation needed for the filling of blood prior to ejection (Bers, 2002). The slow repolarization is maintained by a balance between an inward Ca^{2+} current (I_{CaL}) via the L-type Ca^{2+} channels (LTCC), and outward K^+ currents (rapid I_{Kr} and slow I_{Ks} components of the delayed rectifier). Other contributors to the plateau phase are the late Na^+ current and the Na^+/Ca^{2+}exchanger (NCX) current. The rapid activation of L-type Ca^{2+} channels produces a peak inward I_{CaL}

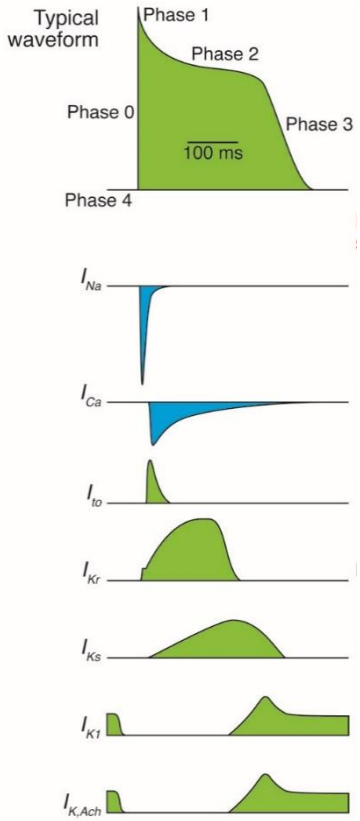

Figure 4 - Ventricular action potential and underlining currents. Schematic representation of a human ventricular AP, its phases (numbers 0-4) and the underlining time course of the currents that contribute to shape the AP. Adopted from (George, 2013).

that triggers the opening of the ryanodine receptors located in the sarcoplasmic reticulum (SR) inducing the Ca^{2+} release from the intracellular store, a phenomenon known as Ca2+-Induced Ca^{2+}-Release (CICR), (Bers, 2002). This massive increase in intracellular Ca^{2+} raises its concentration from 0.1µM up to 1µM to engage contractile filaments and produce mechanical force (Bers, 2002). LTCCs then partially inactivate via voltage- and Ca^{2+}-calmodulin-mediated mechanisms (Peterson et al., 1999), leading to a residual persistent current ("late $I_{Ca,L}$") flowing during the plateau phase of the cardiac AP. At this point **phase 3** starts. The decay of Ca^{2+} entry allows K^+ conductances I_{Kr} and I_{Ks} to govern and repolarize the membrane potential back to -80 mV. To avoid downstream side-effect of Ca^{2+} overload, the surplus of the cation is pumped back to either the extracellular medium via NCX or the SR though the SERCA pump (Fig. 3). This resets the cell to a diastolic state (**phase 4**), during which the myocyte relaxes and prepares for the next electrical activation initiated by the SA node.

1.2 Ventricular arrhythmias

Ventricular arrhythmias define all conditions in which the electrical activity of the ventricles deviates from the normal speed and rhythm of the heart. These conditions range from premature ventricular complex (PVC) to ventricular tachycardia (VT) or fibrillation (VF), with a clinical picture that ranges from a total lack of symptoms to cardiac arrest (Al-Khatib et al., 2018).

VF is the most life-threatening ventricular arrhythmia as it is the major immediate cause of sudden cardiac death, which accounts for approximately 50% of all cardiovascular deaths every year (Priori et al., 2015; Al-Khatib et al., 2018). VF has been defined as rapid, turbulent electrical activity with a ventricular rate > 300 beats per minute. During VF, the high heart rate and the uncoordinated ventricular contraction prevent an adequate pumping of blood such that the arterial pressure suddenly drops to exceedingly low levels, and death usually ensues within less than ten minutes due to lack of oxygen delivery to vital organs. On the ECG, VF appears as a completely aperiodic and irregular beat-to-beat changes in the QRS complex (Jalife, 2000).

Mechanisms of ventricular arrhythmias include enhanced normal automaticity, abnormal automaticity, triggered activity induced by early or late afterdepolarizations, and reentry (Antzelevitch and Burashnikov, 2011; Tse, 2016).

Automaticity

Automaticity is the property of cardiac pacemaker cells, to generate spontaneous action potentials. Spontaneous activity is the result of diastolic depolarization caused by a net inward current, known as "funny" current, during phase 4 of the action potential, which progressively brings the membrane potential to threshold for the activation of Ca^{2+} channels. Abnormal automaticity arises from a partially depolarized membrane potential that commonly results from a reduction of ether K^+ channel conductance or expression, or from an increase in extracellular potassium (Antzelevitch and

Burashnikov, 2011). This condition can arise from channel mutations, hypovolemia, ischemia, or electrolyte disturbances (Tse, 2016).

Reentry

Reentry occurs when an AP fails to extinguish itself and reactivates a region that has recovered from refractoriness. It can be classified into two types. Reentry that occurs in the presence of a physical obstacle, around which an action potential travels to re-excite the site of origin is called circus-type reentry. In circus-type of reentry, all cells recover from excitation one after another so that they can be excited again when the next wavefront arrives. Circus-type reentry is the most common mechanism of ventricular arrhythmia in the presence of structural heart disease, where the anatomic obstacle can be represented, for example, by scar after a myocardial infarct or surgically repaired congenital heart disease. If reentry arises without an obstacle is referred to as reflection and phase 2 reentry. These types of reentry develop in a setting in which each site of reentry differently recovers from refractoriness that exists between one site and another. Thus, the latter recovering site function as a virtual electrode that excites its already recovered neighbour (Antzelevitch and Burashnikov, 2011).

Triggered activity

The concept of triggered activity was introduced 40 years ago to describe extrasystoles and tachycardia events that do not arise from spontaneous or reentry phenomena (Cranefield, 1977; January and Moscucci, 1992; Rosen, 2009). Triggered activity develops at the single cell level, from abnormal action potentials that are evoked by a preceding action potential and do not arise *de novo*. The abnormal impulses appear as positive oscillations of membrane potential that can either **1**) occur early during phase 2 or 3 of the action potential (early afterdepolarizations, **EADs**) or **2**) follow the completion of the repolarization phase (delayed afterdepolarizations, **DADs**), (Fig. 5).

EADs and DADs must be sufficiently large to depolarize the cell membrane to its threshold potential, in order to trigger extra action potentials (Antzelevitch and Sicouri, 1994). These triggered events give rise to premature ventricular complexes (PVCs), which can precipitate in polymorphic ventricular tachycardia (PVT), *torsades de pointes* and ventricular fibrillation (VF), especially in vulnerable tissue (Cranefield and Aronson, 1991; Antzelevitch and Burashnikov, 2011; Wit, 2018).
Multiple conditions predispose to EAD development and include long QT syndromes, hypertrophy, hypoxia , acidosis, electrolyte abnormalities, high concentrations of catecholamines, pharmacologic agents and antiarrhythmic drugs (Antoons et al., 2007; Antzelevitch and Burashnikov, 2011; George, 2013; Karagueuzian et al., 2013). DADs and DAD-induced triggered activity are observed in failing or hypertrophic hearts, or under conditions that augment intracellular Ca^{2+}, such as after exposure

to toxic levels of cardiac glycosides (digitalis), (Rosen et al., 1973) or catecholamines (Priori and Corr, 1990).

The following sections are dedicated to EADs, specifically to the mechanism by which these single-cell phenomena can trigger arrhythmias at the organ level and to the molecular background responsible for EAD upstroke.

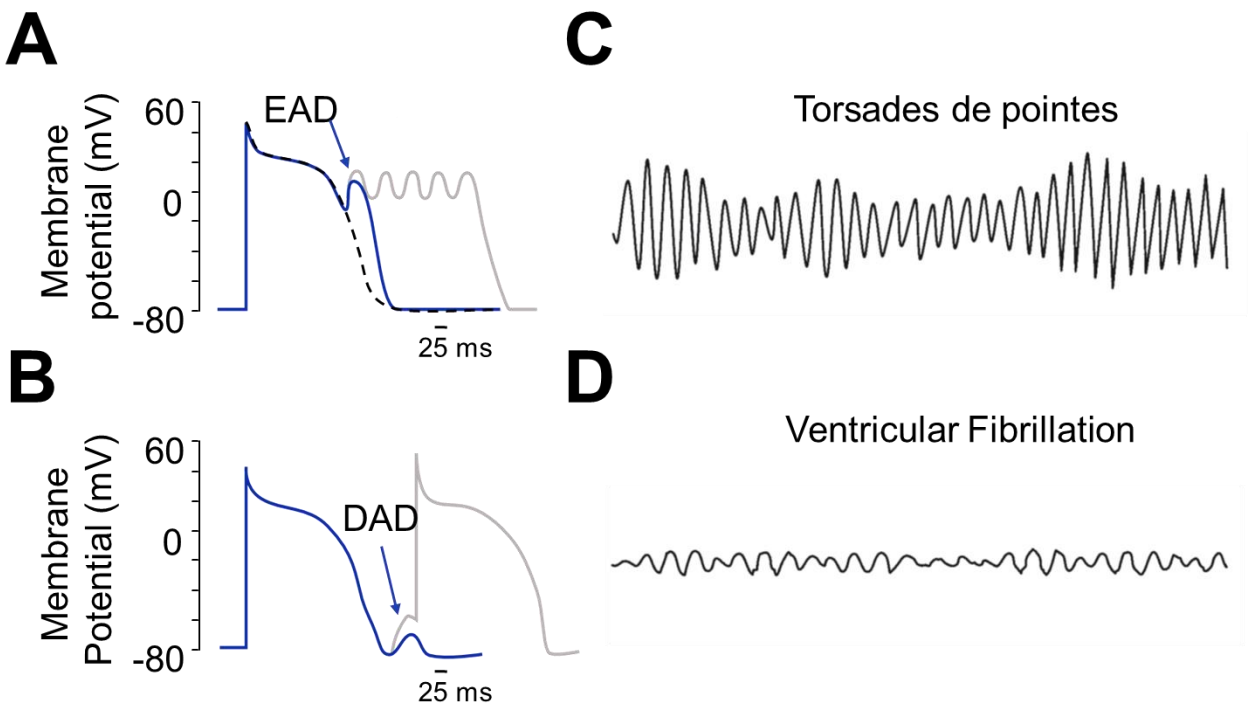

Figure 5 - Afterdepolarizations and associated arrhythmias. Ionic current alterations can result in excessive depolarizing currents that, in turn, elicit EADs and DADs. **A**) EADs are membrane voltage oscillations during the repolarizing phase of the cardiac action potential (AP) causing an action potential prolongation. Black dashed line represents a normal AP. EADs typically result from increased reactivation of voltage-gated L-type Ca^{2+} channels or voltage-gated Na^{+} channels. **B**) Illustration of a DAD generated after completion of the action potential repolarization (blue line) and a triggered impulse arising from it (grey line). DADs are usually elicited either by spontaneous intracellular Ca^{2+} release from the SR which activates the electrogenic exchanger leading to membrane depolarization. **C-D**) ECG recordings representing arrhythmias commonly associated with afterdepolarizations: polymorphic ventricular tachycardia (or torsades de pointes, **C**) and ventricular fibrillation (**D**). C-D adopted from (George, 2013).

1.3 Early after depolarizations

From single cell events to myocardial arrhythmias

The mechanism by which one triggered AP at the single cell level, that usually arise from low pacing rate, could synchronize with the surrounding tissue and degenerate in myocardial arrhythmias with a rapid rate like PVCs or *torsades de pointes* is still under investigation (Sato et al., 2009; Wit, 2018). Few explanations have been proposed combining experimental data and computational simulations.

In a healthy coupled tissue, an aberrant depolarization developed by an individual myocyte will be minimized by the electrotonic potential of the normal-repolarizing neighbors flowing through local gap junctions (Xie et al., 2010). In other words, the depolarizing EAD current from the susceptible myocyte is “diluted” into too many unsusceptible neighbors to cause a significant depolarization (repolarization delay) of the surrounding myocytes. This concept, referred as source-sink mismatch, is well demonstrated by coupling two isolated myocytes, one with EADs and the other without EAD, via a variable resistor: the greater is the coupling, the smaller is the EAD amplitude (Huelsing et al., 2000). As consequence, multiple myocytes must exhibit EADs to overcome the surrounding tissue and spread. In a 3D structure, the number can be as high as 696,910 (Sato et al., 2010). This number drastically decreases by 64% in structural or electrical remodeled heart, where myocytes decoupling makes the myocardium more prone to arrhythmogenic events (Xie et al., 2010). Considering that 70 myocytes can account for a cable of ~10mm, this estimation is still substantial, indicating that the source–sink mismatch in intact tissue functions as a protective mechanism against unsynchronized EADs triggering PCVs (Weiss et al., 2010).

Thus, appearance and propagation of EADs imply some grade of synchronization. However, EADs tend to occur irregularly at intermediate pacing, with the number of EADs and the duration of each AP vary from beat to beat, reducing the probability that all the cells in a given region will develop an EAD simultaneously on the same beat. This apparent irregular behavior follows instead, the laws of deterministic chaos as demonstrated by Sato and colleagues (Sato et al., 2009). As such, sensitivity to initial conditions, which is a property of chaos, guarantees that small differences in AP variables (irregularity of EADs) will be rapidly amplified (“butterfly effect”) creating islands of long AP durations with EADs to appear next to islands of short AP duration without EADs. These multiple foci can shift in space from beat to beat, increasing the risk of a wave break leading to reentry and fibrillation (Sato et al., 2009; Weiss et al., 2010).

Etiology of early afterdepolarizations

EADs were first identify in 1974 by Cranefield and his colleagues in canine Purkinje fibers as oscillatory after-potentials, and subsequently classified as a form of triggered activity that can precipitate into asynchronous electrical activity such as VT and VF (Cranefield and Aronson, 1974; Cranefield, 1977).

EADs appear as aberrant fluctuations of the membrane potential that interrupt phase 2 and early phase 3 of the AP (Fig. 5a). EADs occur in conditions of prolonged AP duration (APD), when the membrane potential fails to repolarize due to a reduced repolarization reserve. APD can be prolonged with bradycardia or partial inhibition of K^+ channels. The latter condition can be a consequence of hypokalemia (which reduces outward I_{K1} and I_{Kr}), pharmacological action (e.g. K channel blockers) or congenital long QT syndromes (linked to mutations that alter I_{Na}, I_{Kr} and I_{Ks}) (Weiss et al., 2010). However, any condition that sufficiently decrease the net outward current can

promote EADs independently from the heart rate (Huffaker et al., 2004). A critical example is the Timothy syndrome of long QT 8. In this disorder, $Ca_V1.2$ mutations impair channel inactivation, producing a greater inward current that overcomes repolarizing K^+ conductance prolonging AP duration and promoting proarrhythmic events (Splawski et al., 2004).

A reduced repolarization reserve by itself is not enough to cause an EAD. A second critical factor is whether the voltage during the AP plateau lingers for a sufficiently long time in that status leading to time- and voltage-dependent recovery of a regenerative inward current. The ventricular AP is shaped by three predominant depolarizing currents and all of them have been attributed to EAD genesis: the

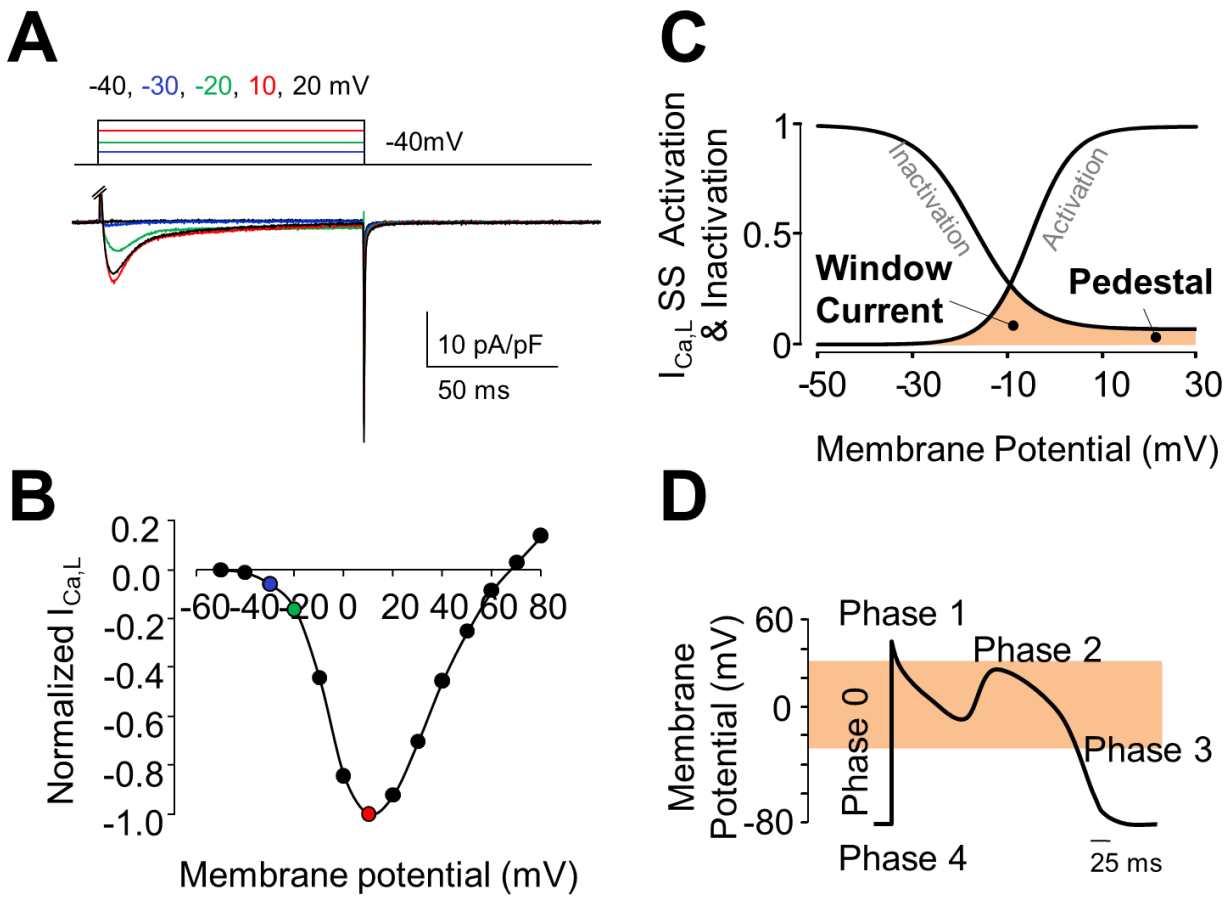

Figure 6 - I_{CaL} window current and its relationship with EADs upstroke. The range of membrane potential in which L-type Ca channels operate corresponds to the range of take-off potentials for EADs. **A** L-type Ca^{2+} current recorded from a mouse ventricular myocyte in voltage-clamp mode. $I_{Ca,L}$ starts to activate at ~ -30 mV (blue trace) reaching the maximal peak value at 10 mV (red trace). The square pulse given as voltage command is reported above the traces. Nifedipine-sensitive $I_{Ca,L}$ was isolated by substituting KCl with CsCl in the external solution to block contaminant I_K current, and by blocking I_{Na} with a 50 ms prepulse at -40 mV and 20 µM tetrodotoxin. **B**) The current-voltage (I-V) relationship, constructed from the traces in A, displays the voltage-dependent activation of L-type Ca^{2+} channels. Values were normalized to the maximal peak current. **C**) $I_{Ca,L}$ voltage-dependent activation and inactivation curves describe the steady state properties of L-type Ca^{2+} channels. The overlap between the two curves, identifies a range of membrane potential (orange) in which channels are available to be activated (as they are not inactivated) and generate an inward (depolarizing) current. This range of membrane potential from -40 to 10 mV equals the critical membrane potentials in which EADs are elicited (orange rectangle in **D**), making $Ca_V1.2$ channels the primary responsible for the regenerative current underlining EADs development (**D**).

persistent $I_{Ca,L}$ (January and Riddle, 1989; Madhvani et al., 2011), I_{Na} (Maltsev et al., 1998; Bengel et al., 2017), and I_{NCX} (Szabo et al., 1994). The relevance of an increased inward $I_{Ca,L}$ in EADs upstroke (especially of phase 2) became clear in the 80's when Marban and colleagues demonstrated that increasing open probability of $Ca_V1.2$ channels with the Ca^{2+} channel agonist Bay K8644, potentiated EADs, while antagonizing their activity with the Ca^{2+} channel blocker Nitrendipine abolished the triggered activity. These effects on EADs occurrence were not observed either by blocking SR Ca^{2+} release with ryanodine nor chelating intracellular Ca^{2+} with BAPTA, ruling out the intracellular Ca^{2+} release as the underlying mechanism (Marban et al., 1986). Additional validation of $I_{Ca,L}$ contribution to EADs came from the discovery that these phenomena ($I_{Ca,L}$ and EADs) share similar voltage dependence (January and Riddle, 1989). $Ca_V1.2$ channels typically activate at -40mV, reaching the maximal current at 10mV (Fig. 6A, B). This range of membrane potential corresponds to the take off potential of most EADs (Fig. 6D), (Damiano and Rosen, 1984). However, these channels undergo voltage-dependent and Ca^{2+}-dependent inactivation at similar voltages. As consequence, overlapping the steady-state activation and inactivation curves of $I_{Ca,L}$, identifies a "window current" region (or voltage interval) in which a fraction of not inactivated L-type Ca^{2+} channels may be available for reactivation (Fig. 6C) (January and Riddle, 1989; Hirano et al., 1992). It means that, as the AP repolarizes into this "window current" region (or voltage interval), some L-type Ca^{2+} channels can reactivate and generate an inward I_{CaL}, causing an extra membrane depolarization, and thus EADs. Furthermore, January and Riddle demonstrated that EADs and the inward current share also similar time-dependent occurrence, showing that lengthening the duration of conditioning voltage step used to elicit EADs, results in both EADs and inward current of increasing amplitude (January and Riddle, 1989). Another direct confirmation that EADs are highly related to the "window current" and biophysical properties of $I_{Ca,L}$ was provided by Madhvani and colleagues (Madhvani et al., 2011; Madhvani et al., 2015). Using the dynamic clamp technique (a hybrid electrophysiological/computational approach), they provided a compelling evidence that reduction of $I_{Ca,L}$ "window current" by either **1**) reducing the non-inactivating (pedestal/late) component, **2**) shifting the $I_{Ca,L}$ steady-state activation in the depolarizing direction by <5 mV, or **3**) shifting the steady-state inactivation curve in the hyperpolarizing direction by <5 mV, are equally effective strategies to suppress EADs (Fig. 7) with an enormous advantage compare to traditional class IV antiarrhythmics. That is, these three maneuvers do not block the early peak $I_{Ca,L}$ required to maintain normal excitation-contraction coupling avoiding the negative inotropic effect of most Ca^{2+} channel blockers (Fig. 7), (Madhvani et al., 2011; Madhvani et al., 2015).

EADs can also occur during repolarization, or phase 3, when they arise at more hyperpolarized membrane potentials (below -40 mV). This type of triggered activity has been attributed to two primary mechanisms: **1**) recovery from inactivation of the Na^+ channels and/or **2**) spontaneous Ca^{2+} release, which depolarizes the membrane potential through the electrogenic NCX (Szabo et al., 1994; Qu et al., 2013; Bengel et al., 2017; Sato et al., 2017). The main reason to exclude L-type

Ca^{2+} current involvement in phase 3 EADs is that Ca^{2+} channels are not active below -40mV (like Na^{+} channels), and therefore unlikely to contribute to EAD formation.

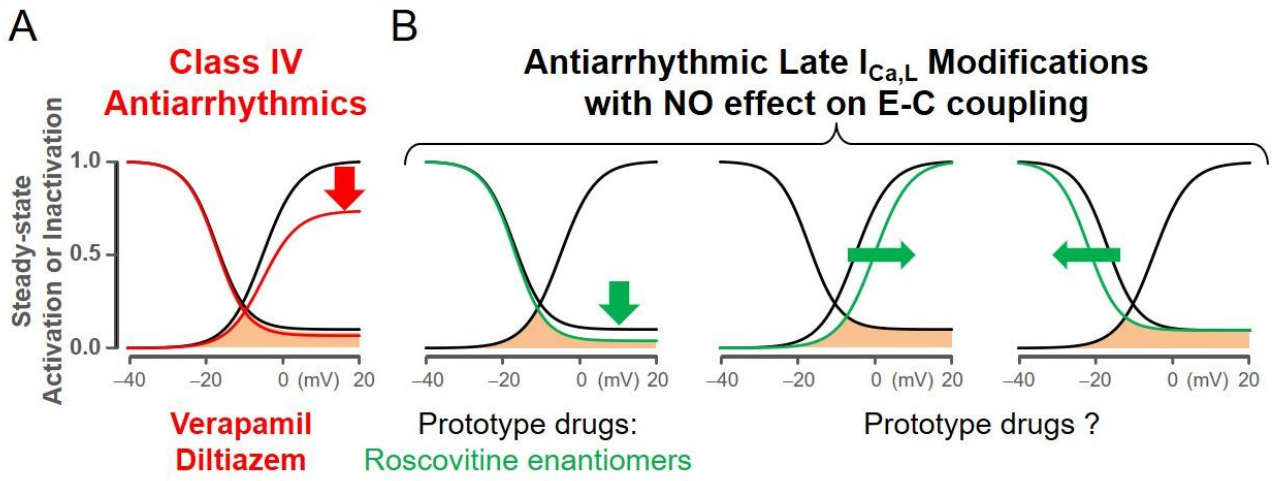

Figure 7 – Late $I_{Ca,L}$ modifications proposed as antiarrhythmic strategies. A) Effect of Class IV antiarrhythmics on $I_{Ca,L}$ steady-state activation-inactivation (red line): they indiscriminately block LTCCs reducing late and peak (red arrow) $I_{Ca,L}$, resulting in the reduction of maximum $Ca_V1.2$ open probability and impairment of EC coupling. **B**) $I_{Ca,L}$ gating modifications, that specifically reduce $I_{Ca,L}$ "window current", were found to potently abolish EADs without affecting maximum $Ca_V1.2$ open probability; therefore peak $I_{Ca,L}$ remains largely preserved. These manoeuvres include: **1**) $I_{Ca,L}$ non inactivating component reduction (late $I_{Ca,L}$,); **2**) a 5 mV depolarizing shift of steady-state activation; **3**) a 5 mV hyperpolarizing shift of steady state-inactivation. From (Karagueuzian et al., 2017).

1.4 L-type calcium channels

The L-type Ca^{2+} channels (LTCCs) are high voltage-gated channels that convert an electrical signal (membrane depolarization) into an influx of Ca^{2+}. Ca^{2+} entering the cell down its electrochemical gradient serves as the second messenger for multiple intracellular events such as contraction, secretion, synaptic transmission, and gene expression (Catterall, 2000). The four members of the LTCC family ($Ca_V1.1$ - $Ca_V1.4$) are distinguished from other Ca^{2+} channels by their **1**) high voltage of activation (-40mV), **2**) long-lasting (L-type) current, **3**) slow voltage-dependent inactivation, **4**) marked regulation by cAMP-dependent protein phosphorylation pathways, and **5**) sensitivity to dihydropyridine (such as nifedipine) and other channel blockers (Catterall, 2000).

The skeletal $Ca_V1.1$ was the first Ca^{2+} channel to be purified (Curtis and Catterall, 1984) and cloned (Tanabe et al., 1987), while the molecular identity of the cardiac L-type Ca^{2+} channel was established by Mikami and colleagues from rabbit hearts in the late 1980s (Mikami et al., 1989).

LTCC $Ca_V1.2$ subunit composition

Ca_V1 channels exist as multimeric protein complexes consisting of the pore-forming α_1 subunit, together with auxiliary β, $\alpha_2\delta$, and γ subunits. The high resolution CryoEM structure of $Ca_V1.1$ (Fig. 8), which is taken as a model for all the Ca_V1 isoforms, shows that the skeletal pore-forming subunit

(α_{1S}) asymmetrically interacts with these three auxiliary subunits in a 1:1:1:1 ratio (Wu et al., 2016), similarly to $Ca_V1.2$ channels (α_{1C}) (Walsh et al., 2009).

All LTCCs derive their voltage dependence properties from the structural assets of the **α_1 pore-forming subunit** (Catterall, 2010). As shown in Figure 9, the α_1 subunit consists of four homologous, but nonidentical, concatenated repeats (I–IV), each composed of six transmembrane segments (S1-S6) that form a voltage sensing domain (VSD, S1–S4 helices) and a quarter of the pore domain (S5–S6) (Fig. 9A, B). The pore domain contains the selectivity filter that confers the channel a higher affinity for Ca^{2+} among all the other extracellular ions. Each VSD contains a conserved repeated motif of positively charged amino acids at every third position of the S4 helix (Fig. 9C). The presence of these charges conveys the VSDs the ability to "sense" membrane depolarization and rearrange in response to it (Catterall, 2010). The movement of S4 segments across the membrane is then electromechanically transduced to S5-S6 transmembrane segments, causing the opening of the

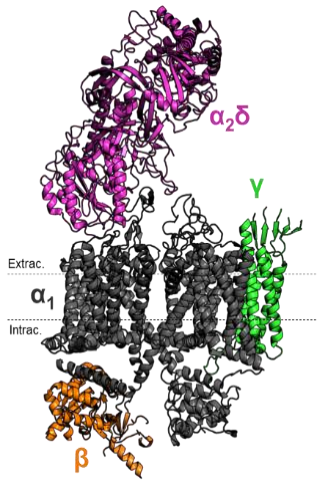

Figure 8 – Ca_V1 channel structure. CryoEM structure of a $Ca_V1.1$ macromolecular complex showing the transmembrane α_1 pore-forming subunit (grey) and γ (green), the intracellular β subunit (orange) and the mostly extracellular $\alpha_2\delta$ subunit. PDB:5jgv (Wu et al., 2016).

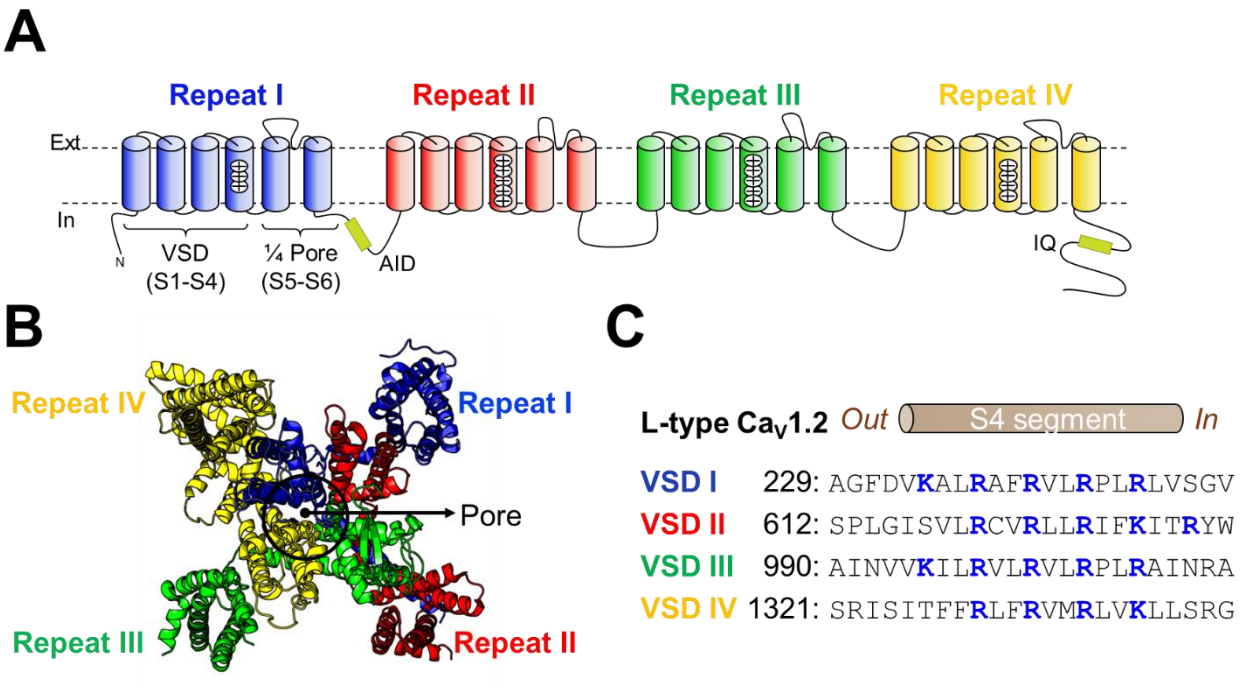

Figure 9 - Topological and structural details of Ca_V channels A) Topology of the α_1 pore-forming subunit showing its four tandem repeats (I-IV), each crossing six times (S1-S6) the plasma membrane, the α-interacting domain (AID) and the isoleucine-glutamine (IQ) motif. **B**) Top view of the atomic structure of the α_1 pore-forming subunit highlighting the central pore formed by the S5-S6 segments of each repeat, and the surrounding voltage sensing domains (VSDs, S1-S4 helices). **C**) Amino acid sequence alignment of each cardiac S4 segment, highlighting the typical R-X-X-R motif of voltage gated channel VSDs. PDB-5GJV, structure from Wu et al., 2016.

pore and the influx of Ca^{2+}. Recently it has been demonstrated that each of $Ca_V1.2$ VSDs possesses unique properties differently contributing to channel activation (Pantazis et al., 2014).

The four repeats are linked through intracellular loops that allocate critical regulatory domains. In the long C terminal region, the isoleucine-glutamine (IQ) motif is recognized by both calmodulin (CaM) and CaM kinase II in the $Ca_V1.2$ channel (Zuhlke et al., 1999). Ca^{2+}/Calmodulin acts as an intrinsic Ca^{2+} sensor modulating Ca^{2+}-dependent inactivation (CDI) and Ca^{2+}-dependent facilitation (CDF), that are central for regulating the level of Ca^{2+} during cardiac AP (Catterall, 2011). In addtion to CDI, Ca_V channels display a slower voltage dependent inactivation (VDI) that is relevant for myocite activity as it limits Ca^{2+} entry during prolonged depolarization, avoiding Ca^{2+} toxic downstream effects. C-terminus is also the target of multiple numerous protein–protein interactions, including protein kinase A phosphorylation sites (Striessnig et al., 2014).
An additional structural determinant of channel function is found in the intracellular linker between repeats I and II which contains the α-interaction domain (AID) that binds the β accessory subunits.
Different mutation in $Ca_V1.2$ α_{1C} subunit has been associated with different cardiac pathologies associated with abnormal heart rhythm, such as Timothy syndrome, and Brugada syndrome (Burashnikov et al., 2010).

The **$\alpha_2\delta$ subunit** is the largest auxiliary subunit of these channels, with a molecular weight of ~175kDa. The mature protein is formed by two peptides, α_2 and δ, which are post-translationally cleaved by an unidentified protease probably during its maturation in the trans-Golgi network (Jay et al., 1991; Dolphin, 2013) and successively linked together by a disulphide bond. α_2 is entirely extracellular interacting only with the α_1 pore-forming subunit (Wu et al., 2016) while δ, that contributes to the C terminal end, anchors the protein to the cell membrane by a glycosyl-phosphatidylinositol motif (Fig. 10), (Davies et al., 2010).
The topology of the $\alpha_2\delta$ comprises four tandem cache domains and one von Willebrand Factor A (VWA) domain, which are well organized domains in the three-dimensional space, but intertwined in the primary sequence (Fig. 10B, C). The role of each domain is still under investigation. However, experimental data collected so far suggest that they are involved in protein-protein interaction and trafficking. VWA domains are generally involved in protein-protein interactions via their metal ion-dependent adhesion site (MIDAS) that coordinates a divalent cation. VWA domain is taught to be involved in Ca^{2+} channels trafficking, since the ability of $\alpha_2\delta$ to increase the plasma membrane expression of Ca_V1 is compromised by a mutation in MIDAS motif (Hoppa et al., 2012). The role of cache domains remains uncertain.

Four genes encoding for as many $\alpha_2\delta$ isoforms ($\alpha_2\delta$-1, $\alpha_2\delta$ -2, $\alpha_2\delta$-3 and, $\alpha_2\delta$ -4) have been identified in the human genome. Among these, $\alpha_2\delta$-1 is the most ubiquitous and represents the main form expressed in cardiac tissue, although $\alpha_2\delta$-3 has been detected at low levels (Gong et al., 2001).

The effect of $\alpha_2\delta$ on channel function depends on the combination of β and $\alpha_2\delta$ isoforms within the complex (Dolphin, 2013). For $Ca_V1.2$ channels, previous experiments in *Xenopus* oocytes showed that co-expression of $\alpha_2\delta$ in combination with $Ca_V1.2/\beta_{2a}$ increased current density suggesting a role in enhancing both channel trafficking and open probability (Shistik et al., 1995). Similarly, $\alpha_2\delta$-1 was reported to shift activation of the $Ca_V1.2/\beta_3$ complex toward more negative potentials (Platano et al., 2000),(Pantazis et al., 2014; Savalli et al., 2016), and increase inactivation kinetics of the current (Shirokov et al., 1998; Dolphin, 2013).

Few mutations in $\alpha_2\delta$-1 gene are associated to human cardiac disfunctions, including the short QT syndrome (Templin et al., 2011) and the Brugada syndrome (Burashnikov et al., 2010).
Physiological relevance of this auxiliary subunit is also proven by the fact that $\alpha_2\delta$-1 is the target for the analgesic drugs gabapentin and pregabalin, two highly effective agents to medicate neuropathic pain (Patel and Dickenson, 2016).

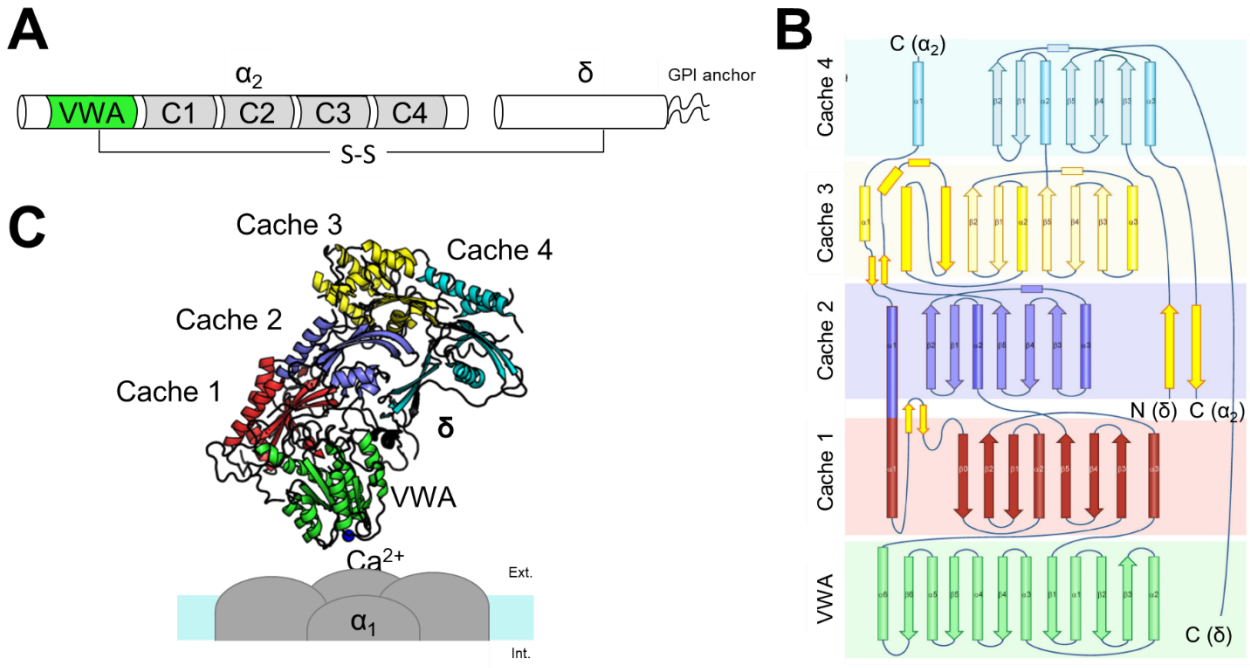

Figure 10 - Topological and structural features of $\alpha_2\delta$-1 subunit. A) Schematic representation of a mature $\alpha_2\delta$-1 protein, cleaved into α_2 and δ peptides. The approximate position of the five domains is shown together with the inter-subunit disulphide bond between α_2 and δ. At the C-terminus of δ peptide a GPI-anchoring element is present. **B**) $\alpha_2\delta$-1 topology shows the interlaced nature of the protein domains to which α_2 and δ differently contribute. The main body of each domain is formed by α_2, while δ subunit completes the cache 4 domain by contributing three β –strands, and extends its ensuing segment to cache1, cache2 and VWA domains. **C**) Structural organization of $\alpha_2\delta$-1 subunit showing a domain coloured α_2 and a black δ subunit. The coordinated calcium cation by MIDAS motif of VWA domain is shown as blue sphere. The same colour code of B was used for each domain. B from Wu et al., 2016.

The **β subunit** is a cytosolic protein of 54 kDa that interacts with the α_1 subunit, through the α-interacting domain (AID) located in the loop between repeats I and II of the α_1 subunit (Fig. 9A), (Pragnell et al., 1994). Upon co-expression of β, Ca^{2+} currents are increased by orders of magnitude,

due to enhanced channel surface expression (Tareilus et al., 1997; Gao et al., 1999) and increased voltage sensitivity (Neely, Olcese et al. 199 Science).

Besides this primary chaperon function, β subunit facilitates channel opening by shifting the voltage-dependence of activation to more hyperpolarized potentials (Neely et al., 1993; Gregg et al., 1996; Weissgerber et al., 2006), increases open probability at single channel level (Colecraft et al., 2002; Dzhura and Neely, 2003), accelerates both VDI and CDI (Buraei and Yang, 2013) and alters both channel activation and inactivation kinetics (Singer et al., 1991; Varadi et al., 1991).

Furthermore, β subunits have been identified as target of lipids, G-proteins, RGK GTPases and other signalling proteins (Buraei and Yang, 2010).

There are four different genes encoding for four distinct β subunits (β_1–β_4) and their multiple splice variants (Buraei and Yang, 2013). Their expression varies with the tissue. In the human heart, β_2 and β_3 isoforms predominate (Hullin et al., 2003), with β_{2b} being the most abundant transcript in ventricular myocytes (Hullin et al., 1992). In pathological condition, such as failing heart, an increased expression of β_{2a} has been observed and associated with pathological membrane excitability and cell death in adult cardiomyocytes (Hullin et al., 2007). Among all the splice variants, β_{2a} produces the largest ionic current and prevents voltage-dependent inactivation, due to its palmytoilated N-terminus that anchors the intracellular subunit to the plasma membrane (Olcese et al., 1994; Dzhura and Neely, 2003; Hullin et al., 2003).

The functional significance of having diverse Ca_V β isoforms and splice variants in the heart is unknown but their expression is critical for embryonic survival and tissue development, as demonstrated by β knockout experimental animal models (Weissgerber et al., 2006). On the contrary, in adult tissues, it has been reported that a cardiac-specific knock-down of β_2 proteins (by 96%), only moderately decreased $I_{Ca,L}$ suggesting that $Ca_V\beta_2$ may not be critical for α_{1C} trafficking in adult ventricular myocytes (Meissner et al., 2011). This observation was recently confirmed in adult transgenic mice carrying a mutation in the AID, which renders the pore-forming α_{1C} subunit incapable of binding β subunits. Despite this mutation, the basal function of β-less Ca^{2+} channels was only minimally altered. Instead, it was found that the β subunit was obligatory for transducing β-adrenergic signals to cardiac $Ca_V1.2$ channels (Yang et al., 2019).

<u>γ subunits</u> are transmembrane accessory proteins that primarily interact with VSD IV of the pore-forming subunit (Fig. 8), (Wu et al., 2016). There are eight distinct γ isoforms (γ_1–γ_8), four of which (γ4, γ6, γ7, γ8) have been detected in human hearts, with only γ_6 confirmed at the protein level in rat hearts (Shaw and Colecraft, 2013). At a functional level, γ_4 and γ_7 slightly left-shift voltage dependent activation ($\alpha_{1C}/\beta_1/\alpha_2\delta$ complex), while γ_8 has the greatest impact on voltage dependent inactivation, shifting the curve toward more positive membrane potentials by ~10 mV (Yang et al., 2011).

1.5 Targeting the Late $I_{Ca,L}$ to suppress EADs

Based on the experimental data reported by Olcese's Laboratory, and our current mechanistic understanding of arrhythmogenesis (Qu and Chung, 2012; Madhvani et al., 2015; Weiss et al., 2015), we hypothesize that a drug able to preferentially reduce "late $I_{Ca,L}$" without affecting "peak $I_{Ca,L}$" and the EC coupling, will have great antiarrhythmic potential (Fig. 7).
A potential candidate to explore this hypothesis is represented by roscovitine. Roscovitine (Seliciclib, R-roscovitine) is a 2,6,9-trisubstituted purine that was originally developed as a selective blocker of cyclin-dependent kinases (Meijer and Raymond, 2003) and is currently in phase II clinical trials as an anticancer drug (Benson et al., 2007; Belani, 2012). Further pharmacological characterization of this compound led to the discovery that the R-enantiomer operates also as an extracellular ligand of α_{1C} pore-forming subunit, since intracellularly-applied (R)-roscovitine failed to affect L-channel activity (Yarotskyy and Elmslie, 2007). The resulting interaction has the unique characteristic of accelerating the voltage-dependent inactivation of $Ca_V1.2$ LTCCs, preferentially reducing "late $I_{Ca,L}$" (non-inactivating component) over "peak" (Yarotskyy and Elmslie, 2007; Yarotskyy et al., 2009; Yarotskyy et al., 2010; Yazawa et al., 2011).

In the following sections, I address our hypothesis by studying the biophysical modification of R-roscovitine on the "late $I_{Ca,L}$" of L-type $Ca_V1.2$ channels, and by investigating the antiarrhythmic effect of R-roscovtine on either EADs induced in isolated rabbit ventricular myocytes and EAD-mediated VT/VF in isolated perfused rabbit and rat hearts.

2. METHODS

2.1 Ethical approval

All animal protocols were approved by the UCLA Institutional Animal Care and Use Committee and conformed to the Guide for the Care and Use of Laboratory Animals published by the US National Institutes of Health.

2.2 Molecular biology

cDNA of human α_{1C} (GenBank accession no. CAA84346) (54) $\alpha_2\delta$-1 (UniProt accession no. P13806) and β_{2b} subunits (UniProt accession no. Q8VGC3), containing a T7 promoter and a poliA tail for heterologous expression in Xenopus oocytes, were transcribed in vitro using the AmpliCap-Max™ T7 High Yield Message Maker Kit, CELLSCRIPT (for details see Chapter 2).

2.3 Oocyte preparation

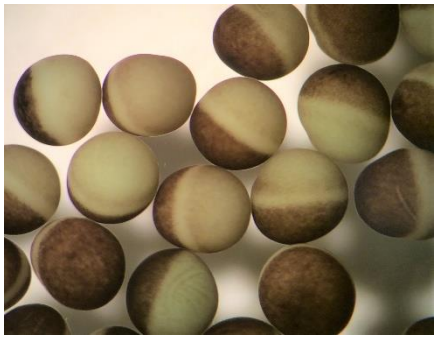

Figure 11 – Mature *Xenopus* oocytes after defolliculation.

Xenopus *leavis* female frogs (NASCO, Modesto, CA) were anesthetized with 0.17% tricaine solution pH 7.0 for 20 minutes and sacrificed. Ovaries were surgically removed and washed from blood contamination in OR-2 solution containing (mM): 82.5 NaCl, 2.5 KCl, 1 MgCl2, 5 HEPES, pH 7. To isolate single oocytes, lobes were open and digested at room temperature in OR-2 supplemented with 207 U/ml Collagenase type I for ~12-15 minutes in continuous agitation. After rinsing six time to remove collagenase excess, oocytes were gradually adapted to increasing Ca^{2+} concentration mixing OR-2 and SOS solutions, with the latter containing (in mM): 100 NaCl, 1.8 $CaCl_2$, 2 KCl, 1 MgCl2, 5 HEPES, 50 µg/ml gentamycin (Gibco) and 10 mg/ml penicillin/streptomycin (Sigma), pH 7. Isolated cells were maintained in SOS solution at 18°C until use (Fig. 11).

2.4 Cut-open oocyte technique

The cRNA of the different subunits of the cardiac LTCC (α_{1C}+β_{2b}+$\alpha_2\delta$-1) was injected into stage VI *Xenopus* oocytes (50 nl at 0.1–0.5 µg/µl). After 3-4 days post-injection, oocytes were voltage-clamped using the cut-open oocyte technique (for more details see Project 2), (Stefani and Bezanilla, 1998; Pantazis and Olcese, 2013). The ionic currents were acquired before and after the addition of (R)-roscovitine (termed roscovitine throughout the elaborate). Roscovitine (LC Laboratories) was dissolved in either ethanol or DMSO (0.02%) and added to the external solution.

External solution (mM): 2 Ba-Methanesulfonate (MES), 120 NaMES, and 10 HEPES, pH 7.0, supplemented with 0.1 ouabain to eliminate current deriving from endogenous Na/K ATPase (Barish, 1983). Internal solution (mM): 120 K-glutamate and 10 HEPES, pH 7.0. Pipette solution (mM): 2700 NaMES, 10 NaCl, and 10 Na-HEPES, pH 7.0. Before experiments, oocytes were injected with 100 mM BAPTA•4K (100 nl), pH 7.0, to chelate Ca^{2+}/Ba^{2+} ions and thus prevent activation of endogenous Ca^{2+}- and Ba^{2+}-dependent Cl− channels.

Ionic current was activated by a depolarizing step from -100 to 100 mV for 25 ms (holding potential at -90 mV). Depolarization was followed by a repolarizing step at -40 mV to elicit tail current. The voltage dependence of channel opening (steady-state activation) was thus obtained from the peak tail current at −40 mV and plotted against the test potential. The steady state activation was empirically characterized by fitting to two Boltzmann functions as:

$$G(V) = \frac{G_{\max}}{1 + e^{\left[z(Vhalf - Vm)\left(\frac{F}{RT}\right)\right]}}$$

where q is the effective charge, V_{half} is the half-activation potential, V_m is the membrane potential, T is the absolute temperature, and F and R are the Faraday and Gas constants, respectively.

For steady-state inactivation, current was elicited from -100 to +30 mV for 2s and then subjected to a 0 mV test pulse for 50 ms. The quasi-steady-state inactivation curves were constructed by plotting the normalized peak current during a test pulse at 0 mV at the various membrane potentials tested. The steady state inactivation was fitted to Boltzmann function:

$$f(\mathrm{V}) = \frac{1 - pdest}{1 + \exp\left[\left(-\frac{qF}{RT}\right)(Vhalf - Vm)\right]} + pdest$$

where pdest is the non-inactivating pedestal of the inactivation.

Five different batches of oocytes were used.

2.5 Ventricular myocytes

For ventricular myocytes isolation, adult (3- to 4-month-old) New Zealand white male rabbits were anesthetized by intravenous injection of 1,000 U heparin sulfate and 100 mg/kg sodium pentobarbital. Once removed from the chest, hearts were washed from residual blood and perfused retrogradely in Langendorff fashion at 37°C with nominally Ca^{2+}-free Tyrode's solution containing (in mM): 136 NaCl, 5.4 KCl, 0.33 NaH_2PO_4, 1 $MgCl_2$, 10 glucose and 10 HEPES, pH 7.4, and supplemented with ≈1.4 mg/mL collagenase (type II; Worthington) and 0.1 mg/mL protease (type XIV; Sigma) for 25 to 30 minutes. After washing out the enzyme solution, hearts were removed from the perfusion apparatus and swirled in a culture dish to obtain a cell suspension. [Ca^{2+}] was slowly

increased to physiological levels (1.8 mM). The cells were stored in Tyrode's solution at room temperature and used within ~8 hours.

2.6 Patch clamp

Myocytes were patch-clamped in whole-cell configuration. For voltage clamp recordings, a modified AP waive-form from a rabbit ventricular myocyte was used to record $I_{Ca,L}$. The voltage command was modified with a prepulse at -40mV to inactivate Na^{2+} voltage-gated channels. The pipette solution contained (in mM): 110 Cs-aspartate, 30 CsCl, 5 NaCl, 10 HEPES, 0.1 EGTA, 5 MgATP, 5 creatine phosphate, 0.05 cAMP, pH 7.2 with KOH. Cells were superfused with a modified Tyrode's solution prepared with (in mM): 136 NaCl, 5.4 CsCl, 0.33 NaH_2PO_4, 1.8 $CaCl_2$, 1 $MgCl_2$, 10 glucose and 10 HEPES, pH 7.4 with NaOH. Bath solution was supplemented with 600 µM H_2O_2 to simulate conditions that would produce EADs in ventricular myocytes (Madhvani et al., 2011). Contaminant K^+ and Na^+ conductances were abolished substituting KCl with CsCl and adding 10 µM tetrodotoxin (TTX) to the bath solution, respectively. $I_{Ca,L}$ was blocked with 20 µM nifedipine. $I_{Ca,L}$ was isolated by subtracting the current after 20 µM nifedipine from the total current. The effect of roscovitine during AP clamp was quantified by normalizing the current in presence of 20 µM roscovitine to the control current (before addition of the drug) at 10, 100, 200 ms. All electrophysiological recordings were performed using an Axopatch 200B amplifier (Axon Instruments) and acquired using custom-made software (G-Patch; Analysis).

AP (current clamp) recordings were captured with a pipette solution containing (in mM): 110 K-aspartate, 30 KCl, 5 NaCl, 10 HEPES, 0.05-0.1 EGTA, 5 MgATP, 5 creatine phosphate, 0.05 cAMP, pH 7.2 with KOH. Borosilicate pipettes (Warner Instruments) with 1-2 MΩ resistance were used. The cells were superfused with Tyrode's solution containing (mM): 136 NaCl, 5.4 KCl, 0.33 NaH_2PO_4, 1.8 $CaCl_2$, 1 $MgCl_2$, 10 glucose and 10 HEPES, pH 7.4 with NaOH. To identify the threshold at which cardiomyocytes produce APs, cells were challenged with stimuli of increasing amplitude with square pulses of 2 ms duration. Threshold was then doubled in amplitude and injected at a pacing cycle length (PCL) of 6 s to elicit regular APs. EADs were induced adding 600 µM H_2O_2 to the superperfusate or reducing the extracellular [K^+] from 5.4 to 2 mM (hypokalemia, hypoK) in the presence of 100 µM H_2O_2. To test EADs suppression, 20 µM roscovitine was added to the EAD-inducing solutions. In the control experiments solution containing the vehicle (0.02% ethanol) was perfused. All experiments were performed at 34 to 36°C. Corrections were made for liquid junction potentials. Action potential duration at 90% of repolarization (APD_{90}) and EAD occurrence (defined as percentage of APs that display a positive voltage deflection (dV/dt) of ≥5 mV) were reported as an average of six consecutive action potentials.

Experiments were performed in at least three different cell preparations. Chemicals and reagents were purchased from Sigma unless indicated.

2.7 Intracellular Ca^{2+} measurements and cell shortening

Changes in cytosolic [Ca^{2+}] were recorded in rabbit ventricular myocytes after incubation with the Ca^{2+} indicator 10 µM Fluo-4 AM (Molecular Probes) for ≈20 minutes at room temperature in Tyrode's. The cells were then washed and placed in a heated chamber at 35°C on an inverted microscope implemented with a sCMOS camera (Hamamatsu ORCA) operating at ≈50 frames/s.

Cells were field-stimulated by a pair of platinum electrodes carrying square-wave pulses of 2 ms duration, and 2 nA amplitude, injected every 6 s. Baseline fluorescence was acquired exposing myocytes to the light for 30 s after 2 min stimulation, needed to reach steady state intracellular Ca^{2+} concentrations. The recording of Ca^{2+} transients (Cai) was then repeated with the same protocol, after addition of roscovitine or vehicle (Tyrode's solution + DMSO 1:5000). Fluorescence changes (ΔF) were defined as ΔF = (Fmax-F0)/F0 where Fmax is the intensity of fluorescence at the peak and F0 is the intensity of fluorescence before the stimulation. The values of ΔF in the presence of roscovitine or vehicle solution were normalized to the baseline Ca^{2+} transients.

Ca^{2+} transient duration at half maximum was the duration of the Cai at 50% of the peak amplitude. Cell shortening was measured by dividing the cell length at maximal shortening during each beat by the resting cell length and expressed as percentage. Myocytes from at three different cell isolations were used.

2.8 Isolated perfused heart

Male New Zealand White rabbits (6–8 months old) or and Fisher344 rats (3–4 months old were anesthetized and sacrificed as stated before. Isolated hearts were cannulated through aorta and mounted in Langendorff fashion (Bell et al., 2011). Retrograde perfusion was achieved at 37°C with Tyrode's solution containing (in mM): 125 NaCl, 24 $NaHCO_3$, 4.5 KCl, 1.8 NaH_2PO_4,0.5 $MgCl_2$, 1.8 $CaCl_2$, 5.5 glucose, pH 7.4 gassed with 95%O_2-5%CO_2. Arrhythmias were induced by oxidative stress (100 µM H_2O_2) or combining hypokalemia (1 mM K^+) with 100 µM H_2O_2. Roscovitine (20 or 50 µM) was added to the solution as described below either before or after stressors perfusion. Spontaneously beating hearts were continuously monitored to record local bipolar left atrial-, right ventricular- electrograms and a pseudo-electrocardiogram (LA, RV, p-ECG, respectively) as show in Fig. 12.

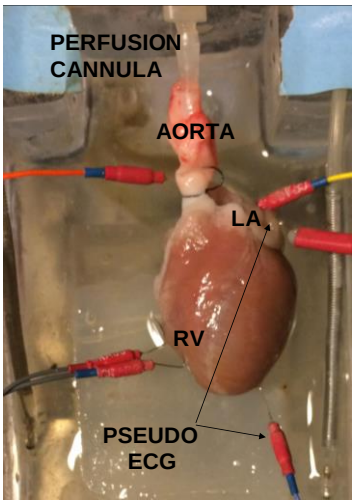

Figure 12 - **Langendorff perfusion setting for rabbit heart.** Illustration of electrodes positioning for left atrial-, right ventricular- electrograms pseudo-ECG recordings. LA = left atrium, RV = right ventricle.

2.9 Statistical analysis

Data are presented as means ± SEM. Paired or unpaired Student's t tests were used to assess statistical significance for $I_{Ca,L}$ inactivation and action potential duration (APD) differences. Kaplan-

Meier curves were constructed to compare the time to onset of VT/VF in the absence or presence of roscovitine at different [drug], using the log rank (Mantel-Cox) test. Differences were considered statistically significant when p value <0.05.

3. RESULTS

3.1 Roscovitine modifies $Ca_V1.2$ channels properties, reducing the non-inactivating component of $I_{Ca,L}$

To estimate whether roscovitine exclusively affects the non-inactivating channel population of the human $Ca_V1.2$, we overexpressed in *Xenopus* oocytes the LTCC complex comprising the human α_{1C} pore-forming subunit and the most common auxiliary subunits find in the human ventricular tissue, namely $\alpha_2\delta$-1 and β_{2b} subunits. Cells expressing the reconstituted $Ca_V1.2$ were voltage-clamped using the cut-open oocyte voltage clamp technique (Stefani and Bezanilla, 1998) and ionic currents were recorded as described in material and methods before and after the addition of roscovitine to the external solution. Ba^{2+} was used as a charge carrier to avoid Ca^{2+}-dependent inactivation.

The presence of 100 μM roscovitine in the external solution had a prominent kinetics effect compared to the control, accelerating the rate of voltage-dependent inactivation. This caused a reduction of the non-inactivating current component (late $I_{Ca,L}$,) with a minimal effect over the maximal current flowing at the beginning of the pulse, e.g. the peak current (Fig. 13A).

The effect was quantified by comparing the normalized steady state inactivation current in control and after the addition of the drug. This comparison was made at 0 mV, when $Ca_V1.2$ channels produce the maximal inward current. Normalized current values were then expressed in percentage. On average, 100 μM roscovitine reduced the quasi steady-state, non-inactivating component of $I_{Ca,L}$ from 27 ± 3% to 15 ± 2%, (p=0.006, N=7, Fig. 13B). Notably, the effect on $I_{Ca,L}$ inactivation was not a consequence of a shift in voltage dependence of steady state activation and inactivation, which remained largely unaffected by roscovitine (Fig. 13B).

This set of experiments establishes that roscovitine modulates the human $Ca_V1.2$ channel, specifically accelerating channel inactivation, or in other words, reducing the fraction of channels that do not inactive and are available for activation (Fig. 13B). As consequence, roscovitine reduces the number of L-type channels that are operative in the range of voltage that defines Ca_V window current and is critical for EADs onset, reproducing one of the therapeutic strategies that Madhvani and colleagues predicted to be highly effective to suppress EAD-triggered arrhythmias (Fig. 7), (Madhvani et al., 2015).

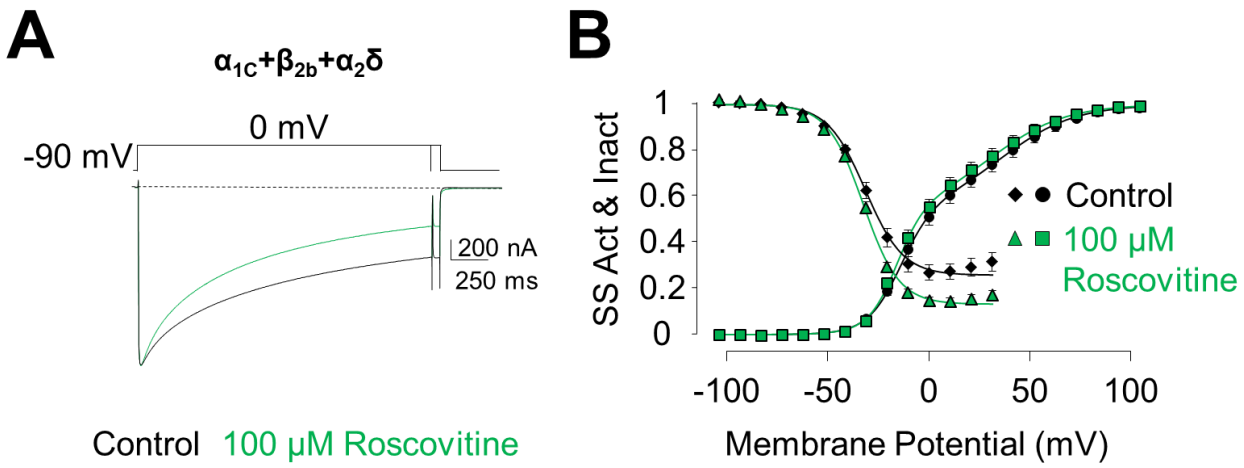

Figure 13 - Roscovitine reduces the non-inactivating component of $I_{Ca,L}$. A) Superimposed Ba^{2+} currents from human $Ca_V1.2$ channels expressed in oocytes ($\alpha_{1C}+\beta_{2b}+\alpha_2\delta$) before (black) and after 100 µM roscovitine (green). **B**) Average steady-state activation and inactivation curves before and after roscovitine. Smooth lines are Boltzmann fits to the activation and inactivation curves. Note the highly-desirable effect of roscovitine selectively reducing "late $I_{Ca,L}$" (N=7).

3.2 Roscovitine reduces late $I_{Ca,L}$ in rabbit ventricular myocytes

Since roscovitine modulates the human $Ca_V1.2$ channel as it does with the rabbit clone with different accessory subunits (Yarotskyy and Elmslie, 2007; Yarotskyy et al., 2010), we used freshly dissociated ventricular rabbit myocytes to determine the effects of roscovitine on endogenous $Ca_V1.2$ channels, and thus on $I_{Ca,L}$ in native conditions. Under AP clamp (Fig. 14), rabbit cardiomyocytes were challenged with a voltage command reproducing an AP waveform, previously obtained from a ventricular myocyte and modified to include a 50 ms prepulse at −40 mV to inactivate voltage-gated Na channels. The Ca^{2+} current exclusively generated by $Ca_V1.2$ channels, defined as nifedipine-sensitive current, was isolated from the total current to which also T-type channels contribute, by subtracting the residual current remaining after the perfusion of the L-type channel blocker nifedipine. Nifedipine-sensitive $I_{Ca,L}$ was measured before and after exposure to 20 µM roscovitine but in constant presence of H_2O_2 to enhance the $I_{Ca,L}$ produced toward the end of the AP and thus simulate a borderline condition for EADs (Xie et al., 2009; Madhvani et al., 2011).

Figure 14A shows that the amplitude of Ca^{2+} current flowing during the late plateau phase of the AP is reduced in presence of roscovitine. To quantify current decrease, we calculated the ratio "*late* $I_{Ca,L}$*"* / $I_{Ca,L}$ *Peak control* at three different time points during the AP clamp (Fig. 14A, dotted lines). The results are reported in Figure 14B. In average, at 200 ms, the fraction of the persistent current (late $I_{Ca,L}$) was reduced by roscovitine by 42% ± 5% (p=0.001, N=4), while at 10ms, representing the peak current, the ratio was not significantly affected by the presence of the drug, as the current was reduced only by 4% ± 2%, suggesting that the maximal influx of Ca^{2+} at early stages of the AP does

not change in presence of the compound. In principle, this feature should preserve proper EC coupling and in turn myocyte contractility.

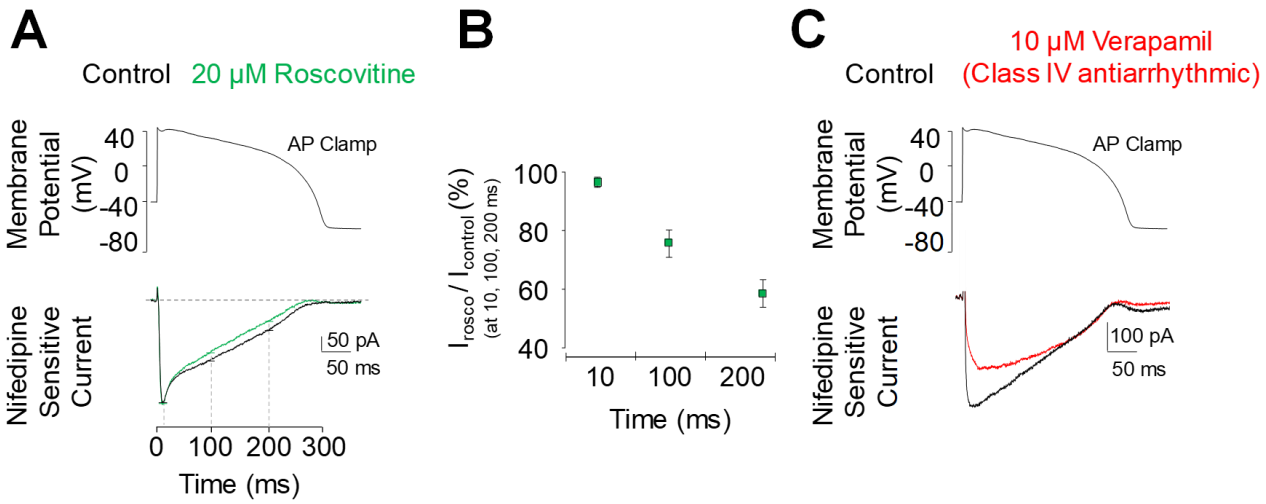

Figure 14 - Roscovitine reduces the late (non-inactivating) component of $I_{Ca,L}$ in native conditions. A) Representative endogenous $I_{Ca,L}$ recorded in the presence of 600 µM H_2O_2 using an action potential waveform protocol (voltage-clamp mode) in rabbit ventricular myocyte. $I_{Ca,L}$ is recorded in control (black) and in presence of 20 µM roscovitine (green). **B)** Quantification of I_{CaL} measured at different time points of the AP, (N=4). Data are mean ± SEM. Roscovitine reduces "late $I_{Ca,L}$" without affecting the "peak $I_{Ca,L}$"**. C)** Nifedipine-sensitive $I_{Ca,L}$ recorded as in A, in control (black) or in presence of 10 µM calcium channel blocker Verapamil (red).

By contrast, commonly-used antiarrhythmic drugs, such as the LTCC blocker Verapamil, dramatically reduced $I_{Ca,L}$ peak current in myocytes stimulated with the same AP waveform (Fig. 14C). This effect is likely consistent with the negative inotropic side-effects reported for Verapamil (Rosen et al., 1975).

These results demonstrate that roscovitine produces a selective reduction of the Ca^{2+} current flowing during the late phase of the AP (late $I_{Ca,L}$) also in cardiac myocytes, confirming that the potential therapeutic effect observed on the heterologously-expressed human $Ca_V1.2$ clone (Fig. 13B) is also applicable to native cardiac L-type channels.

3.3 Roscovitine potently suppresses EADs induced by oxidative stress in isolated rabbit ventricular myocytes

Electrophysiological-computational studies postulated that drugs modifying LTCC gating properties by reducing late $I_{Ca,L}$ by ~ 4%, should potently suppress EADs (Fig. 7), (Madhvani et al., 2015). Since roscovitine can pharmacologically produce this beneficial LTCC gating modification in both clone and endogenous channels (Figs. 13-14), we tested its effectiveness to reduce EAD susceptibility in isolated rabbit ventricular myocytes.

To induce EADs, a model of oxidative stress at the cellular level was applied using 600 µM H_2O_2 which is known to reduce repolarization reserve affecting various ion channels, such as I_{to} (Zhao et al., 2012), the late I_{Na} (Ward and Giles, 1997) and $I_{Ca,L}$ (Xie et al., 2009).

Under current clamp, we recorded ventricular APs injecting a current twice the amplitude current needed to fire an AP in each specific cell. A pacing cycle length (PCL) of 6 s was applied to reproduce the bradycardic stimulation that favors EADs onset and their regular appearance “beat to beat” (Sato et al., 2009; Sato et al., 2010; Weiss et al., 2010). We first exposed myocytes to 600 µM H_2O_2, that prolonged the AP duration (APD) and caused the concomitant appearance of a stable EAD regime within 6 minutes after stressor perfusion.

Specifically, EADs developed in 83.2% ± 5.4 of the APs, prolonging the APD measured at 90% repolarization (APD_{90}) from 276 ± 43 ms to 860 ± 178 ms. Perfusion of 20 µM roscovitine suppressed H_2O_2-induced EADs in all myocytes tested, despite the continuous presence of H_2O_2 (Fig. 15) and restored a normal APD_{90} to 232 ± 25 ms (Fig. 15, control vs roscovitine, p=0.354, N=7). In control experiments, the perfusion of the vehicle (0.02% ethanol) did not suppress the EAD regime (Fig. 16, N=4) or revert the APD_{90}.

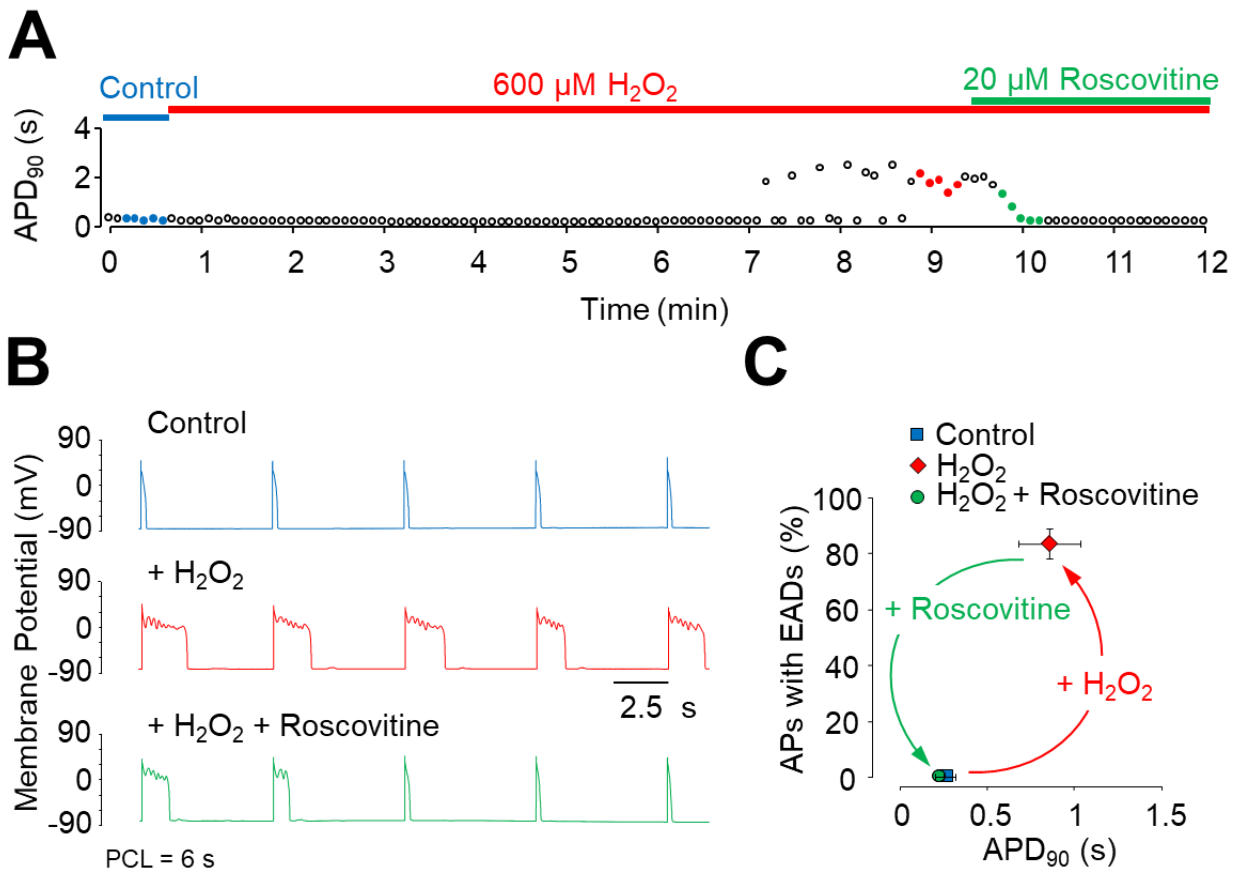

Figure 15 - Roscovitine abolishes H_2O_2-induced EADs in ventricular myocytes. A) Time course of action potential duration (APD_{90}) for a representative experiment. APs (circles) were elicited with 2ms-2nA pulses under current clamp conditions in rabbit ventricular myocyte. APD_{90} dramatically increased after ~ 6 min exposure to 600µM H_2O_2, exhibiting a robust and stable EAD regime. Addition of 20 µM roscovitine completely abolished EAD occurrence and restored the normal APD despite the continuous presence of H_2O_2 in the bath solution. **B)** Demonstrative APs in control condition (blue), H_2O_2 (red) and after the addition of roscovitine (green) that are highlighted as filled circle in the time course in A. **C)** Plot summarizing the average changes in APD_{90} and EAD occurrence during experiments performed as in A. Roscovitine abolished EADs and restored the normal APD, despite the presence of H_2O_2 (N=7 cells, mean ± SEM).

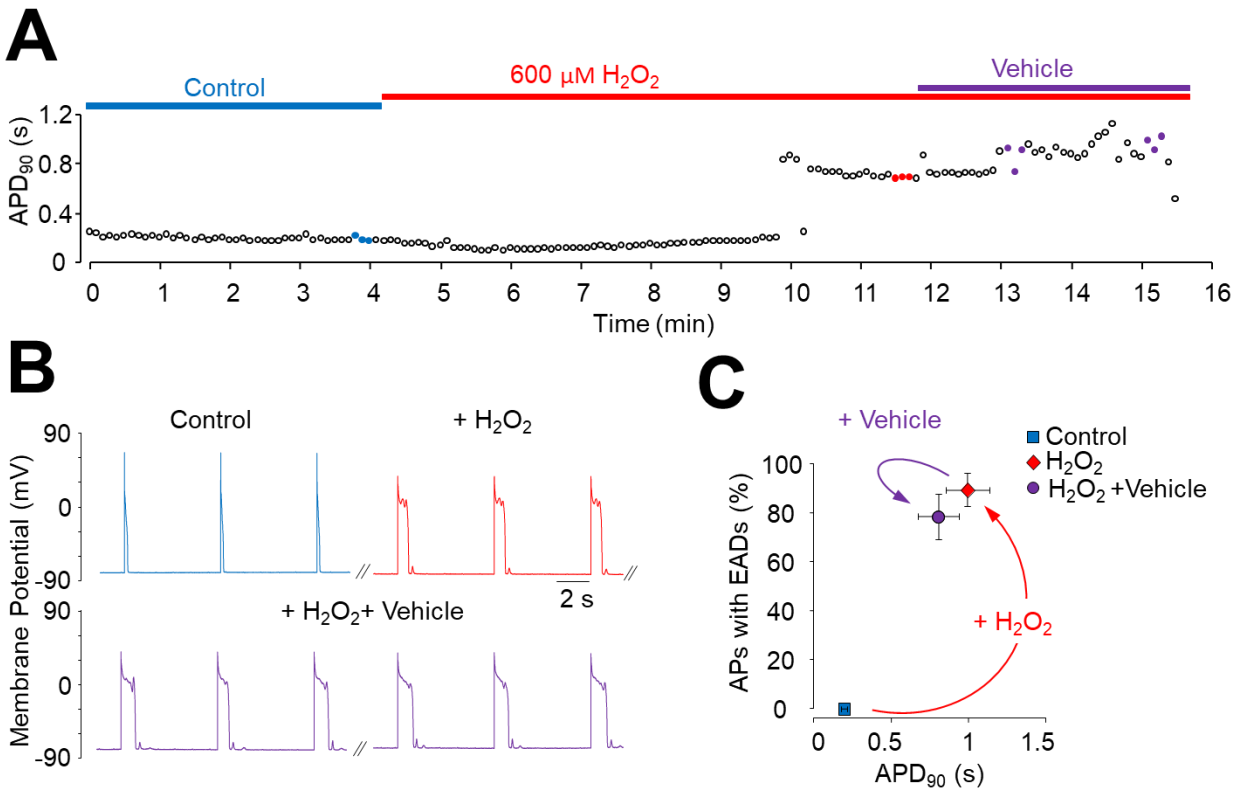

Figure 16 - H_2O_2-induced EADs regime persists in presence of the vehicle. A) Time course of AP duration in rabbit ventricular myocyte perfused with 600 µM H_2O_2, to which vehicle (0.02% ethanol) was then added. **B)** Representative APs in A (coloured circles) are shown for control (blue), H_2O_2 (red) and H_2O_2 + vehicle. **C)** Data quantification shows that the addition of vehicle solution had no effect on APD prolongation and EADs development (N=4 cells, mean ± SEM).

3.4 Roscovitine strongly suppresses EADs induced by oxidative stress and hypokalemia in isolated rabbit ventricular myocytes.

The ionic background of EADs is usually very complex as multiple ionic currents are required to change in order to set the conditions for a reduced repolarization reserve and a prolongation of the AP (Weiss et al., 2010). Thus, testing the "anti EADs" effect of roscovitine in a contest where more ionic currents are compromised would further confirm the robustness of its potential therapeutic effect.

To increase the strength of the type of stressors used to induce the EAD regime, we combined oxidative stress (100 µM H_2O_2) with a reduction of the external potassium from 5.4 mM to 2 mM. Hypokalemia (hypoK) has direct effect on repolarization reserve and contributes to EAD development in rabbit ventricular myocytes (Pezhouman et al., 2015; Trenor et al., 2018).

Under control conditions in normal Tyrode's solution, isolated ventricular myocytes displayed an APD_{90} of 224 ± 39 ms which quadruplicated up to 827±178 ms (N=5) while perfusing both H_2O_2 + hypoK stressors. This intervention produced a stable regime of EADs in 97.1 ± 2.8% of APs elicited within 5-10 mins from stressor application and caused a hyperpolarization of the membrane potential from ~-80 mV to ~-110 mV, likely caused by the reduction of external potassium (Fig. 17), (Trenor

et al., 2018). As with H_2O_2-induced EADs, perfusion with 20 µM roscovitine completely prevented EADs occurrence, restoring the APD_{90} to 324 ± 32 ms (Fig. 17; control vs roscovitine, p=0.067, N=5). These results indicate that roscovitine which we have shown to selectively reduce late $I_{Ca,L}$ (Fig. 14), effectively suppressed EADs of different etiology, pointing out that controlling the non-inactivating population of $Ca_V1.2$ during the AP might be a precious intervention to control aberrant electrical activity at tissue level.

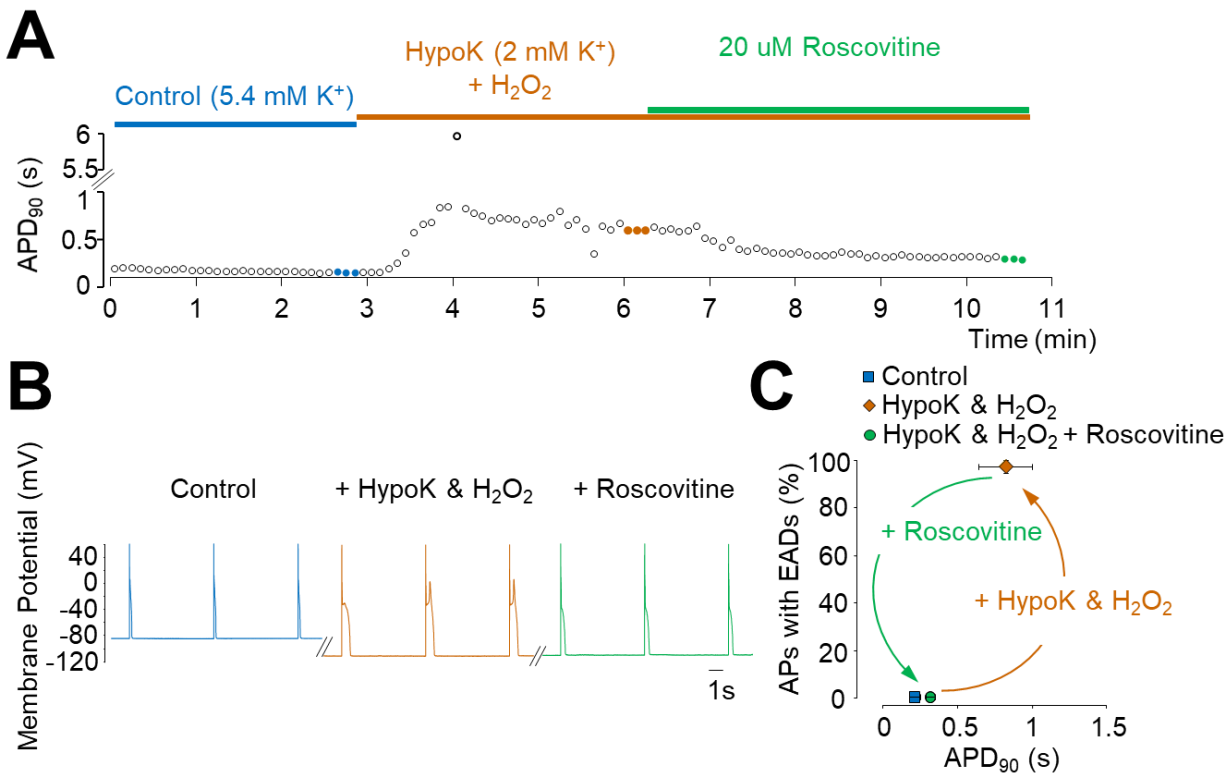

Figure 17 - Roscovitine suppresses Hypokalemia+H_2O_2-induced EADs in rabbit ventricular myocytes. **A)** Time course of AP duration in rabbit ventricular myocyte perfused first with Hypokalemia (2 mM K^+) + 100 µM H_2O_2, followed by 20 µM roscovitine. **B)** Representative APs highlighted in the time course are shown for control (blue), Hypoklaemia+H_2O_2 (orange) and after the addition of roscovitine (green). **C)** Plot summarizing the average changes in APD_{90} and EAD occurrence during experiments performed as in A (N=5 cells, mean ± SEM).

3.5 Roscovitine does not compromise Ca^{2+} transient (Cai) and cell shortening in isolated rabbit ventricular myocytes.

Early Ca^{2+} influx is very rapid and massive in phase 1 and 2 of the AP and is essential to maintain a functional EC coupling as it is needed to trigger Ca^{2+} release from the SR (Bers, 2002). This peak $I_{Ca,L}$, is not affected by roscovitine (Fig. 14). Therefore, it is reasonable to hypothesize that the Ca^{2+} transient (Cai), representing the total cytoplasmic change of Ca^{2+} from RyR2 activation to cell relaxation, and cell shortening would not be compromised by the compound at the concentration used to abolish EADs.

To measure the pure effect of roscovitine on Ca^{2+} transients, we quantified fluorescence signal produced by the intracellular Ca^{2+} indicator Fluo-4AM loaded into rabbit ventricular myocytes in absence of all stress stimuli. Cells were repeatedly stimulated with square pulses to mimic a regular rhythm and induce Ca^{2+} release from the SR. Recordings reporting the change in intracellular Ca^{2+} are shown in Fig. 18A. Roscovitine did not significantly altered Cai amplitude (Fig. 18B. control 92% ± 17, roscovitine 86% ± 2 %, n.s) or duration at half maximal amplitude (Fig. 18C, control 232 ± 23.14 ms, roscovitine 234 ± 30.76 ms, n.s.). In agreement with these findings, cell shortening with roscovitine was comparable to control conditions (Fig. 18D, control 7.23% ± 0.81, roscovitine 7.56 % ± 0.53, n.s.).

Thus, the potent EAD-suppressing effect of roscovitine seems to occur without perturbing Ca^{2+} signaling and cell shortening at the cellular level, indicating that roscovitine will largely preserve cardiac contractility at the modest concentration used to abolish EADs.

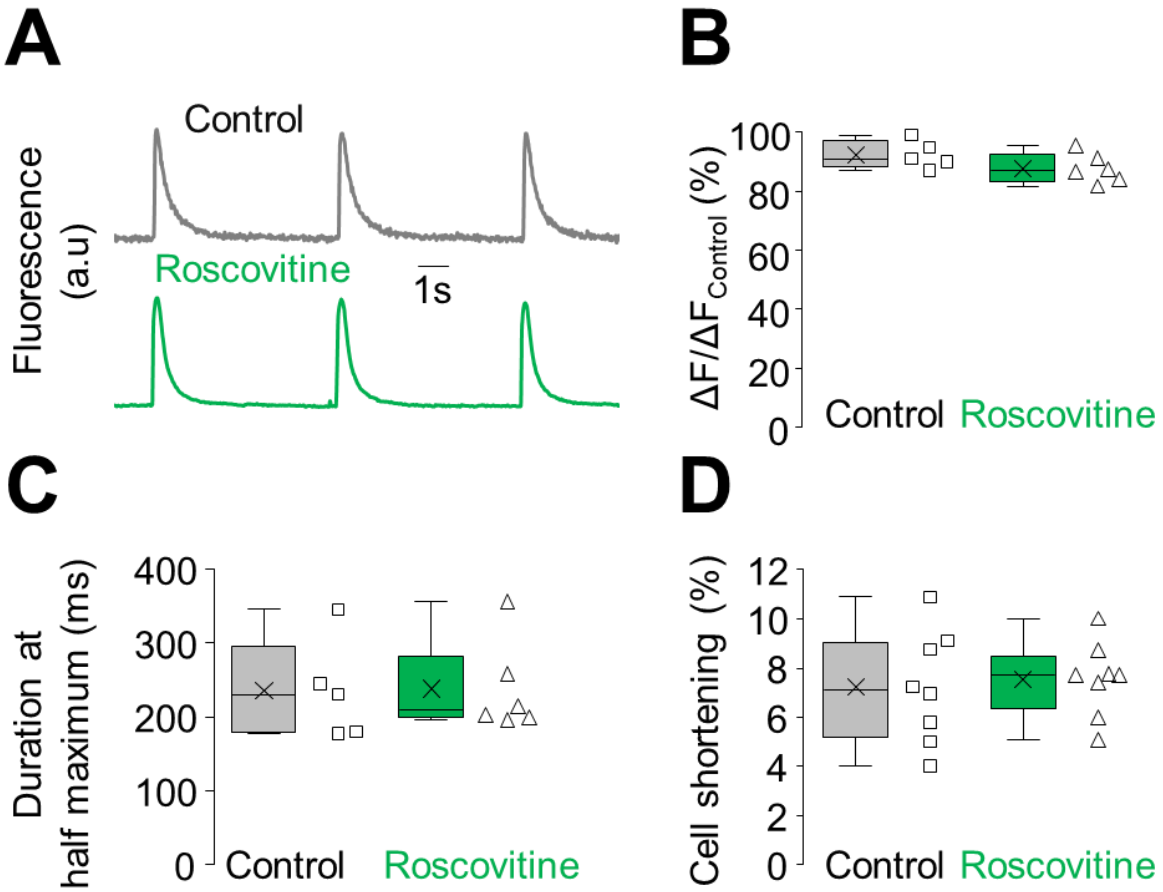

Figure 18 - Ca^{2+} transient and cell shortening in ventricular myocytes are unaffected by roscovitine. A) Representative Ca^{2+} transients from field-stimulated ventricular myocytes loaded with Fluo-4 AM in control (grey) or 20 µM roscovitine (green). **B)** Average change in Ca^{2+} transient amplitude following control or roscovitine addition. **C)** Average change in transient duration measured at half-maximum amplitude for control and roscovitine (control: N=5 cells; roscovitine: N=6). **D)** Cell contraction ability in control conditions or in presence of roscovitine (N=8 each).

3.6 Roscovitine suppresses H_2O_2-induced EADs in *ex vivo* rat hearts.

EADs are arrhythmogenic events that appear at the cellular lever. However, upon synchronization they can trigger premature ventricular complexes that in turn, might result in ventricular tachycardia (VT) or even fibrillation (VF) at tissue level (Sato et al., 2009; Weiss et al., 2010). As consequence, roscovitine, which we have shown to suppress H_2O_2- and/or HypoK-induced EADs in isolated ventricular myocytes (Figs. 15, 17), could be equally effective in repressing at the organ level, the arrhythmogenic events that are triggered by EADs.

Thus, we performed *ex vivo* experiments in isolated rat hearts perfused in Langendorff fashion with a modified Tyrode's solution containing either 100 µM H_2O_2 or 2 mM K^+ (hypoK) to trigger VT/VF. Both oxidative stress and hypokalemia are considered pro-arrhythmic. Specifically, H_2O_2 promotes EADs and mixed focal-reentrant VT/VF in aged fibrotic rat hearts (Morita et al., 2009), while low extracellular K^+ effect is thought to initiate arrhythmias by reducing both K^+ conductance, and thus repolarization reserve and the activity of the Na^+/K^+-ATPase, subsequently leading to Ca^{2+} and Na^+ overload (Weiss et al., 2017; Skogestad and Aronsen, 2018). Electrical activity of the heart was then constantly monitored with Pseudo-electrocardiogram (pECG). As shown in Fig. 19A, H_2O_2 produced a sustained regime of VT/VF in all 8 hearts tested. Perfusion of 20 µM roscovitine effectively suppress VT/VF, converting arrhythmias to sinus rhythm in 8 out of 8 rat hearts (p=0.0024) within 13min ± 2.8 min despite the presence of H_2O_2 (Fig. 19B).

Analogously to oxidative stress, K^+ deficit produced a sustained VF regime in rat hearts that was suppressed by 20 µM roscovitine in 5 out 6 experiments (p=0.045) within 28 ± 9.1 min (Fig. 20).

These *ex vivo* experiments demonstrated that roscovitine possesses antiarrhythmic properties on the whole organ, producing the proof of concept that reducing the late $I_{Ca,L}$, *i.e*. reducing the non-

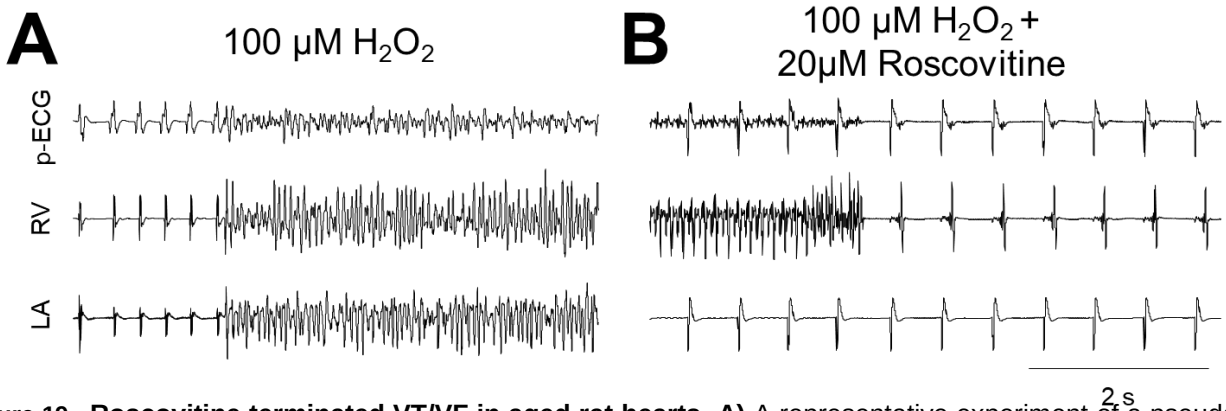

Figure 19 - Roscovitine terminated VT/VF in aged rat hearts. A) A representative experiment of a pseudo-ECG recordings from right atrial-left ventricular leads (top) and RV (middle) and LA (bottom) bipolar electrograms showing the initiation of VT/VF ~ 38 min after exposure to 100 µM H_2O_2 in an isolated-perfused aged rat heart in Langendorff setting. **B)** Same heart, as in **A.** VF is suppressed 16 min after the addition of 20 µM roscovitine to the perfusate in the continuous presence of H_2O_2. Sinus rhythm was restored by roscovitine in 8/8 hearts within 13 ± 2.8 min.

inactivating component of $Ca_V1.2$ channels, could be effective in suppressing EAD-mediated arrhythmogenic events not only at single cell level, but also in the tissue.

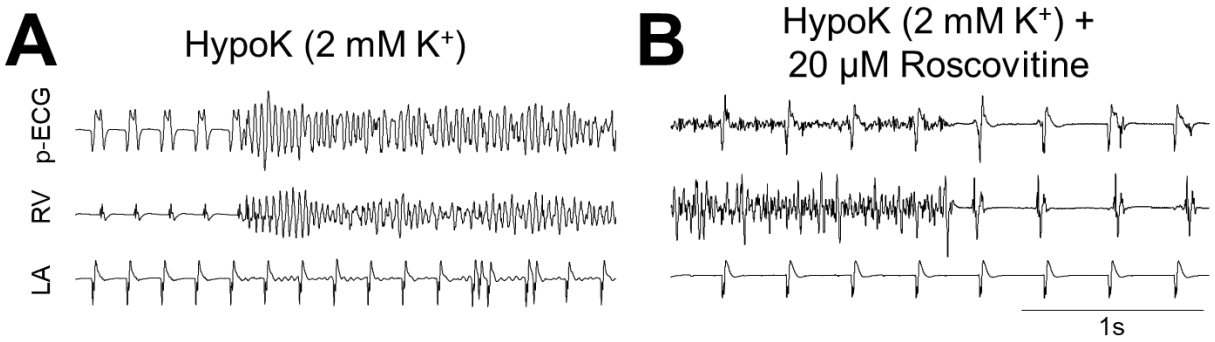

Figure 20 - Roscovitine suppresses hypokalemia-induced VT/VF in aged rat hearts. A) A representative experiment showing initiation of VF in a rat heart after 12 min of exposure to hypokalemia (Tyrode's with 2 mM K^+) recorded with a pseudo-ECG, bipolar electrograms from the RV and LA. **B)** Recordings from the same heart as in **A**, showing suppression of VF 8 min after the addition of 20 µM roscovitine to the perfusate in the continuous presence of hypokalemia.

3.7 Roscovitine prevents H_2O_2- and hypokalemia-induced VT/VF in *ex-vivo* perfused rabbit hearts.

Motivated by the evidence that roscovitine suppresses ventricular arrhythmias in rat hearts (Figs. 19-20), we investigated whether this drug could have also a preventive action on the onset of EADs (rather than abolishing them).

To test this hypothesis, we used rabbit hearts as their AP displays a more prominent plateau phase that resembles the one of humans. Hypokalemic conditions (1mM K^+), as well as oxidative stress (100 µM H_2O_2) were used as a model of cardiac arrhythmia (Pezhouman et al., 2015; Pezhouman et al., 2018).

The control group was exposed to hypoK and 100 µM H_2O_2 which induced VT/VF in 5 out of 5 rabbit hearts within 20 ± 11 mins (Fig. 21A, B). In this condition, H_2O_2- and hypoK-induced arrhythmia did not terminate spontaneously.

The preventive efficacy of roscovitine was tested by arterial perfusion of roscovitine alone 15 minutes before adding H_2O_2 and hypokalemia to the perfusate. Prophylactic perfusion of 50 µM roscovitine prevented VT/VF initiation in 4 out 5 hearts ($P<0.05$) monitored for about one hour in the presence of roscovitine and H_2O_2 and hypokalemia stressors. However, the pretreatment of rabbit hearts with 20 µM roscovitine only prevented emergence of VT/VF in 2 out of 5 hearts tested ($p>0.05$), (Fig. 21D). These results provide substantial compelling evidence that the pharmacological reduction of the late $I_{Ca,L}$ by roscovitine suppresses and prevents VT/VF induced by hypokalemia and/or oxidative stress.

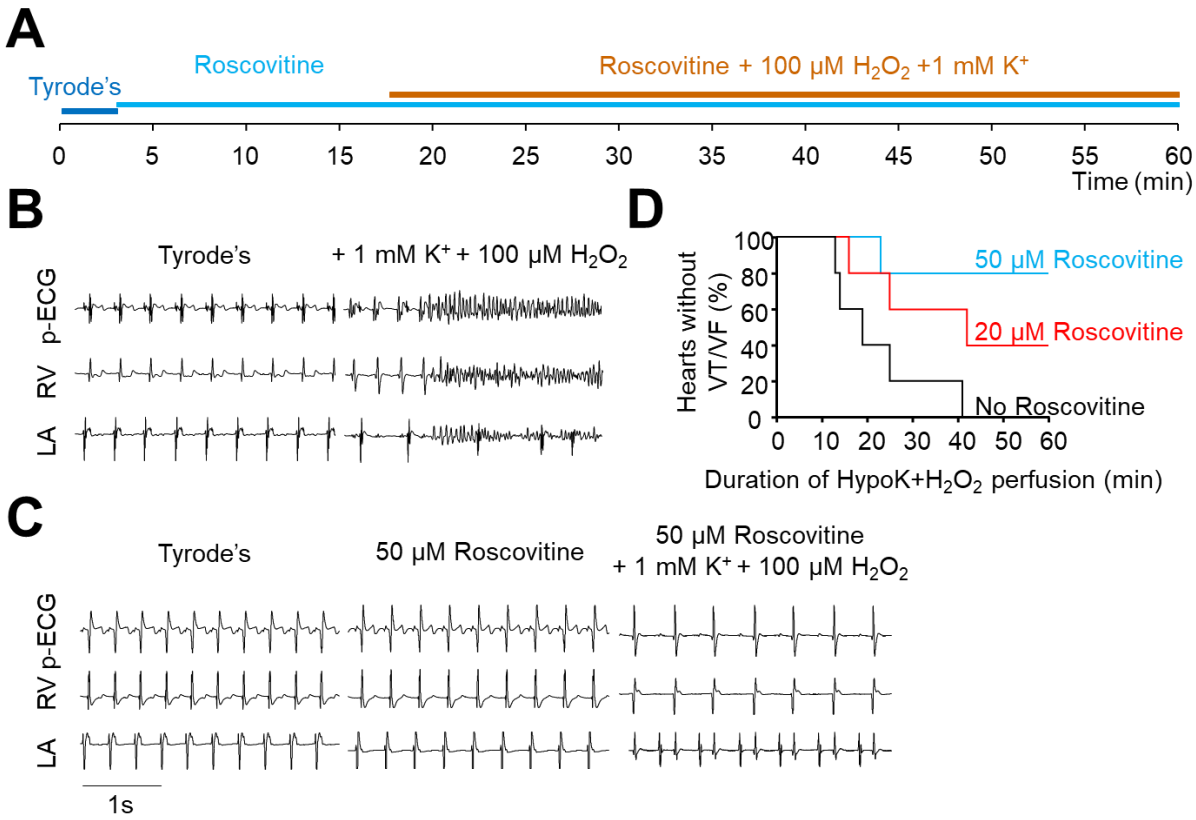

Figure 21 - Roscovitine prevents Hypokalemia+H_2O_2-induced VT/VF in isolated rabbit hearts. A) Scheme of the experimental protocol showing sequential administration of roscovitine and stressors. **B)** Left panel showing sinus rhythm during normokalemia, as recorded with a pseudo-ECG, bipolar electrograms from the RV and LA. Right panel shows initiation of ventricular arrhythmia 14 min after the perfusion of Tyrode's containing 1mM K^+ (hypoK) + 100 µM H_2O_2. **C)** Representative experiment for preventive effect of 50 µM roscovitine. Left, sinus rhythm during normokalemia. Middle panel shows the same heart during 15 min pretreatment with roscovitine. Right panel illustrates recordings 60 minutes after the perfusion of HypoK (1 mM K^+) + 100 µM H_2O_2 in continuous presence of roscovitine. **D)** Kaplan–Meier survival curves comparing time to onset of VT/VF for hearts perfused with HypoK (1mM K^+) + 100 µM H_2O_2 only (control, black) or pretreated with roscovitine 20 µM (red) or 50 µM (blue).

4. DISCUSSION

Ventricular tachyarrhythmias are the most common cause of sudden cardiac death worldwide (Priori et al., 2015; Al-Khatib et al., 2018). Despite the dramatic improvements over the past decades, clinicians and researchers still struggle in identifying therapeutic approaches that are indicated for most patients and economically sustainable. A better understanding of the molecular mechanism underlying arrhythmias would make progress toward innovative therapies.

At the cellular level, early after depolarizations (EADs) provide the most common mechanisms for ectopic excitation, resulting the primary trigger of arrhythmias at the organ level, especially in long QT syndromes and heart failure (Damiano and Rosen, 1984; Cranefield and Aronson, 1991; Antzelevitch and Burashnikov, 2011; Wit, 2018). EADs are driven by the regeneration of inward currents during plateau phase of the AP, in a setting of reduced repolarization reserve (Weiss et al., 2010). Since $I_{Ca,L}$ is the principal depolarizing current during phase 2 of AP, it can recover from inactivation and gain sufficient amplitude to produce a late $I_{Ca,L}$ and evoke a triggered beat (January and Riddle, 1989; Hirano et al., 1992; Weiss et al., 2010; Madhvani et al., 2011). As recently demonstrated by an electrophysiological-computational approach by the Olcese's Laboratory (Madhvani et al., 2015), selectively reducing this EAD-causing current could be one possible strategy to successfully prevent EADs formation while preserving the early Ca^{2+} influx necessary for EC coupling (Fig.7). The experimental data here reported, provide evidence that pharmacological reduction of the late $I_{Ca,L}$ over the peak $I_{Ca,L}$, by roscovitine, is highly effective to suppress EADs. In agreement with previous studies (Yarotskyy and Elmslie, 2007; Yarotskyy et al., 2010), roscovitine selectively reduced the fraction of non-inactivating component of $I_{Ca,L}$ in heterologously-expressed human $Ca_V1.2$ clone and in rabbit ventricular myocytes, diminishing the persistent current at late stage of phase 2 (Figs. 13,14) but leaving EC coupling (e.g. cell contractility) unaffected (Fig.18). This action was translated in a potent suppression of EADs and VT/VF, in single ventricular myocytes and isolated hearts, respectively (Figs. 15-17, 19, 20), as well as in an effective prevention of tachycardia in rabbit hearts (Fig. 21). Moreover, EADs were induced using oxidative stress and/or hypokalaemia, which increase Na^+ and Ca^{2+} inward current or decrease K+ conductance, respectively (Ward and Giles, 1997; Xie et al., 2009; Zhao et al., 2012). Consequently, roscovitine efficacy implies that exclusively targeting the "late $I_{Ca,L}$" is a very effective strategy regardless of the specific ionic mechanism by which EADs were generated. This is also in line with previous reports demonstrating that roscovitine restores electrical activity and Ca^{2+} handling in induced pluripotent stem cells (iPSCs)-derived cardiomyocytes that carry a gain-of-function mutation in $Ca_V1.2$ channels that leads to EADs and Timothy syndrome (TmS), (Yazawa et al., 2011; Song et al., 2015). In addition, we reported that roscovitine was able to recover sinus rhythm in rat hearts and to

prevent the arrhythmia in two different species (rabbit and rat, respectively), despite the different ionic characteristics of the respective APs (Figs. 19-21).

L-type calcium channels: old targets for new therapeutic strategies

Since the discovery of Verapamil in the early 70's, LTCCs have been recognized as interesting targets for antiarrhythmic drugs. At present, the Class IV antiarrhythmics includes Ca^{2+} blockers such as Verapamil and Diltiazem that are used for the treatment and prevention of various cardiac arrhythmias (Rosen et al., 1975; Grace and Camm, 2000; Szentandrassy et al., 2015). Their pharmacological action relays on the overall block of LTCC conductance, indiscriminately reducing both "late $I_{Ca,L}$" and "peak $I_{Ca,L}$" (Fig. 14C). Consequently, these drugs suppress EADs at the single myocyte level, but also compromise cardiac EC coupling (January et al., 1988; Shimizu et al., 1995; Hensley et al., 1997). Thus, their antiarrhythmic action is accompanied by an undesirable negative inotropic effect, that limits their therapeutic value especially in patients with compromised cardiac function (Rosen et al., 1975).

By contrast, drugs that selectively target the "late $I_{Ca,L}$" could be both sufficient and highly potent in suppressing EADs of various etiologies and at the same time safe, as they are predicted to preserve Ca^{2+} signalling (Fig. 18), (Madhvani et al., 2011; Madhvani et al., 2015; Bengel et al., 2017).

Thus, LTCC gating modifiers that selectively reduce "late $I_{Ca,L}$" could constitute a new Class of antiarrhythmic action. Since roscovitine pharmacologically implements selective "late $I_{Ca,L}$", it stands as the archetype for this new class (Karagueuzian et al., 2017).

Moreover, therapeutic compounds that target the "late I_{Na}" are already in development or on the market (such as Ranolazine, GS-967), (Antzelevitch et al., 2004; Belardinelli et al., 2013; Pezhouman et al., 2014; Bengel et al., 2017; Bossu et al., 2018), suggesting the feasibility of developing drugs that selectively reduce "late $I_{Ca,L}$", given the structural similarity between Ca_V and Na_V channels.

Potential off-target effects of roscovitine

As roscovitine has been described to acts on several proteins, some potential off-target effects of our pilot antiarrhythmic compound might be taken into consideration.

Cycline-dependent Kinases.

Roscovitine was initially identified as a potent cyclin-dependent kinase (CDK) inhibitor highly selective for CDK1, CDK2, CDK5, and CDK7, resulting in cell proliferation arrest and cell apoptosis with maximal efficacy at 20 μM after 24h from drug administration (Meijer and Raymond, 2003). At the same concentration, but with shorter exposure, roscovitine did not compromise Ca^{2+} handling and successfully recovered APD in cells displaying EADs. Despite no cytotoxic effects were observed in our experimental setting, a longer exposure to this compound could result in cell damage, hampering its preclinical use as an antiarrhythmic drug, as roscovitine is under phase II

clinical trial as an anticancer compound. However, the promising results here reported, make roscovitine (or better, its mechanism of action) an appealing prototype drug/strategy to suppress or prevent arrhythmogenic events. As consequence, we expect that better pharmacological alternatives could be formulated for clinical antiarrhythmic modulation. In this regard, the existence of roscovitine analogues with reduced CDK inhibition (Liang et al., 2012; Tarr et al., 2013), suggests that future derivative compounds could target more selectively LTCCs.

HERG.

Besides its CDK-inhibition effect, roscovitine remains the only drug available to preferentially reduce "late $I_{Ca,L}$", but in the past few years it has been described to interact with multiple ion channels. In particular, roscovitine has been found to block voltage-dependent potassium channels hERG (Ganapathi et al., 2009) and $K_V4.2$ channels (Buraei et al., 2007) expressed in heterologous systems. In most cases, the block of hERG is associated with an AP prolongation and acquired long QT syndrome that can potentially cause lethal ventricular arrhythmia called torsade de pointes (Sanguinetti and Tristani-Firouzi, 2006). As opposite, no instances of cardiac proarrhythmia have been reported in clinical trials (Fischer and Gianella-Borradori, 2003; Benson et al., 2007). Furthermore, our experimental data demonstrate that roscovitine potently suppressed EADs and restored APD to normal values in isolated ventricular myocytes overcoming the potential drug-induced APD prolongation observed by blocking hERG channel or other potassium channels.

In conclusion, our results provide experimental evidence that L-type Ca^{2+} channel gating modifiers could conceptually represent a new Class of antiarrhythmics that suppress EAD-mediated arrhythmias by selectively reducing "late $I_{Ca,L}$" and avoiding the negative inotropy caused by traditional Ca_V channel blockers that belong to Class IV Antiarrhythmics.

Project 2

Differential modulation of L-type $Ca_V1.2$ and $Ca_V1.1$ channels by the $\alpha_2\delta$-1 subunit

1. INTRODUCTION

1.1 Excitation-contraction coupling and physiological role of L-type calcium channels

Muscle excitation-contraction (EC) coupling defines the process by which the electrical activation of muscle cells leads to the activation of contraction. In its broadest use, EC coupling refers to all the events that intervene between action potential (AP) stimulation and cell contraction. In both cardiac and skeletal muscle cells these events can be summarized as follow: **1**) voltage-dependent activation of L-type Ca^{2+} channels (LTCCs) at the plasma-membrane level to activate the ryanodine receptors (RyRs), **2**) activation of the RyRs which release Ca^{2+} from the sarcoplasmic reticulum (SR) into the cytoplasm, **3**) increase in intracellular Ca^{2+} that shortens the sarcomere units and induces cell contraction, **4**) extrusion or SR re-uptake of Ca^{2+} surplus to favour cell relaxation (Bers, 2002; Calderon et al., 2014).

All these events take places at the dyadic (cardiac) or triadic (skeletal) junctions, where one invagination of the sarcolemma, known as T-tubule, encounters one or two cisternae of the SR, respectively. Here, the distance between the plasma-membrane and the SR is reduced to few nm (~10-15 nm), so that RyRs on the SR are in close proximity to LTCCs channels in the T-tubule (Fawcett and McNutt, 1969). The structural organization of these micro-domains has a clear functional implication: it increases coupling efficiency between LTCCs and RyRs such that activation of LTCCs results in a faster and uniform Ca^{2+} release from the SR (Eisner et al., 2017).

However, cardiac and skeletal junctions differ for LTCC and RyR isoforms expressed and for their reciprocal distribution at the junctional space. In the dyads, the cardiac LTCC $Ca_V1.2$ channels are distributed randomly with one channel every 4-10 cardiac RyR (RyR2), while the skeletal triads appear to be more rigid, since four $Ca_V1.1$ channels forms tetrads that sit above every other RyR1 (Bers and Stiffel, 1993). This stoichiometric arrangement between the two channels functionally explains why in the heart it is the influx of Ca^{2+} via $Ca_V1.2$ that activates the adjacent RyRs (Bers, 2002). By contrast, in the skeletal muscle, the rigid junctional arrangement favours a mechanical interaction between $Ca_V1.1$ and RyR1 such that the SR Ca^{2+} release is not triggered by the entry of extracellular Ca^{2+} like in the heart (Armstrong et al., 1972; Dirksen and Beam, 1999) but requires a depolarization-induced rearrangement in $Ca_V1.1$ to activate RyR1 (Rios and Pizarro, 1991). In other words, cardiac and skeletal muscles engage the SR Ca^{2+} release by two different mechanisms: the former relays on Ca^{2+}-Induced Ca^{2+}-release (CICR) phenomenon, whereas the second exploits a Depolarization-Induced Ca^{2+}-release (DICR) process (Fig. 22). The following sections will discuss these two mechanisms.

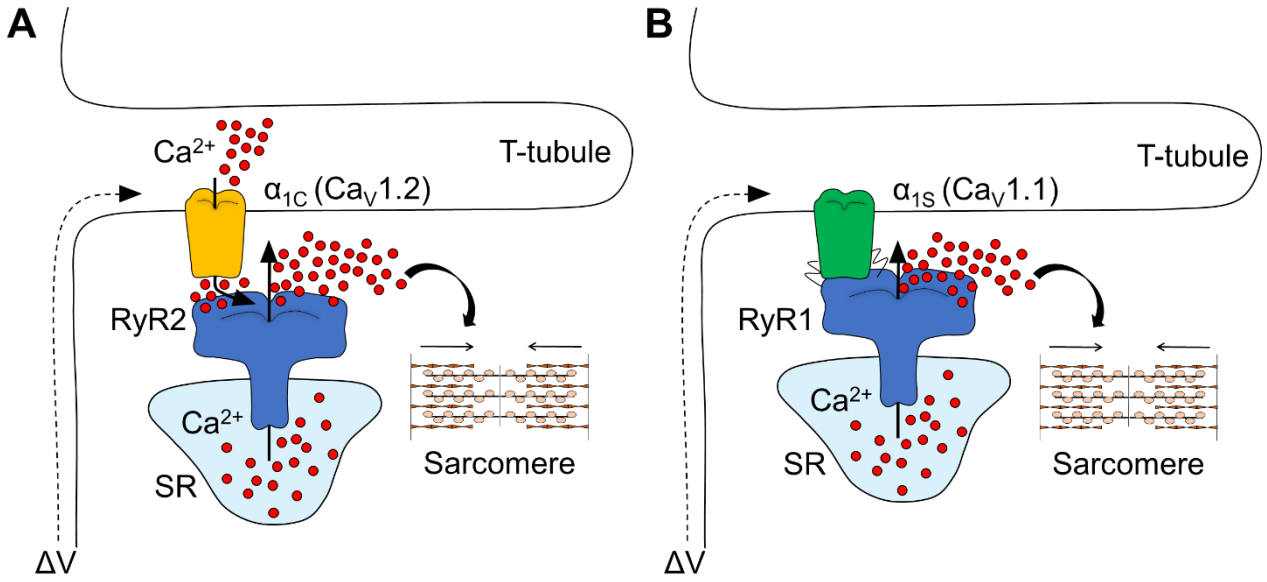

Figure 22 – Excitation-contraction coupling in cardiac and skeletal muscle. A) Schematic representation of Ca^{2+}-induced Ca^{2+} release in cardiac muscle. Cardiac $Ca_V1.2$ opens upon membrane depolarization (ΔV). The massive calcium (Ca^{2+}) influx through the channel pore activates the proximal RyR2 and start Ca^{2+} release from the SR. **D**) Depolarization-induced Ca^{2+} release in skeletal muscle. Upon membrane depolarization, $Ca_V1.1$ channels undergo a conformational change that is mechanically transduced to RyR1 which in turn activates to initiate SR Ca^{2+} release.

$Ca_V1.2$ channels role in Ca^{2+}-Induced Ca^{2+}-Release

Ca^{2+}-induced Ca^{2+}-release (CIRC) was discovered in the heart in the early 70's (Fabiato et al., 1972; Fabiato and Fabiato, 1978), and defined as the process whereby an increase of the intracellular Ca^{2+} concentration causes the release of Ca^{2+} from the intracellular stores, further rising cytosolic Ca^{2+} concentration (Rios, 2018). Thus, CIRC reflects the ability of intracellular Ca^{2+} channels, the RYRs, to be activated by Ca^{2+} when it rises above a threshold level. The voltage-dependence of the Ca^{2+} transients, as well as the cell contraction corresponds to that of the L-type current of Cav1.2 ($I_{Ca,L}$), (London and Krueger, 1986; Beuckelmann and Wier, 1988). Thus, it generally assumed that the activation of $Ca_V1.2$ channels is the principal entry pathway of Ca^{2+} in the heart. As consequence, the threshold is reached upon extracellular Ca^{2+} entry via $Ca_V1.2$ channels, which are estimated to bring in ~10 µmol/L cytosol of Ca^{2+} (Sipido et al., 1995; Sham et al., 1998). Under physiologic conditions, it is believed that one $Ca_V1.2$ should raise the local Ca^{2+} enough to activate at least one RyR2 that, in turn, can recruit more neighbouring RyRs (Bers, 2002). This positive feedback increases the local Ca^{2+} concentration ~100 times and explains why $Ca_V1.2$ channels can irregularly lie around RyR2 at dyadic junction and properly activate CIRC. The resulting Ca^{2+} release is not an all-or-none or self-sustaining phenomenon, as it might be expected. It is instead graded according to the amount of Ca^{2+} influx, as it is inhibited by high (supra-optimal) levels of external Ca^{2+} (Bers, 2002). Moreover, during the late phase 2 of the AP, the current produced by $Ca_V1.2$ opening ($I_{Ca,L}$) decreases by ~ 50% as the SR release and the contraction get larger. This reduction reflects a Ca^{2+}-

dependent inactivation of $I_{Ca,L}$ operated by the SR Ca^{2+} release (Puglisi et al., 1999). As consequence, both $I_{Ca,L}$ and SR Ca^{2+} release control each other to limit the positive feedback of the CIRC guarantying the refractory period that is necessary to complete contraction before a second stimulus is received.

$Ca_V1.1$ channels role in Depolarization-Induced Ca^{2+} Release

The conclusion that skeletal EC-coupling is mostly voltage-dependent rather than reliant on Ca^{2+} influx, has been inferred from four major observations. First, the skeletal muscle can contract for several minutes after depletion of Ca^{2+} from the bath solution (Armstrong et al., 1972), which is instead essential for cardiac contraction (Ringer, 1883). Second, skeletal $I_{Ca,L}$ activates so slowly (at room temperature, $I_{Ca,L}$ peaks after ~ 200 ms while the cardiac $I_{Ca,L}$ reaches the peak in ~5 ms) minimizing Ca^{2+} influx during the fast (5 ms) skeletal AP (Sanchez and Stefani, 1978). Third, RyR1 is less strongly activated by Ca^{2+} alone, and requires more Ca^{2+} to activate than RyR2 (Meissner, 2017). Fourth, skeletal myocytes still release Ca^{2+} from the SR when all known ionic currents (including Na^{2+} and Ca^{2+}) are blocked (Fig.23), (Rios and Pizarro, 1988).

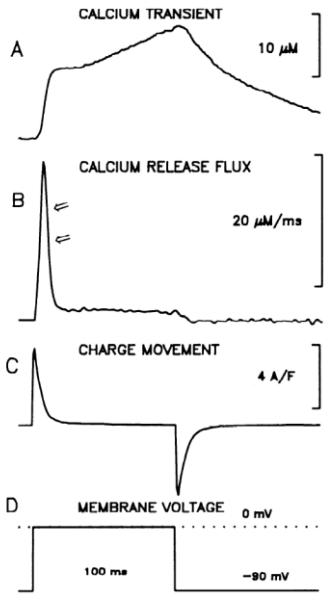

Figure 23 - Ca^{2+} release and intramembrane charge movement in skeletal muscle. Voltage-clamp recordings from a frog semitendinosus fiber reporting **A**) Ca^{2+} transient, **B**) Ca^{2+} release and **C**) charge movement during a depolarizing pulse at 0mV showed in D. A Ca^{2+}-sensitive dye was added to the intracellular solution to measure Ca^{2+} transient in A, that was used to calculate the Ca^{2+} release flux in B. From these experiments, the author suggested that charge movement during the depolarizing pulse could be responsible for activating the SR Ca^{2+} release (Schneider and Chandler, 1973). From (Rios and Pizarro 1988).

In this condition of "ionic block", an intramembrane charge movement, which is synchronized with the Ca^{2+} release, is still visible (Fig 24). This movement is attributed to $Ca_V1.1$ channels gating as **1**) Dihydropyridine Ca^{2+} antagonist (nifedipine) inhibits charge movement as well as contraction (Lamb and Walsh, 1987; Rios and Pizarro, 1988) and **2**) dysgenic myotubes lacking the α_{1s} pore-forming subunit of $Ca_V1.1$ do not display charge movement or signs of contraction (Tanabe et al., 1988; Adams et al., 1990). $Ca_V1.1$ channels are thus referred to as the voltage sensors of the skeletal EC-coupling (Rios and Pizarro, 1991; Calderon et al., 2014). By contrast, the cardiac $Ca_V1.2$, even when injected in dysgenic myotubes, gates RyR1 opening only in presence of extracellular Ca^{2+} (Tanabe et al., 1990; Garcia et al., 1994; Kasielke et al., 2003).

Interestingly, CICR is present in developing skeletal muscle. At embryonical stages, skeletal EC coupling is governed by an alternative splice variant of $Ca_V1.1$ channels ($Ca_V1.1e$), with faster kinetics and greater conductance, resembling those of the cardiac $Ca_V1.2$ (Tuluc et al., 2009; Flucher and Tuluc, 2017). The ability to

conduct big and fast Ca^{2+} current is then lost during muscle maturation, when DICR takes over and $Ca_V1.1e$ channels are replaced with slow activating channels, implying that reducing Ca^{2+} influx might be physiologically relevant for muscle homeostasis (Flucher and Tuluc 2017).
It is although recognized that the adult $Ca_V1.1$ may conduct a small Ca^{2+} current during long-lasting tetanic stimulation or repeated trains of APs, to refill the SR Ca^{2+} stores and thus sustain muscle performance during prolonged activity (Robin and Allard, 2015).

1.2 $Ca_V1.1$ and $Ca_V1.2$ interaction with the ryanodine receptor

DICR implies mechanical interaction between Ca_V and RyRs, respectively. However, the past 60 years of experimental data did not completely clarify whether $Ca_V1.1$ and RyR1 are directly coupled or whether a third protein is needed to mediate their interaction, nor they unravelled the mechanism by which $Ca_V1.1$ rearrangement gates the opening of the RyR1 receptors (Calderon et al., 2014; Bannister, 2016).
So far, the most concrete evidence of the intermolecular interaction comes from electron freeze-fracture replicas capturing the highly organized structure of the skeletal tetrads (Block et al., 1988). Therefore, any structural element whose absence compromised this rigid organization or the EC coupling machinery was proposed as the connecting ring between Cav1.1 and RyR1 channels. Among the three auxiliary subunits that form Cav1.1 macromolecular complexes (β_{1a}, γ_1, $\alpha_2\delta$), only β_{1a} displayed such requirements. In absence of β_{1a} auxiliary subunit, the “chessboard“ framework of the tetrads becomes irregular and EC-coupling fails to happen, suggesting a critical role of β_{1a} in the electromechanical coupling (Gregg et al., 1996; Strube et al., 1996; Schredelseker et al., 2005). However, its hypothetical role as a “glue” between the two Ca^{2+} channels is still controversial since its ability to bind RyRs *in vitro*, independently from the α_{1s} subunit, was not confirmed *in vivo* (Dayal et al., 2010; Rebbeck et al., 2011).
Areas of direct physical contact between $Ca_V1.1$ and RyR1 have also been identified. Chimeric approaches based on $Ca_V1.1$-$Ca_V1.2$ fusion proteins, identified the intracellular $Ca_V1.1$ linker between the voltage sensing domain (VSD) II and VSD III as the indispensable connecting site for skeletal-type EC coupling. In particular, the central residues of this region (720-764/5) were considered “critical” for this function (Nakai et al., 1998; Kugler et al., 2004). The same linker was found to mediate the interaction with another central protein for the EC coupling, named Stac3, confirming the relevance of this sequence as the interface between $Ca_V1.1$ and RyR1 (Horstick et al., 2013; Nelson et al., 2013; Linsley et al., 2017; Wong King Yuen et al., 2017).

Instead, the emerging picture for the cardiac $Ca_V1.2$ and RyR2 channels is of a much less robust interaction than in skeletal muscle. That is consistent with the total absence of DICR in the cardiac muscle and the stoichiometric arrangement of the two channels at the dyads, where there is a 4-10-

fold excess of RyR2 over $Ca_V1.2$ and no tetradic organization (Bers and Stiffel, 1993). Few reports support this weak interaction in the heart. El-hayek and Ikemoto found that a short peptide (Ac-10C) in the II-III loop of the cardiac α_{1C} pore-forming subunit could activate the skeletal RyR1 (El-Hayek and Ikemoto, 1998), and induce SR Ca^{2+} release in skinned (permeable) skeletal muscle (Lamb et al., 2000). By contrast, in ferret ventricular myocytes, RyR2 opening and spontaneous release of Ca^{2+} were reduced by the presence of Ac-10C (Li and Bers, 2001). Beside the opposing results in terms of function, the analogy of this peptide with the skeletal II-III loop suggests that α_{1C} and RyR2 might interact, but further analysis is surely needed.

1.3 L-type Ca^{2+} channels voltage-sensing mechanism and generation of gating currents

Beside the different mechanism used to gate RyR, both Cav1.1 and Cav1.2 need to be activated by membrane depolarization to fulfil their function. How they sense the change in voltage depends either on the structure of their α_1 pore-forming subunit and on the electrical nature of the plasma membrane.

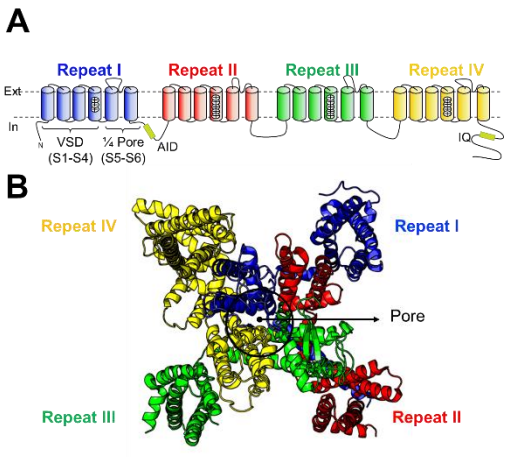

Figure 24 – Topology and structure of α_1 pore-forming subunit of Ca_V1 channels. **A**) Topology of a1 subunit showing the four repeats and their six transmembrane helices. The charged helices indicate the S4 segments. **B**) Top view of the α_1 subunit highlighting the central pore and the surrounding voltage sensing modules. PDB:5gjv, (Wu et al., 2016).

As described in the previous project, Ca_V α_{1S} and α_{1C} subunits are formed by four homologous repeats that arrange around a central pore (Fig. 24). Each repeat has six transmembrane α-helices (S1-S6) that are spatially organized to form a voltage sensing domain (VSD, S1-S4) and to contribute to ¼ of the pore (S5-S6). Each VSD is critical for channel operation as it contains multiple charged residues concentrated in the S4 segment. All the six repeats of α_1 subunit are embedded in the phospholipid bilayer where they are directly exposed to an electric field that is determined by ions diffusing across the membrane, down their electrochemical gradient.

Changes in this electric field can orientate a charge within a protein causing a conformational change that may affect its function. (Bezanilla, 2008). This charge orientation phenomenon takes place also in voltage-gated ion channels, mainly at their S4 transmembrane segments that are rich in Arg and Lys. Here, the translocation of charges during membrane depolarization moves the S4 transmembrane segments in concert with the surrounding α-helices to allosterically open the channel pore (Catterall, 2010). As the S4 charges move across the electric field, they produce a small (but measurable) transient current of few milliseconds that always precedes pore opening. For this reason, it is called

gating current. The transient nature of this current is given by the fact that the movement of the S4 segments is mainly limited to its transmembrane location (Catterall, 2010). Thus, the time course of the transient depends on the mobility and the path of the gating charge.

The S4 movement can be described by a “two-state” model, where the sensor (and the associated gating charge) can be in only two positions: the resting and the active state (Bezanilla, 2018). The two states are separated by an energy barrier that makes the spontaneous transition from one to another energetically unfavourable. To move, the charge must overcome the barrier, which usually happens as a transmembrane potential is imposed (Fig. 25).

As consequence, the strength of the local electric field and the magnitude of the charge influence the extent and the kinetics of this charge movement. For example, a weak electric field determines a “slow” charge movement that can produce a decaying gating current. By contrast, a fast transition can be observed when a charge crosses a high-energy barrier (Bezanilla, 2008).

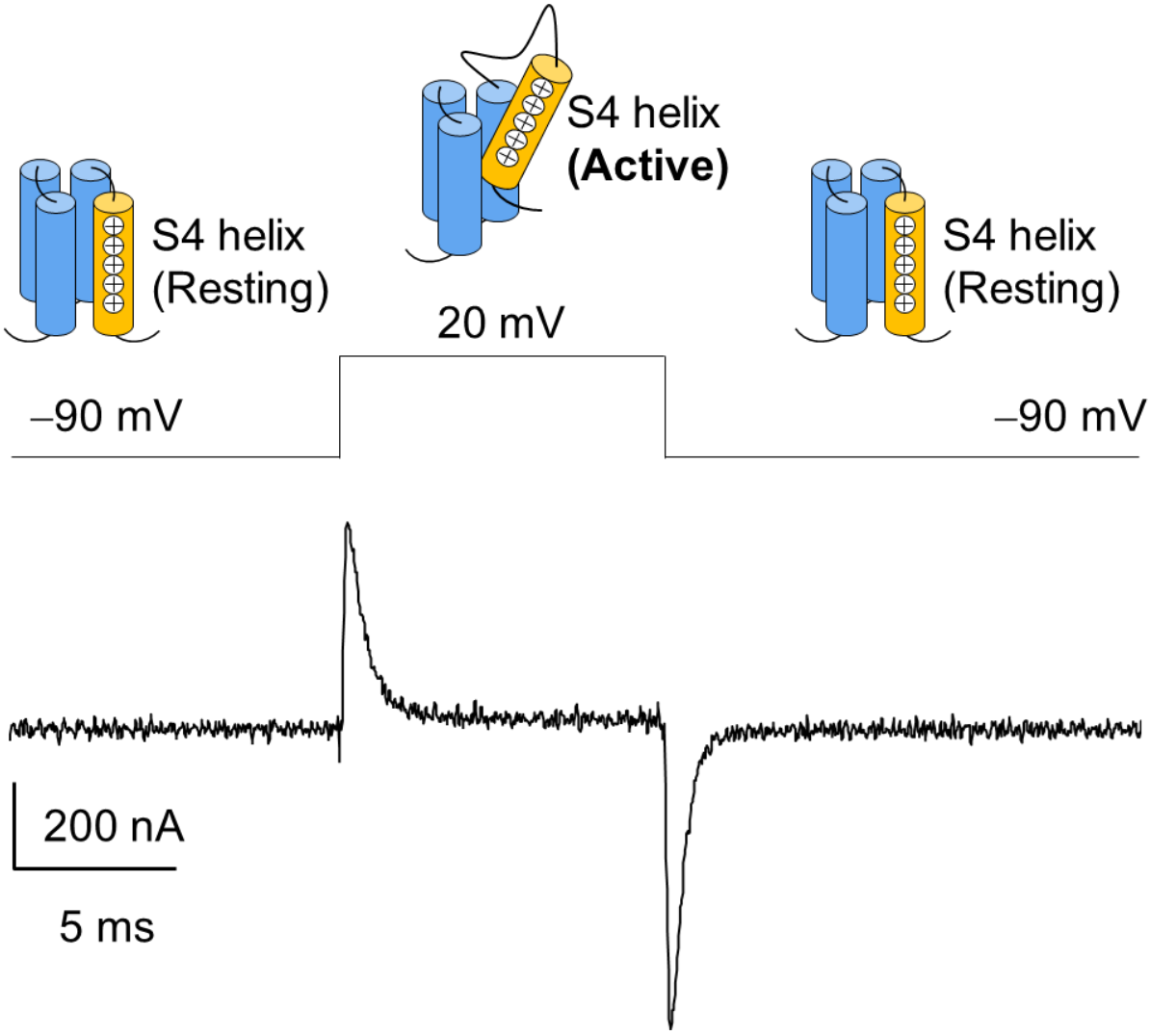

Figure 25 - Two-state model of the S4 segment. Top) Schematic representation of the S4 transition from a resting state, when membrane potential is at rest (-90 mV), to an active (outward) state during membrane depolarization (20 mV). **Bottom)** Representative trace of the transient gating current at 20 mV generated by the movement of the S4 segments in $Ca_V1.1$ channels (α_{1S}/β_{1a}) overexpressed in *Xenopus* oocytes. Gating current was isolated blocking the pore conductance with 0.1 mM $LaCl_3$ and 0.5 mM $CdCl_2$.

In voltage-gated Ca^{2+} channels, the gating current is generated by the conformational change (movement) of the four homologous but non-identical voltage sensing domain (VSDs), (Fig. 24), (Catterall, 2011). Given their structural heterogeneity, each VSD experiences a different electric path from its resting to its active state. This path determines the intrinsic properties of the VSDs, such as voltage dependence, voltage sensitivity and kinetics.

In cardiac $Ca_V1.2$, VSDs movement accounts only for pore opening, in skeletal $Ca_V1.1$, VSDs operation might mechanically influence the opening of the RyR1 (Ferreira Gregorio et al., 2017).

1.4 $Ca_V1.1$ and $Ca_V1.2$ modulation by auxiliary subunits

An intensive work over the past decades has established that L-type Ca^{2+} channels can gain different properties, and thus differently sense membrane depolarization, from the interaction with their auxiliary subunits (Catterall, 2011).
The skeletal α_{1S} subunit associates with multiple proteins, analogously to $Ca_V1.2$ channels (explained in detail in the introduction of Project 1). Specifically, α_{1S} forms macromolecular complexes with β_{1a}, $\alpha_2\delta$-1 and γ_1 subunits, as they are the only variants expressed in skeletal tissue (Bannister and Beam, 2013). At this picture, it must be added the non-canonical auxiliary subunit Stac3, recently discovered (Horstick et al., 2013; Nelson et al., 2013).

Among the four known **$\alpha_2\delta$ auxiliary subunits**, $\alpha_2\delta$-1 associates with both $Ca_V1.1$ and $Ca_V1.2$ channels. $\alpha_2\delta$-1 is an entirely extracellular protein anchored to the plasma membrane that influences channel trafficking and/or biophysical properties depending on Ca_V isoform and subunit composition (Dolphin, 2013). In $Ca_V1.2$ channels, the presence of $\alpha_2\delta$-1 remodels the voltage sensitivity of three VSDs out of four, increasing their coupling to pore opening and thus facilitating channel activation (Savalli et al., 2016). Moreover, $\alpha_2\delta$-1 accelerates ionic current activation kinetics (Bangalore et al., 1996; Tuluc et al., 2007; Savalli et al., 2016). On the other hand, in $Ca_V1.1$ channels, $\alpha_2\delta$-1 is determinant to confer the typical slow kinetics of the skeletal $I_{Ca,L}$ but irrelevant for both channel voltage dependent activation and EC coupling (Obermair et al., 2005). In addition, Gach and colleagues provide evidence that prolonged depolarization or repetitive stimulations, normally occurring *in vivo*, require the presence of $\alpha_2\delta$-1 to sustain an adequate Ca^{2+} release, suggesting that $\alpha_2\delta$-1 plays a role in physiological muscle contraction (Gach et al., 2008).

β subunits are intracellular proteins that generally function as chaperones favouring channel trafficking to the membrane and modulate the biophysical properties of Ca_V (Buraei and Yang, 2013). $Ca_V1.2$ channels interact with different β subunits (Hullin et al., 1992), while $Ca_V1.1$ isoform exclusively associates with β_{1a}. β_{1a} knockout mice die after birth from ataxia (Gregg et al., 1996). Muscle fibers isolated from these animals fail to elicit Ca^{2+} transient and display a reduced $I_{Ca,L}$ secondary to an impaired membrane expression of α_{1S}, suggesting that β_{1a} subunit is essential for

both EC coupling and channel trafficking (Gregg et al., 1996; Strube et al., 1996). As confirmed later, the latter is a function of β_{1a} contribution to tetrads formation (Schredelseker et al., 2005). Besides these chaperone-like roles, β_{1a} seems implicated also in $Ca_V1.1$ channel activation/inactivation (Varadi et al., 1991; Strube et al., 1996).

γ auxiliary subunits are transmembrane proteins. Eight genes encode for eight distinct γ isoforms. In the cardiac tissue, the RNA of γ4, γ6, γ7, γ8 subunits has been detected but their role remains uncertain (). In the skeletal muscle, only γ_1 is expressed and associates with $Ca_V1.1$ channels through their VSD IV (Wu et al., 2016). The main modulatory effect of this subunit is to hyperpolarize voltage-dependent inactivation (Freise, Held et al. 2000). It has been recently shown that γ_1 is also important for channel trafficking (Polster et al., 2016).

Stac3 adaptor protein. Stac3 belongs to a family of src homology 3 (SH3) and cysteine rich domain (Stac) proteins. Among the three family members, only Stac3 is expressed in the skeletal tissue and localize to T-tubules (Nelson et al., 2013), where it seems to interact with the α_{1S} subunit via the II-III linker between VSD II and VSD III (Wong King Yuen et al., 2017). Stac3 is a key element of EC coupling (Horstick et al., 2013; Nelson et al., 2013; Polster et al., 2016), favouring α_{1S} trafficking (Polster et al., 2015) and tetrads assembly (Linsley et al., 2017). Stac proteins, which are not essential for membrane trafficking of $Ca_V1.2$ channels, were shown to bind to the cardiac isoform slowing down the time-dependent properties of inactivation (Polster et al., 2015).

1.5 Investigating the molecular mechanism of $\alpha_2\delta$-1 subunit modulation on L-type $Ca_V1.1$ channels

L-type voltage-gated Ca^{2+} channels are expressed in striated muscles ($Ca_V1.1$ in skeletal muscle and $Ca_V1.2$ in cardiac muscle) and play a fundamental role in EC coupling. Both channels share ~70% sequence similarity (with the highest homology covering the transmembrane segments) and associate with β and $\alpha_2\delta$ auxiliary subunits.

Despite all these similarities, the modulation by the $\alpha_2\delta$-1 auxiliary subunit has striking opposing effects on the two channel isoforms: in $Ca_V1.2$ channels, $\alpha_2\delta$-1 accelerates activation and greatly facilitates channel opening (Platano et al., 2000; Savalli et al., 2016); in $Ca_V1.1$, $\alpha_2\delta$-1 slows down activation and has negligible effect on voltage dependence (Obermair et al., 2005). The question as how such similar channels are differently modulated by the same $\alpha_2\delta$-1 arises spontaneous.

While it is known that the $\alpha_2\delta$-1 subunit facilitates $Ca_V1.2$ voltage-dependent activation by remodelling voltage sensors activation (Savalli et al., 2016), the molecular mechanisms underlying $Ca_V1.1$ modulation by $\alpha_2\delta$-1 remain unknown.

In the following section, I address this question by studying the effect of $\alpha_2\delta$-1 on the voltage-dependent activation properties of the voltage sensing apparatus in the human $Ca_V1.1$.

2. MATERIALS AND METHODS

2.1 Molecular biology

The following clone were used for all the experiments: human α_{1S} (NCBI Reference Sequence: NP_000060.2), rabbit $\alpha_2\delta$-1 (UniProt accession no. P13806), rabbit β_{1a} and mouse Stac3 (kind donation from S. Cannon's Lab, University of California, Los Angeles, CA).

Mutagenesis: To introduce Cysteines in strategic position of α_{1S} protein, DNA single point mutations were generated with the QuikChange Site-Directed Mutagenesis Kit (Stratagene, CA), which allows site specific mutation in double-stranded plasmids. Reactions were performed using PfuUltra™ high-fidelity DNA polymerase and custom-made primers designed with Clone Manager software (© 2016 Scientific & Educational Software, CO). PCR products were controlled on a 1% agarose gel and then transformed into competent XL1-blue bacteria, using the appropriate selective antibiotic. To confirm predicted mutations and exclude extra modification, α_{1S} gene was fully sequenced.

Four Cysteine mutants of α_{1S} pore-forming subunit were generated, one for each VSDs (Fig. 26). Positions analogous to those previously published for $Ca_V1.2$ channels were chosen (Pantazis et al., 2014; Savalli et al., 2016). In VSD I, Cysteine substituted a Leucine in position 159 in the S3-S4 loop (L159C); for VSD II, Cysteine substituted a Methionine in position 519 in the S3-S4 loop (M519C); for VSD III, Cysteine substituted a Valine in position 893 in the S3-S4 loop (V893C); for VSD IV, Cysteine substituted a Serine in position 1231 in the S3-S4 loop (S1231C).

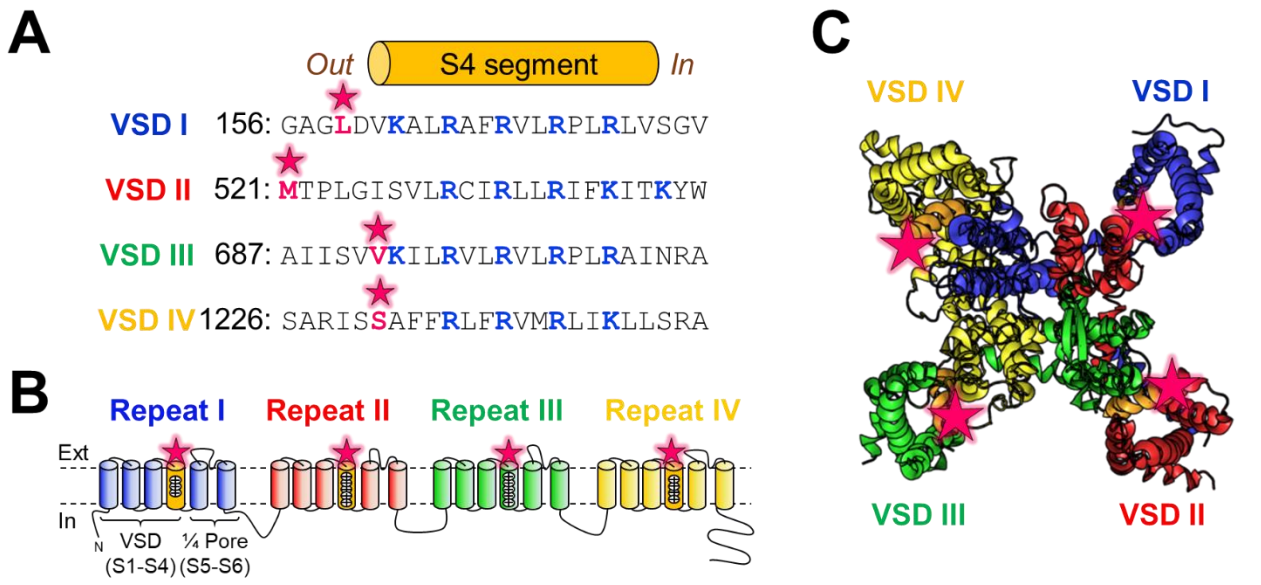

Figure 26 – Cysteine position strategy. A) Amino acid sequence alignment of the S4 segment of the four $Ca_V1.1$ VSD. In bold pink are indicated the amino acids that were substituted with the Cysteine. **B, C**) Topology and top view of the α_{1S} pore forming subunit showing the S4 segment of each repeat in orange and the approximative position of the Cysteine (star). PDB: 5gjv from Wu et al., 2016.

In vitro transcription: The plasmids carrying cDNAs of Stac3, β_{1a}, $\alpha_2\delta$-1 and α_{1s} pore-forming subunit (either wild type (WT) or cysteine-mutant channels) were linearized with a specific single-cutter restriction enzyme at 37°C overnight: Nhe I (New England Bioloab) for Stac3, β_{1a}, and α_{1s}, and Xho I (New England Biolab) for $\alpha_2\delta$-1. cDNA digestion was confirmed on 0.8% agarose gel. The linear cDNA was then used as the template for the in vitro transcription (1 µg per reaction) to produce capped RNA (cRNA) using KIT (AmpliCap-Max™ T7 High Yield Message Maker Kit, CELLSCRIPT). cRNA mimics most eukaryotic mRNAs found in vivo, because of a 7-methyl guanosine cap structure at the 5' end. The reaction of the in vitro transcription kit includes the cap analogue [m7G(5')ppp(5')G], which is incorporated as the first or 5' terminal G of the transcript. The reaction ran at 37°C for 3h. After $LiCl_2$ precipitation at -20°C, cRNA was resuspended in RNA storage solution (Invitrogen). RNA concentration was assessed measuring absorbance at 260 nm with a spectrophotometer prior to confirm RNA quality by 1% agarose gel. cRNA was stored at –80ºC in aliquots.

2.2 Oocyte preparation and injection

Xenopus laevis (NASCO, Modesto, CA) oocytes are an excellent system where to express ion channels for electrophysiological studies, as their large size (~1 mm diameter) allows the micro-injection of cloned RNA into their cytosol, which they readily translate into functional proteins.

As described in Chapter I, oocytes (stage V-VI) were mechanically and enzymatically defolliculated in a Ca^{2+}-free solution. The same day of preparation or the day after, oocytes were injected with 50 nl of total cRNA (0.01-0.1 µg/µl) encoding for the human pore-forming subunit α_{1s} and the accessory subunit β_{1a} and Stac3 with/without $\alpha_2\delta$-1 using a Drummond nano-injector. The auxiliary subunits were injected in excess molar ratio to completely saturate all α_{1s} proteins available. Injected oocytes were maintained at 18ºC in an amphibian saline solution containing 50% Leibovitz15 medium (Gibco) and 50% distilled water, supplemented with 1 % horse serum (Gibco), kanamycin, penicillin and streptomycin (Gibco). Four-five days after injection, oocytes were stained with membrane-impermeable, thiol-reactive fluorophores, as follows: 5 min on ice with 20 µM (2-((5(6)-Tetramethyl-rhodamine)carboxylamino)ethyl methanethiosulfonate, MTS-TAMRA - Santa Cruz Biotechnology), or 15 min on ice 10 µM II (tetramethylrhodamine-5'-maleimide, TMRM - Molecular Probes, Eugene, OR) in a depolarizing K^+ solution containing in mM: 120 KMES, 2 $Ba(MES)_2$, and 10 HEPES, pH=7. TMRM and MTS-TAMRA stocks (100 mM) were dissolved in DMSO and stored at -20°C. Prior to being mounted in the recording chamber, oocytes were thoroughly rinsed in SOS and injected with the Ca^{2+} chelator BAPTA (100nl at 80mM) to prevent activation of endogenous Ca^{2+}- and Ba^{2+}-dependent Cl− channels (Barish, 1983).

2.3 Voltage clamp fluorometry

Ba^{2+} current flowing through Cav1.1 complex and its conformational change during different voltage steps were recorded using the voltage clamp fluorometry (VCF).

VCF is a powerful technique to optically track protein conformational rearrangements that are elicited by changes in voltage together with the corresponding ionic current. In our specific case, VCF was used to track the “outward” and “inward” movement of the voltage sensing membrane segment S4 during channel activation and deactivation.

Protein movement can cause a change in the surrounding environment (solvent exposure, for example) that can be reported by fluorophores which are sensitive to their local environment (Lakowicz, 2006). It is possible to conjugate such fluorophores to a specific protein site and, if this area undergoes a motion that results in a change of the fluorophore environment, a deflection in the fluorescence emission will be observed. In our case, protein labelling was achieved using malemide-derived fluorophores that can specifically react with thiol groups present in cysteines, forming stable bonds.

Voltage clamp fluorometry was pioneered in Shaker K^+ channels expressed in oocytes clamped by two-electrode voltage clamp (Mannuzzu et al., 1996), and was shortly after implemented in the Cut-open Oocyte Vaseline Gap (COVG) voltage clamp technique(Cha and Bezanilla, 1997).

The COVG technique (Stefani and Bezanilla, 1998) is a large signal-to-noise, fast clamp technique that allows for resolving low magnitude gating currents, rapid ionic current activation, and deactivation while controlling the intracellular environment. As schematically shown, the oocyte is mounted in a chamber consisting of three compartments. The top and bottom blocks are drilled to allocate the oocyte. The hole diameter of the top chamber is ~ 600 µm and isolate ~1/5 of cell surface (Fig. 27). The voltage clamp circuit is then assembled around the mounted oocyte by the placement of six salt bridges and one intracellular electrode, imposing three simultaneous voltage clamps. The three chamber compartments are electrically-isolated by Vaseline gaps. The upper chamber isolates the oocyte upper domus and maintains it under clamp. Fluorescence and current are simultaneously recorded from the membrane area isolated by this chamber. The middle chamber provides a guard shield against leakage currents by clamping the middle part of the oocyte to the same potential as the upper chamber. The bottom chamber isolates the bottom domus of the oocyte which is open (cut open) by permeabilization. This allows to clamp the intracellular compartment to ground (Gandhi and Olcese, 2008). The optical setup consists of a Zeiss Axioscope FS microscope with filters appropriate for TMRM excitation/emission (Omega Optical, Brattleboro, VT). The light source is a 100 W microscope halogen lamp. A TTL-triggered Uniblitz VS 25 shutter (Vincent Associates, Rochester, NY) is mounted on the excitation light path. The Objective (Olympus LUMPlanFl, 40×, water immersion) has a numerical aperture of 0.8 and a working distance of 3.3 mm (Olympus Optical). The emission light is focused on a PIN-08-GL photodiode (UDT Technologies, Torrance,

CA). A Dagan Photomax 200 amplifier is used for the amplification of the photocurrent and background fluorescence subtraction.

The external solution contained (mM): 120 NaMES, 2 $Ba(MES)_2$, 10 HEPES, pH=7.0. The internal solution contained (mM): 120 K-Glutamate, 10 HEPES, pH=7.0. Pipette solution contained (mM): 2700 NaMES, 10 NaCl, 10 Na-HEPES, pH=7.0. Bottom dome of the oocyte was permeabilized with 0.1% saponin dissolved in the internal solution.

Ionic current was activated by a depolarizing step from -90 to 100 mV for 25 ms (holding potential at -90 mV). Depolarization was followed by a repolarizing step at -40 mV to elicit tail current. For fluorescence recordings, the molecular rearrangement of each VSD was recorded from -160mV to 120mV depolarizing steps.

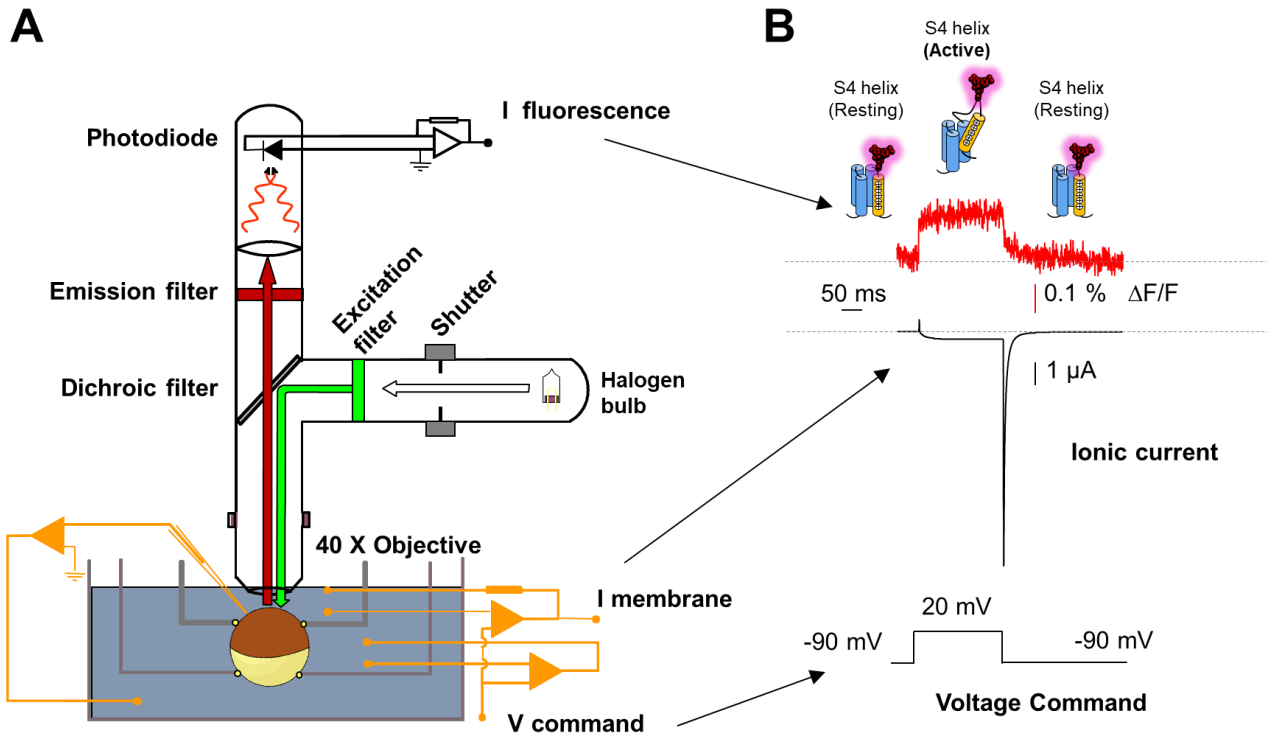

Figure 27 - The cut open voltage clamp fluorometry apparatus. A) Schematic representation of a cut-open oocyte set-up implemented for epifluorescence measurements. A labelled oocyte is mounted in the 3-level chamber. The light (green), produced by the LED lamp, passes through the excitation filter and is reflected by the dichroic, through the objective lens, onto the oocyte upper domus, at the right wavelength. Emitted light (brown) passes through the objective, the dichroic and the emission filter, to reach the photodiode detector. Structural rearrangements of S4 helix during channel gating are recorded in real time via differences in fluorescence emission caused by changes in the probe exposure to solvent (e.g., moving from aqueous to lipid phases) and/or to quenching groups. The fluorescence is monitored at a fixed wavelength with a photodiode while the gating state of the channel is controlled with a voltage-clamp. A change in protein structure near the probe is reported as a dimming or brightening of fluorescence (ΔFs). **B**) An example of a fluorescence trace (red) and the corresponding current (black): the molecular rearrangement of a VSD from its resting state to its active state is reported as an increase of fluorescence (unquenching direction). That the conformational change of the VSD has either modified the surrounding solvent or moved a quenching group. Modified from (Pantazis and Olcese, 2013).

Analysis: Experimental data were analysed with a custom-made program developed in in the Department of Anesthesiology at UCLA. Fit routines were run using Solver tool in Microsoft Excel. The G(V) curves were obtained from the peak tail current at −40 mV and plotted against the test potential. Data for the membrane conductance (G(V)) and the fluorescence (F(V)) curves were fitted to one (or the sum of two when indicated) Boltzmann distributions of the form:

$$G(V) = \frac{G_{\max}}{1 + e^{-\left[z(Vhalf - Vm)\left(\frac{F}{RT}\right)\right]}}$$

$$F(V) = \frac{F_{\max} - F_{\min}}{1 + e^{-\left[z(Vhalf - Vm)\left(\frac{F}{RT}\right)\right]}} - F_{\min}$$

where G_{max} and F_{max} are the maximal G and F; F_{min} is the minimal F; z is the effective valence of the distribution; V_{half} is the half-activating potential; V_m is the membrane potential; F, R and T are the usual thermodynamic values.

2.4 Statistical Analysis

Data are reported as mean ± SEM. Statistical significance was tested using unpaired Student's t test. For p value < 0.05, differences were considered statistically significative.

3. RESULTS

3.1 The co-expression of $\alpha_2\delta$-1 subunit decelerates activation kinetics of $Ca_V1.1$ channels and accelerates deactivation kinetics.

To gain insights on $\alpha_2\delta$-1 subunit modulation on $Ca_V1.1$ channels, we expressed, in *Xenopus* oocytes, $Ca_V1.1$ complexes containing the pore-forming α_{1S} subunit, and the skeletal accessory proteins β_{1a} and Stac3, in the presence or absence of $\alpha_2\delta$-1. Oocytes were voltage-clamped using the cut-open oocyte technique to record ionic current elicited by increasing depolarizations (Stefani and Bezanilla, 1998). Ba^{2+}, instead of Ca^{2+}, was used as the charge carrier to avoid the engagement of Ca^{2+}-dependent inactivation.

We first evaluated the effect of $\alpha_2\delta$-1 on the time-dependent properties (kinetics) of $Ca_V1.1$ channel activation. Channels were activated with a depolarizing step of 200 ms that is needed to reach the quasi-steady state where all channels are open. $\alpha_2\delta$-1 slowed down channel activation, as manifested by the slower activation kinetics than control (NO $\alpha_2\delta$-1), (Steccanella et al., 2019). This result suggests that the transition from the close to the open state requires more time in the presence of the accessory subunit (Fig. 28A-C).

The effect was quantified at ~20 mV when the inward current reaches its peak. A double-exponential function was used to fit the current traces as it better described the channel transition from close to open state. In the absence of $\alpha_2\delta$-1 (α_{1S}/β_{1a}/Stac3), the time constants τ_{slow} (78.5 ± 13.2 ms) and τ_{fast} (13.2 ± 1.2 ms) equally contributed to the current amplitude (A), accounting for 49 ± 1% and 51 ± 1% respectively (N=4). The presence of $\alpha_2\delta$-1 increased both time constants (τ_{slow} 84.9 ± 2.4; τ_{fast} 23.5 ± 2.2 ms; without vs with $\alpha_2\delta$-1 p_{slow}= 0.704, p_{fast}=0.023), and changed their relative contribution, favouring the slow component over the fast (A_{slow}, 77 ± 1%, A_{fast}, 23 ± 1%, N=3).

These findings are consistent with previous studies in mouse dysgenic myotubes and skeletal muscle BC3H1 cells, showing that the $\alpha_2\delta$-1 subunit mainly modulates activation kinetics properties of $Ca_V1.1$ channels (Obermair et al., 2005), but are opposite to those studies reporting that the same subunit accelerates activation kinetics of $Ca_V1.2$ channels (Tuluc et al., 2007).

A slow activation kinetics could indicate that $Ca_V1.1$ channels preferentially populate a closed state in the presence of the $\alpha_2\delta$-1 subunit. To investigate this possibility, we analysed the deactivation kinetics of the tail current. Tail currents are recorded at a fixed voltage at the cessation of the depolarizing step and provide information on the time course of the closing of the channels when the voltage is returned to rest. In our specific conditions, tail currents were produced by stepping to -40 mV as voltage command after the depolarizing pulse as shown in Fig. 28D. At this membrane potential most of the Ca_V channels are closed. The presence of $\alpha_2\delta$-1 subunit greatly accelerated deactivation kinetics. The deactivation time course of the tail currents was fitted with a double-exponential function to adequately describe the slow and fast components (Fig. 28D).

In the absence of the $\alpha_2\delta$-1 subunit, the following deactivation kinetics parameters were obtained: τ_{slow} = 15.8 ± 1.8 ms and τ_{fast} = 2.7 ± 0.7 ms, contributing 32 ± 1% and 68 ± 1% to current amplitude, respectively (N=3). In cells co-expressing $\alpha_2\delta$-1, both time constants became faster than control, and the contribution of the fast component to the current amplitude slightly prevailed (τ_{slow} 10.0 ± 0.8 ms, 22 ± 2% and τ_{fast} 1.7 ± 0.2 ms, 78 ± 2%, N=3; without vs with $\alpha_2\delta$-1 p_{slow}= 0.026, p_{fast}=0.245).

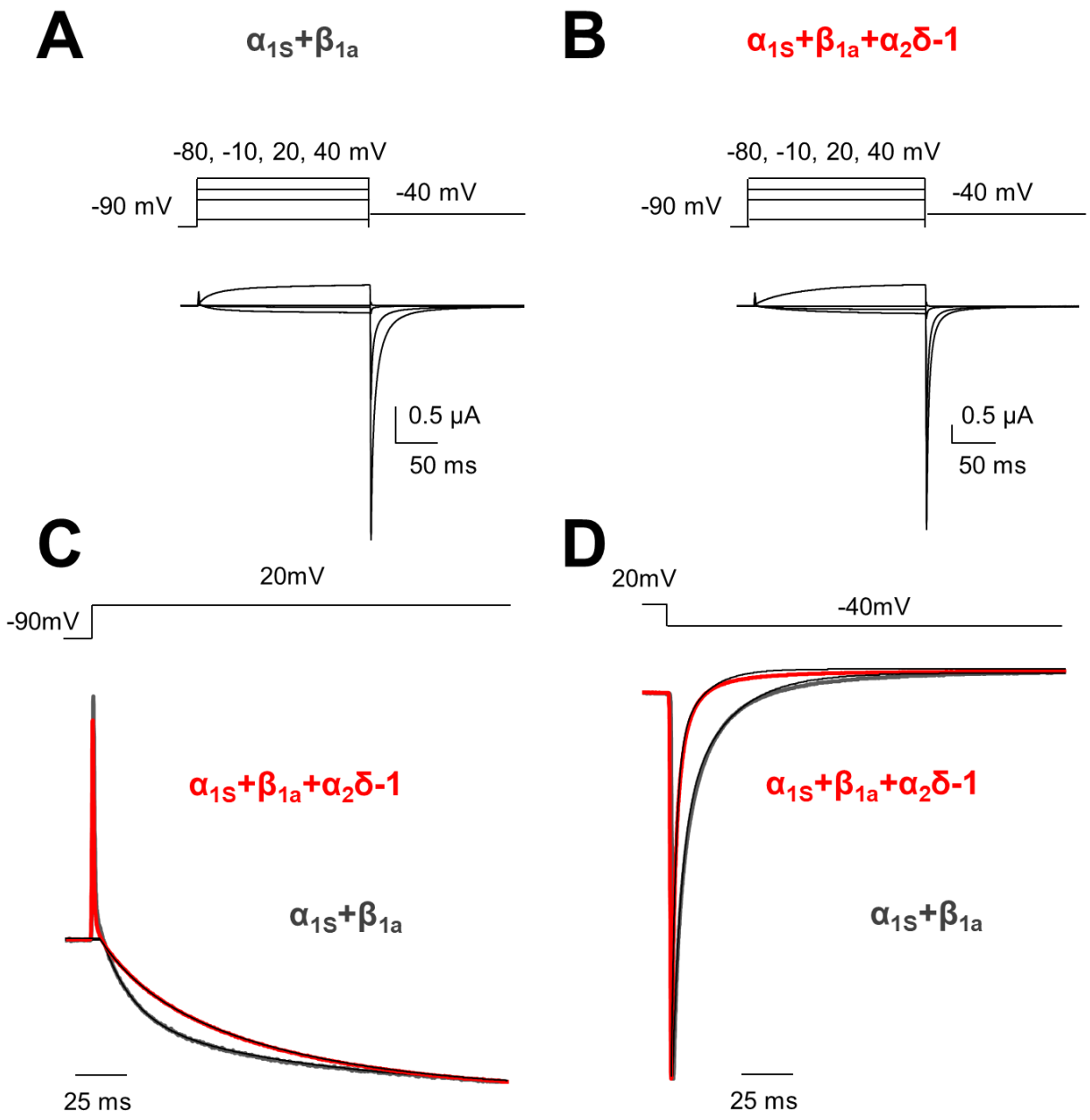

Figure 28 - The $\alpha_2\delta$-1 subunit modifies $Ca_V1.1$ ionic current kinetics. **A,B**) Representative current traces from *Xenopus* oocytes expressing human $Ca_V1.1$ channel complexes (α_{1S}+β_{1a}+Stac3) in the absence (**A**) or presence of $\alpha_2\delta$-1 auxiliary subunit (**B**). The voltage protocol used is reported above. **C**) Representative traces of channel activation from a 200ms-depolarizing step at 20 mV in the absence (grey) or presence of $\alpha_2\delta$-1 (red) are shown superimposed. **D**) Representative traces of channel deactivation kinetic from the same voltage-step as in C, repolarizing back to -40 mV. Traces in **A** and **B** are normalized to the peak inward current. Double exponential fits are shown superimposed as black lines. $\alpha_2\delta$-1 subunit decelerates $Ca_V1.1$ activation while speeds up channel closing.

Taken together, these experiments demonstrate for the first time, that the presence of $\alpha_2\delta$-1 not only slows down channel activation, but also favours channel deactivation. These two kinetics effects suggest that in $Ca_V1.1$ channels $\alpha_2\delta$-1 causes an overall reduction of Ca^{2+} influx, a result that is the opposite of what is observed in $Ca_V1.2$ channels modulation by the same subunit.

3.2 In contrast with $Ca_V1.2$, $\alpha_2\delta$-1 subunit has a relatively small effect on $Ca_V1.1$ channel voltage dependent activation.

As $\alpha_2\delta$-1 subunit affects how $Ca_V1.1$ channels transit from a closed conformation to an open state and vice versa (Fig. 28), it could regulate the voltage-dependent activation of the pore. To evaluate this hypothesis, the voltage dependence of ionic conductance G(V) of channels with or without $\alpha_2\delta$-1 subunit was extrapolated from the peak of the tail currents at -40 mV, that estimates the fraction of channels that were open for any given depolarization step. In the absence of $\alpha_2\delta$-1, the voltage dependence of channel activation was described by a single Boltzmann function with the following parameters for the half activation potential (V_{half}) and the valence (number of charges translocated per gating transition, z): V_{half} = 35.4±2.0 mV, z = 1.9±0.02 e^0 (Fig. 29; N=3). Co-expression of $\alpha_2\delta$-1 subunits facilitated $Ca_V1.1$ channel opening by shifting the V_{half} of the G(V) curve by ~10 mV toward more hyperpolarized potentials (Fig. 29, p=0.0121 at values corresponding to 50% open probability), a small shift that was not previously appreciated in data obtained from myotubes and skeletal muscle-derived BC3H1 cells (Obermair et al., 2005).

The effect of $\alpha_2\delta$-1 on $Ca_V1.1$ was much smaller than that reported for Cav1.2 in the same heterologous system (Platano et al., 2000; Savalli et al., 2016). However, also in Cav1.1 channels, the addition of $\alpha_2\delta$-1 to channel complex introduced a shallow component, such that G(V) curve was well described by the sum of two Boltzmann functions with distinct voltage-dependent properties: V_{half1} = 17.8 ± 1.0 mV, z_1 = 2.8 ± 0.07 e^0, G_1 = 62.4 ± 3.2%, V_{half2} = 48.9 ± 1.4 mV, z_2 = 1.5 ± 0.04 e^0, G_2 = 37.6 ± 3.2%; N = 4, where G is the conductance and represents the rate of ion travelling through the channel at a specific membrane potential (Fig. 29). The presence of a second component indicates that the voltage-dependent mechanism in the presence of $\alpha_2\delta$-1 could comprise more than one voltage-dependent opening transition.

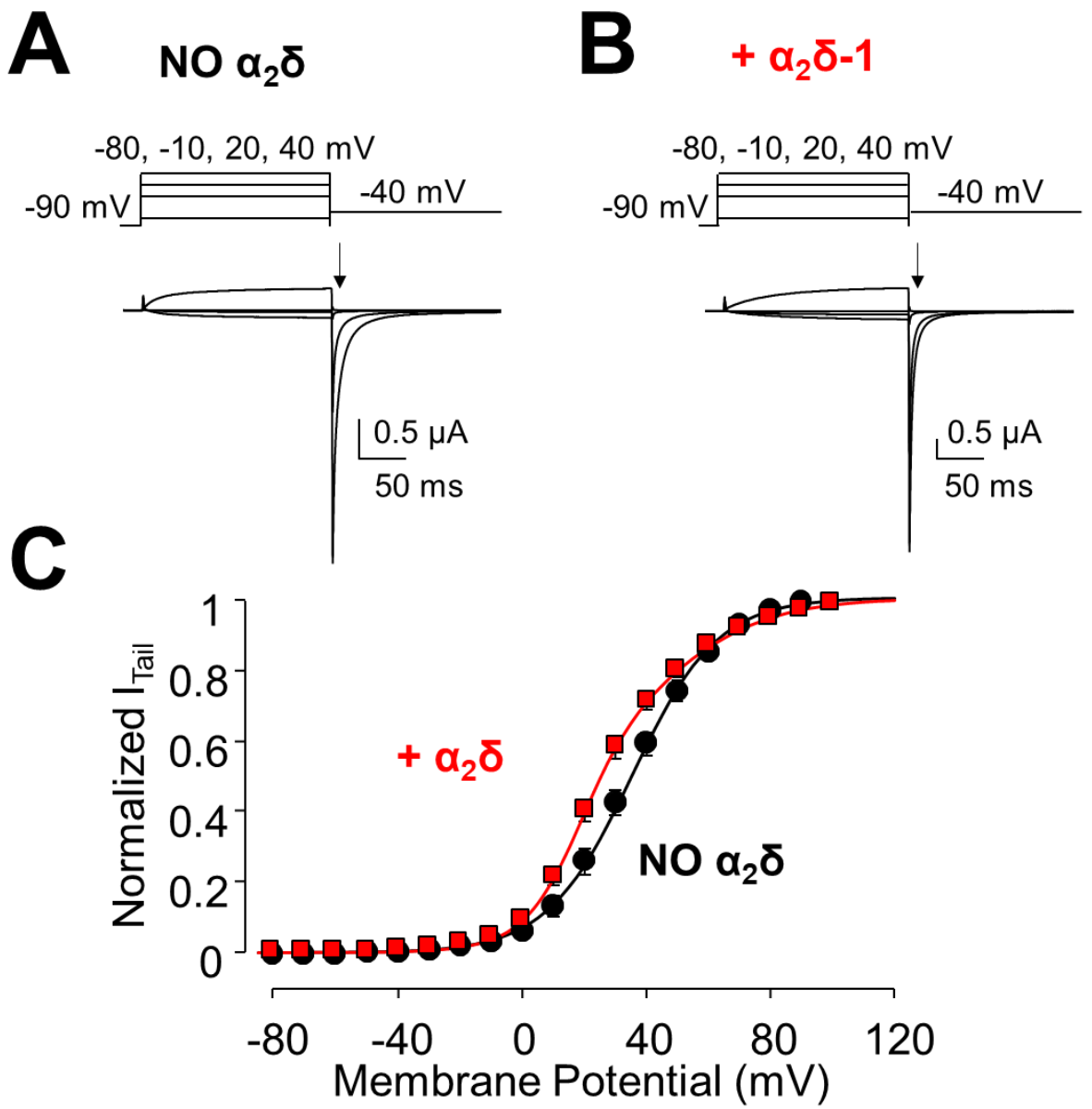

Figure 29 - The $\alpha_2\delta$-1 subunit facilitates activation of $Ca_V1.1$ channels. A, B) Representative current traces from Xenopus oocytes expressing human $Ca_V1.1$ channel complexes (α_{1S}+β_{1a}+Stac3) in the absence (**A**) or presence of $\alpha_2\delta$-1 auxiliary subunit (**B**). The voltage protocol used is reported above. The arrows indicate the approximative position where the G(V) was measured. **C**) G(V) curves constructed from tail currents reported in A and B. Data points were fitted to one (NO $\alpha_2\delta$-1, ●, N=3) or to the sum of two (with $\alpha_2\delta$-1, ■; N=4) Boltzmann distributions (smooth lines). Vertical bars ± SEM.

3.3 The $\alpha_2\delta$-1 subunit remodels VSD I, leaving the other VSDs largely unaffected

In voltage-gated channels, the pore opening is driven by the VSDs rearrangement while exploring different membrane potentials. In the cardiac $Ca_V1.2$ isoform, the contribution of each VSD to pore-opening is extremely different and affected by channel subunit composition (Pantazis et al., 2014; Savalli et al., 2016). Given the high sequence similarity between the two Ca_V channels, we expected a similar picture for the skeletal $Ca_V1.1$. In particular, we hypothesized that the small but significant

shift in voltage-dependent activation produced by the $\alpha_2\delta$-1 subunit should involve the modification of one or more VSDs.

To investigate the voltage-dependent activation of each VSD in the presence or absence of $\alpha_2\delta$-1 subunit, we individually tracked the movement of the four S4 segments at different membrane potentials, while recording simultaneously the ionic current, using the Voltage Clamp Fluorometry (VCF) technique (Gandhi and Olcese, 2008). The α_{1s} pore-forming subunit was engineered by substituting a Cysteine residue in strategic positions flanking the S4 segment of each VSD to achieve site-directed fluorescent labeling with membrane-impermeant, thiol-reactive fluorophores which are sensitive to environmental changes and able to report protein conformational changes (Lakowicz, 2006). Cysteine positions are indicated in Figure 26.

Since changes in DNA sequence may result in critical impairment of protein function, we first verified if mutant Cysteines compromised channel properties. We compared current kinetics and voltage-dependent activation G(V) of WT and "mutated" channels, expressing α_{1s}, β_{1a} and Stac3 subunits (Fig. 30). Current kinetics, as well as voltage dependent activation, of both Cysteine mutants and

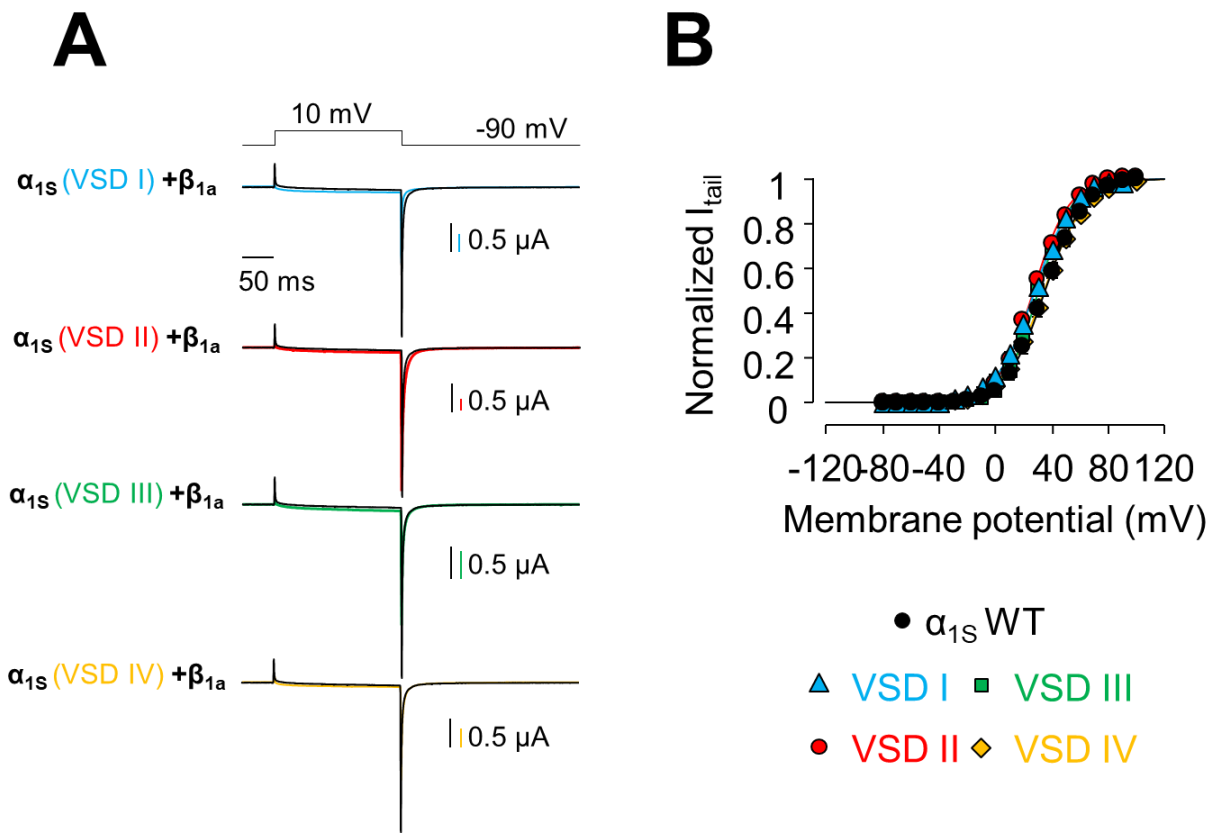

Figure 30 - Kinetics and voltage-dependent activation are not compromised in engineered Cysteine mutants. **A**) Superimposed ionic current traces recorded from *Xenopus* oocytes expressing WT channels (black) or Cysteine mutants for each voltage sensing domain (VSD, coloured traces) with the indicated subunit composition. The voltage command is reported above. **B**) G(V) curves of WT and Cysteine mutants and correspondent Boltzmann fits are reported with the same colour code in A.

WT channels were comparable (Fig. 30, Table 1), confirming that the engineered cysteines did not altered channel properties.

Table 1 - Boltzmann fitting parameters for the Half Activation Potential (V_{half}) and the effective valence (z) of WT channels and Cysteine mutants.

α_{1S}	V_{half} (mV)	z (e^0)	N
WT	35.4 ± 2.0	1.9 ± 0.02	3
VSD I (L159C)	28.5 ± 1.1	1.9 ± 0.02	6
VSD II (M519C)	28.5 ± 0.7	2.0 ± 0.6	5
VSD III (V893C)	31.3 ± 1.6	2.1 ± 0.7	5
VSD I (S1231C)	34.1 ± 1.8	1.7 ± 0.4	5

VCF was thus applied to the Cys mutants (labelled with MS-TAMRA or TMRM) to optically track the voltage-dependent movements of the individual $Ca_V1.1$ VSDs, from their resting state to their active state while exploring different membrane potentials. In all four Cys mutants, a change in fluorescent signal was detected as either a positive (unquenching) or negative (quenching) deflection (Fig. 31). As opposite, no voltage-dependent change in fluorescence was detected in oocytes expressing wild type (WT) $Ca_V1.1$ channels labelled with MS-TAMRA (Fig. 32), confirming that label conjugation of native Cys, if present, did not contaminate voltage-dependent evoked fluorescence in channels with introduced Cys.

Each of the four VSDs exhibited specific activation and deactivation kinetics properties. Specifically, VSD I and II displayed both a slow and a fast component (Fig. 31A-B, red and blue) while VSD III and IV activated and deactivated fast (Fig. 31A-B, green and yellow). Moreover, in the absence of $\alpha_2\delta$-1 subunit, fluorescence emitted from labelled VSDs I and III (Fig. 31A, blue and green) decreased upon membrane depolarization, suggesting that their S4 segments undergo a voltage-dependent conformational change that results in quenching of the attached fluorophore. Instead the emission of the fluorophore conjugated to VSD II and IV increased at more depolarized membrane potential (Fig. 31A, red and yellow), indicating that the fluorescence group is more efficiently quenched in the resting state of these domains than in the active state. In this heterogeneous scenario, the presence of $\alpha_2\delta$-1 subunit dramatically altered VSD I (Fig. 31A, B). Co-expression of $\alpha_2\delta$-1 reversed the fluorescence sign, suggesting that $\alpha_2\delta$-1 may produce a conformational change in VSD I that either modifies solvent exposure of the fluorophore or reports the effect of a different quenching group. Conversely, VSDs II, III and IV were practically unchanged (Fig. 31A, B).

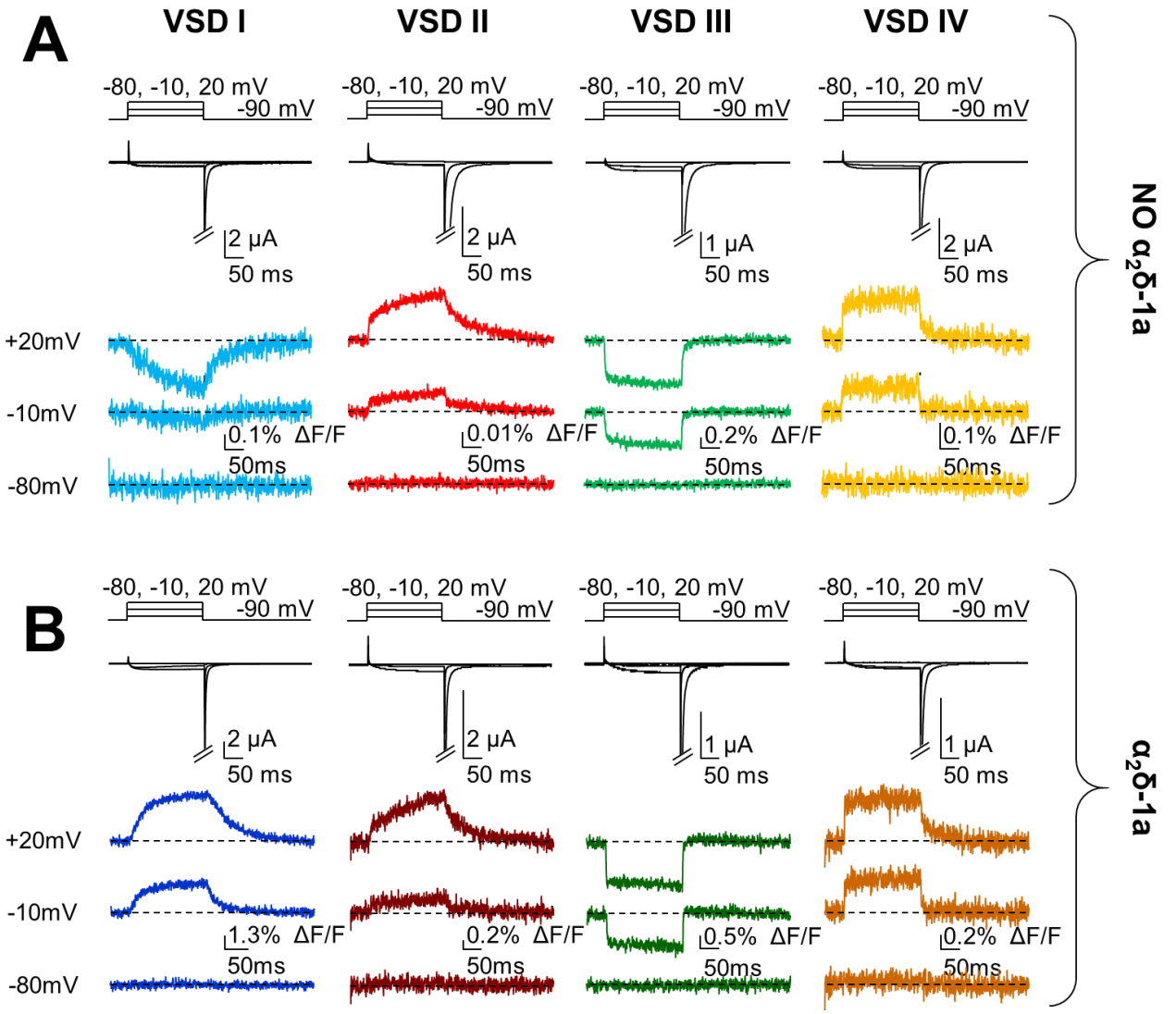

Figure 31 - Voltage-dependent rearrangements of the skeletal $Ca_V1.1$ VSDs in the presence and absence of the $\alpha_2\delta$-1 subunit. Representative current traces and the corresponding fluorescence recordings from *Xenopus* oocytes expressing VSD I, VSD II, VSD III or VSD IV (from left to right) cysteine mutant in the absence (**A**) or presence (**B**) of $\alpha_2\delta$-1 auxiliary subunit. Voltage command is reported above.

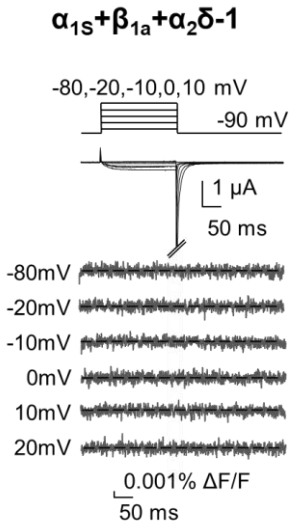

Figure 32 - Endogenous Cysteines in skeletal $Ca_V1.1$ channels do not interfere with thiol-maleimide reaction. Ionic current (top) and the corresponding fluorescence traces (bottom) recorded from maleimide-labelled Xenopus oocytes expressing WT α_{1S} and β_{1a}/Stac3/$\alpha_2\delta$-1 subunits. Despite the presence of many native thiol groups, wild type channels do not generate fluorescent signal once labelled with maleimide fluorophores.

As the fluorescence reports the transmembrane movement of the four charged VSDs from the resting to the active state, it can be used to derive the voltage-dependent activation curve (F(V)) of each VSD. Fluorescence intensity (ΔF) was measured at the end of the depolarizing pulse and plotted against the membrane potential (F(V) curve). Data were fitted to one Boltzmann distribution to extrapolate the membrane potentials at which the VSDs reached 50% probability of activation (V_{half}) and the sensitivity of each VSD to changes in the membrane potential (valence, z), (Fig. 33 and Table 2). Independently from the presence of $\alpha_2\delta$-1, all F(V) V_{half} ranged from near ~ – 40 mV (VSD IV) to ~ +5 mV (VSD II), while z varied between 0.7 e^0 (VSD IV) to 3 e^0 (VSD I).

Although the general picture was not dramatically perturbed by the $\alpha_2\delta$-1 subunit, its association with the channel greatly remodelled voltage dependent-activation of VSD I. As shown in Figure 33A and

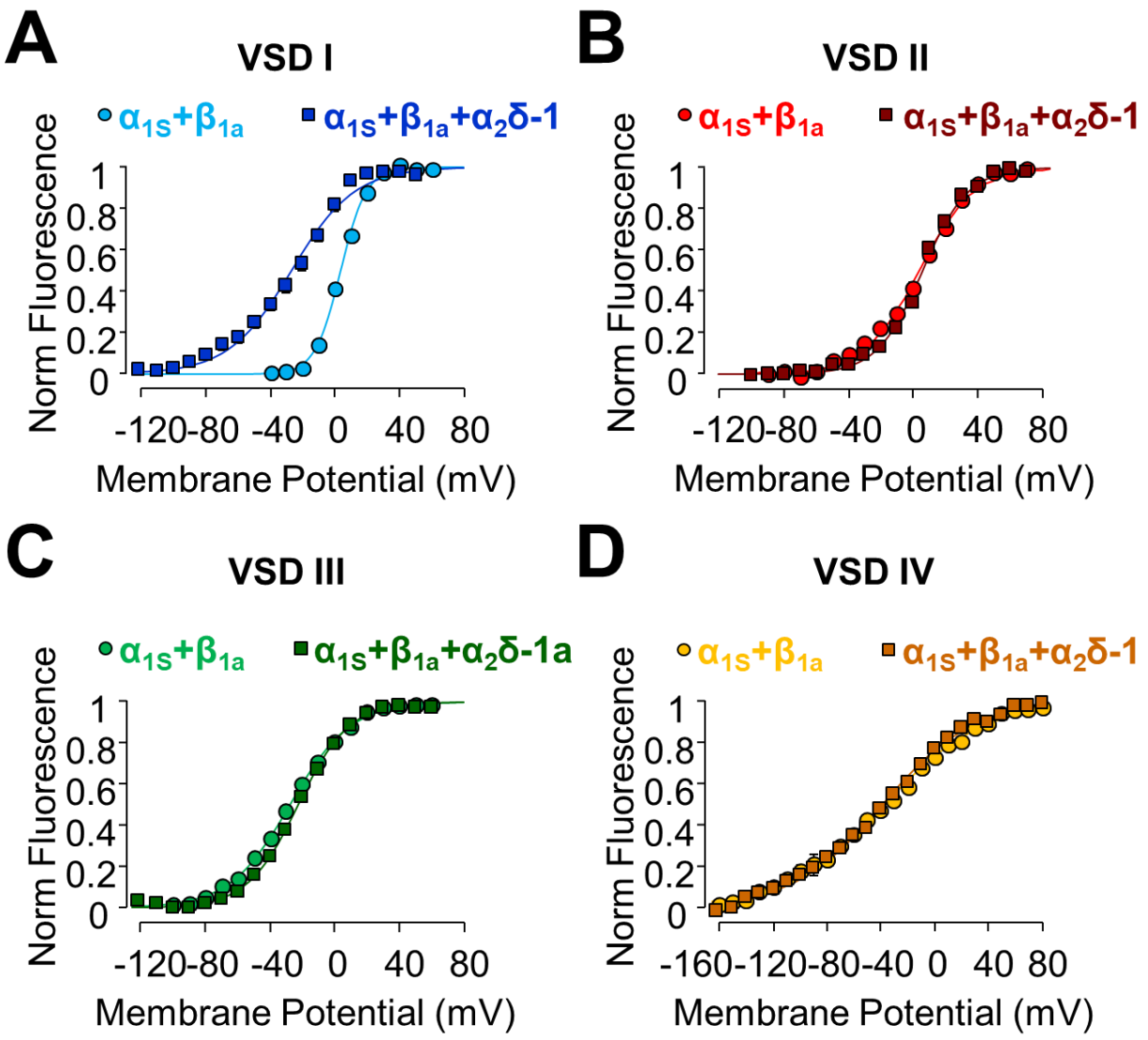

Figure 33 - The $\alpha_2\delta$-1 subunit facilitates activation of VSD I, leaving VSD II, III and IV unaffected. **A-D**) The voltage-dependent activation curves for each VSD in the absence (●) or presence (■) of $\alpha_2\delta$-1 were constructed from fluorescence traces reported in Fig.31, Data point were fitted to a single Boltzmann distribution (smooth line) and reported as mean ± SEM.

table I, the presence of $\alpha_2\delta$-1 produced ~20 mV shift of the F(V) curve toward more hyperpolarized potentials (NO $\alpha_2\delta$-1: V_{half} = 4.2 ± 0.8 mV, N=6 vs. WITH $\alpha_2\delta$-1: V_{half} = -23.2 ± 1.7 mV, N=5; without vs with $\alpha_2\delta$-1 p<0.001) and decreased VSD I voltage sensitivity from 3.0 ± 0.05 e^0 to 1.4 ± 0.05 e^0 (NO $\alpha_2\delta$-1 vs. WITH $\alpha_2\delta$-1,=5; without vs with $\alpha_2\delta$-1 p<0.001). As opposite, the remaining VSDs were marginally affected by the presence of $\alpha_2\delta$-1 (Fig. 33 and Table 2).

Table 2 - **Fitting parameters for the Boltzmann functions fitting the fluorescence data reported in Fig. 33.**

VSD	Parameter	NO α2-δ	α2-δ	P (Unpaired Student's t test)
I	V_{half} (mV) Z (e^0)	4.2 ± 0.8 (n=6) 3.0 ± 0.05	-23.2 ± 1.7 (n=5) 1.4 ± 0.05	P<0.001 P<0.001
II	V_{half} (mV) Z (e^0)	3.5 ± 0.9(n=5) 1.5 ± 0.04	5.7 ± 1.0 (n=4) 1.7 ± 0.04	P=0.141 P=0.006
II	V_{half} (mV) Z (e^0)	-26.9 ± 1.1 (n=5) 1.4 ± 0.01	22.4 ± 0.9 (n=8) 1.6 ± 0.03	P=0.073 P<0.001
IV	V_{half} (mV) Z (e^0)	-36.8 ± 1.5 (n=5) 0.7 ± 0.02	39.4 ± 2.1 (n=5) 0.8 ± 0.03	P=0.488 P=0.132

Given that VSD I activation shifts in the same direction of the G(V) in the presence of $\alpha_2\delta$-1, these data strongly suggest that the remodeling of VSD I is the underlining mechanism by which $\alpha_2\delta$-1 facilitates channel activation, and that VSD I may have a major role in pore opening (Fig. 34).

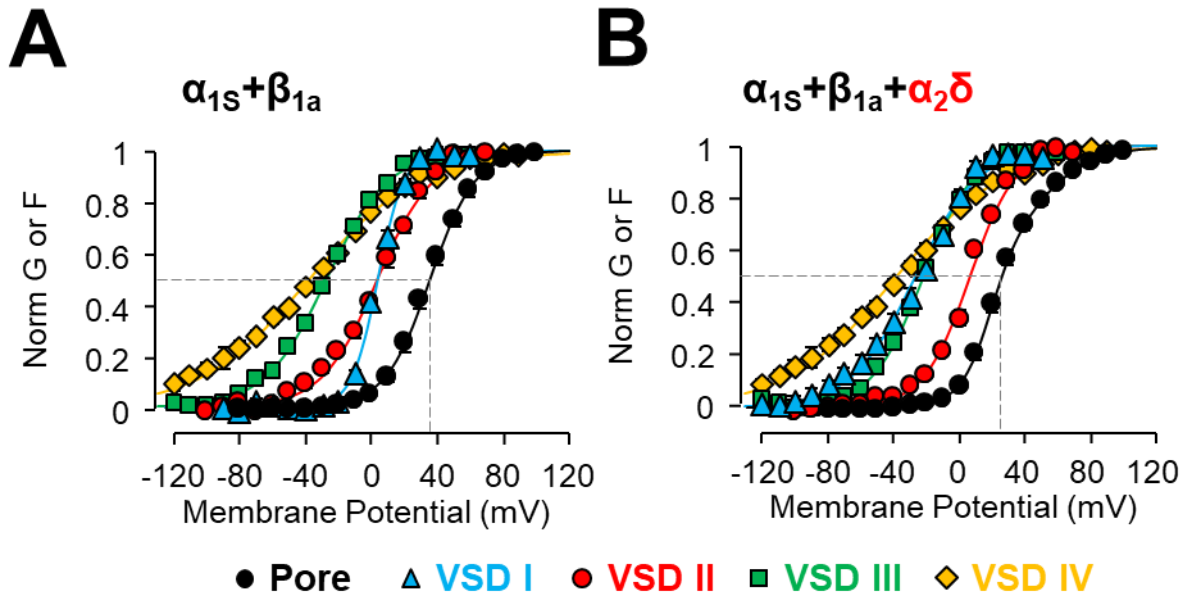

Figure 34 - Voltage-dependent activation of Cav1.1 VSDs in absence or presence of $\alpha_2\delta$-1 subunit. **A**) Mean normalized G(V) and F(V) data points from $\alpha_{1S}+\beta_{1a}$ (**A**) or $\alpha_{1S}+\beta_{1a}+\alpha_2\delta$-1 (**B**) channels and the corresponding Boltzmann fits are shown superimposed (mean ± SEM). These results suggest that the facilitation of voltage-dependent pore activation by $\alpha_2\delta$-1 subunits could be mediated by the remodelling of VSDs I.

4. DISCUSSION

Voltage-gated Ca^{2+} channels derive their biophysical properties from their four voltage sensing domains (VSDs) and from the association with multiple regulatory subunits (Dolphin, 2016). Interestingly, the cardiac $Ca_V1.2$ and skeletal $Ca_V1.1$ isoforms, despite their high sequence similarity, appear to be modulated by the $\alpha_2\delta$-1 auxiliary subunit in an opposite manner. Interaction of $\alpha_2\delta$-1 with the cardiac $Ca_V1.2$ isoform accelerates channel kinetics and promotes its activation by remodelling three out of four VDSs (Savalli et al., 2016). However, the molecular mechanisms underlying the $\alpha_2\delta$-1 modulation in $Ca_V1.1$ channels have not been investigated yet. To biophysically characterize the effect of this regulatory subunit on $Ca_V1.1$ we reconstituted $Ca_V1.1$ macromolecular complexes in *Xenopus* oocytes and applied for the first time the voltage clamp fluorometry technique to investigate the biophysical properties of each VSD and how they are affected by $\alpha_2\delta$-1 subunits. Using the voltage clamp fluorometry technique, we found that each skeletal VSD has unique biophysical properties in terms of voltage dependence and kinetics (Figs. 31, 33) and that the co-assembly with $\alpha_2\delta$-1 subunit remodels VSD I, facilitating its activation by ~20 mV shift in the hyperpolarizing direction (Figs. 31, 33) that likely explains 3) the small hyperpolarizing shift of the voltage-dependent activation of the channel pore (Fig. 29).

$\alpha_2\delta$-1 subunit modulates time-dependent properties of Cav1.2 and $Ca_V1.1$ channels in an opposite fashion

In agreement with previous reports in mouse myotubes and muscle cells (Obermair et al., 2005; Gach et al., 2008), we found that $\alpha_2\delta$-1 subunit is determinant to confer the typical slow activation kinetics of the skeletal $Ca_V1.1$ isoform, when overexpressed in *Xenopus* oocytes (Fig. 28A). We also observed a faster deactivation rate from the tail current of $\alpha_2\delta$-1-expressing channels (Fig. 28B) that was not previously described. By contrast, in the same expression system, the same auxiliary subunit accelerates cardiac current activation (Platano et al., 2000). Equivalent results can be observed in dysgenic myotubes expressing either α_{1S} or $\alpha_{1C,}$ (Kasielke et al., 2003; Tuluc et al., 2007). In skeletal myotubes, α_{1C} pore-forming subunit conserves its typical fast kinetics despite the presence of skeletal auxiliary subunits (β_{1a}, γ_1), (Kasielke et al., 2003), suggesting that the different kinetics modulation operated by $\alpha_2\delta$-1 on cardiac and skeletal Ca_Vs is not biased by the association with different β and/or γ isoforms. Thus, the specific fast and slow current kinetics of cardiac and skeletal L-type Ca^{2+} channels, respectively, relays on the intrinsic properties of the α_1 subunits rather than on $\alpha_2\delta$-1. However, it is the presence of the $\alpha_2\delta$-1 subunit to make the activation of skeletal current slow and the one of cardiac current fast.

In skeletal and cardiac channels, current kinetics is principally controlled by VSD I, particularly through its S3 segment and S3-S4 loop, as demonstrated by chimeras constructed with either $Ca_V1.1$/$Ca_V1.2$ channels (Nakai et al., 1994; Tuluc et al., 2016) or adult vs embryonal splice variants of the skeletal channel (Tuluc et al., 2016), where substitution of the IS3-S4 loop results in a faster

activation kinetics. These results suggest that in $Ca_V1.2$ channels, $\alpha_2\delta$-1 is essential to make $I_{Ca,L}$ fast enough to ensure an efficient opening of RyRs that are disperse in the dyads, whereas in $Ca_V1.1$ channels, $\alpha_2\delta$-1 reduces Ca^{2+}conduction reinforcing the idea that in mature skeletal muscle, $I_{Ca,L}$ has a nil physiological role for EC coupling (Flucher and Tuluc, 2017).

$\alpha_2\delta$-1 subunit facilitates $Ca_V1.2$ and $Ca_V1.1$ voltage-dependent activation to a different extent

We reported that $Ca_V1.1$ channels opening is facilitated by ~ 10 mV by $\alpha_2\delta$-1 subunit (Fig. 29). However, the hyperpolarizing shift is 5-fold larger for the cardiac isoform in similar experimental conditions (Savalli et al., 2016) and is physiologically relevant as it ensure $Ca_V1.2$ opening at membrane potential that are normally explored by myocytes during the AP. Instead, the physiological meaning of the small effect on the skeletal $I_{Ca,L}$ remains uncertain ad it seems irrelevant for the EC coupling. Moreover, previous works on $Ca_V1.1$ in dysgenic myotubes and skeletal muscle-derived BC3H1 cells, reported that the presence of $\alpha_2\delta$-1 seems ineffective at modulating pore activation (Obermair et al., 2005; Gach et al., 2008). In these muscle-derived systems, $\alpha_2\delta$-1 subunit modulation could be compensated by other elements of the EC-coupling apparatus that are not present in *Xenopus* oocytes. By contrast, amphibian cells possess endogenous $\beta_{3\text{-like}}$ subunits that have been reported to affect both protein expression and channel opening, as most of the β isoforms do (Tareilus et al., 1997). However, we feel confident to exclude these β proteins from interfering with $Ca_V1.1$ activation since these channels poorly express in absence of skeletal-specific β_{1a} subunits (data not show), suggesting a minimal interaction with the endogenous subunit.

$\alpha_2\delta$-1 subunit remodels the voltage-dependent activation of $Ca_V1.1$ VSD I, while in $Ca_V1.2$ channels three VSDs are affected

VSDs are important determinant of pore function, as they are responsible for sensing changes in membrane potential. Consequently, the facilitation in the channel opening observed in the presence of $\alpha_2\delta$-1 must be explained by a perturbation of one or more VSDs controlling voltage-dependent channel opening. Using VCF technique in $Ca_V1.1$ channel complexes with or without $\alpha_2\delta$-1, we found that this auxiliary subunit facilitates VSD I activation (Fig. 33A), explaining the hyperpolarizing shift of the G(V) relationship (Fig. 29). By contrast, VSD II, III and IV remain largely unaffected by the presence of $\alpha_2\delta$-1, suggesting that VSD I contributes to control pore opening in $Ca_V1.1$ channels (Fig. 32). Although a mathematical model can be used to corroborate this hypothesis, the high relevance of VSD I in channel opening is further experimentally supported by a natural-occurring mutation that, neutralizing the innermost arginine of VSD I with a tryptophan, impairs the sensor causing a depolarizing shift of both G(V) and F(V) curves of ~ 30 mV and reducing its voltage sensitivity (valence z) such that the channel is unable to open at physiological membrane potentials (Savalli et al., 2019). Recent studies also report the involvement of VSD IV in voltage-dependent activation of $Ca_V1.1$ channels, (Tuluc et al., 2016). The conclusion was made using the embryonic $Ca_V1.1e$ splice variant that lack of a small amino acid sequence in VSD IV, which is instead present

in the adult $Ca_V1.1$ channels and may contribute to reduce the relevance of this VSD to channel activation.

By contrast, analogous characterization of $Ca_V1.2$ channels in *Xenopus* oocytes by the Olcese laboratory, has demonstrated that the association of $\alpha_2\delta$-1 subunit promotes a drastic remodelling of the voltage-dependent activation of VSD I, II and III (Fig. 35A, top vs. bottom), (Savalli et al., 2016). Although the effect on skeletal channel activation resembles that on the cardiac isoform, it is more restrained and limited to VSD I (Fig. 33B, top vs. bottom). The different magnitude of the effect

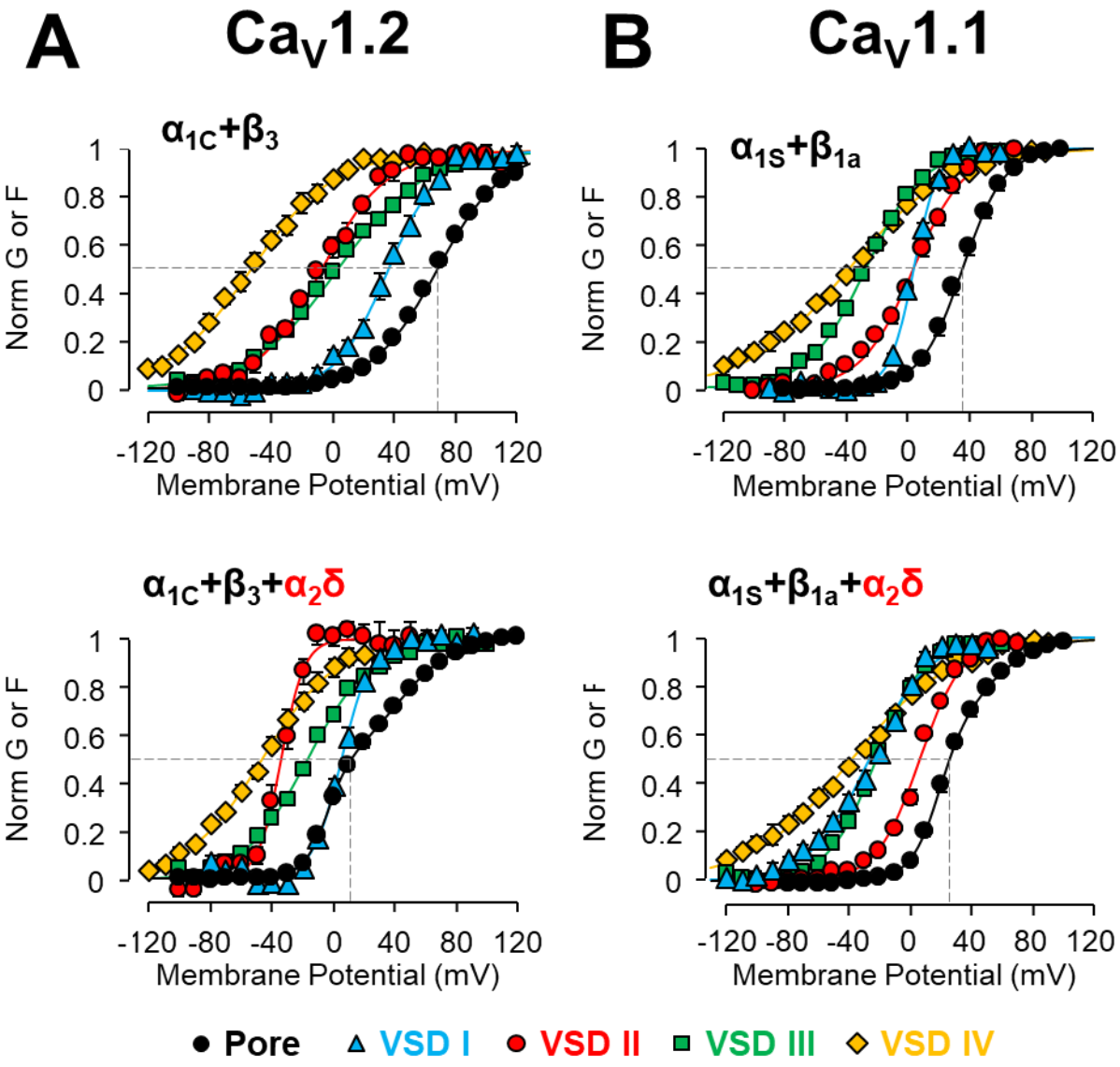

Figure 35 - The $\alpha_2\delta$-1 subunits differently modulates $Ca_V1.1$ and $Ca_V1.2$ channels. Comparison of voltage dependence of activation of cardiac (**A**) and skeletal (**B**) LTCC isoforms in absence (**top**) or presence (**bottom**) of $\alpha_2\delta$-1 subunit. Each chart shows the voltage-dependent activation of the pore (black) and the four VSDs (color code indicated in the legend at the bottom). **A**) In $Ca_V1.2$, voltage-dependent activation of VSD I (blue), II (red) and III (green) is dramatically changed by $\alpha_2\delta$-1 (top vs. bottom). This remodeling has a great effect on pore opening, shifting its voltage-dependent activation by ~50 mV to more hyperpolarized membrane potentials in the presence of $\alpha_2\delta$-1 (Savalli et al., 2016). **B**) In the skeletal $Ca_V1.1$, $\alpha_2\delta$-1 remodels only VSD I (blue, top vs. bottom), which accounts for a small hyperpolarizing shift of the voltage dependence of pore opening (black, top vs. bottom). For A, data from Savalli, Pantazis et al. 2016 with permission.

could be explained by a different interaction between the auxiliary subunit and the VSDs in the two channels. Specifically, the skeletal cryoEM structure shows that VSD I directly interacts with the MIDAS motif of $\alpha_2\delta$-1 to coordinate a cation, presumably a Ca^{2+} ion (Fig. 36A), (Wu et al., 2016). By contrast, in a low-resolution structure of Cav1.2, $\alpha_2\delta$-1 subunit is seen as a cap that covers ~3/4 of the extracellular surface of the α_{1C}, that could correspond to the position occupied by the three VSDs remodelled by $\alpha_2\delta$-1 (Fig. 36B).

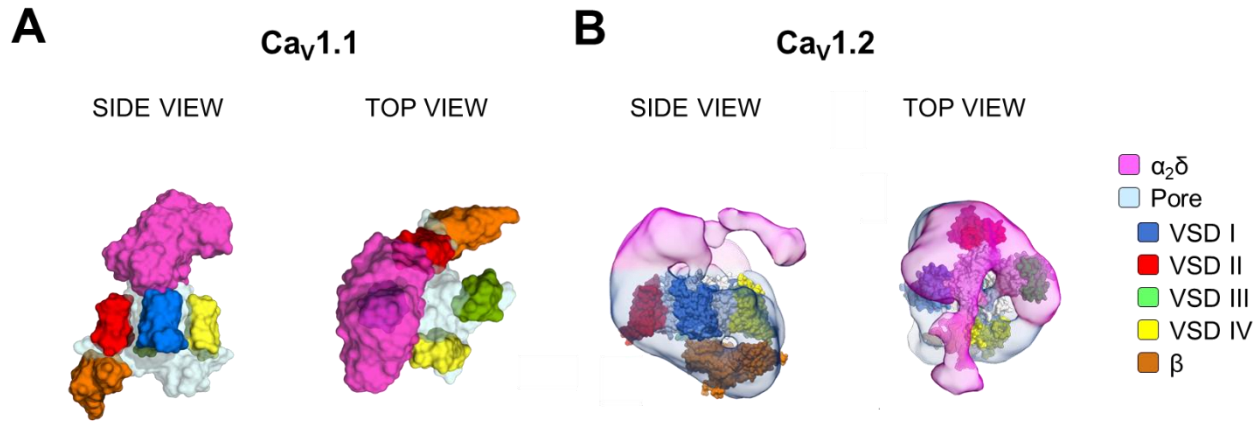

Figure 36 - $\alpha_2\delta$ interaction with $Ca_V1.1$ and $Ca_V1.2$ channels. Side and top view of CryoEM structures of $Ca_V1.1$ and $Ca_V1.2$ channels, respectively, illustrating the interaction between the pore forming subunit α_1 and the $\alpha_2\delta$-1 subunit in the two channel isoforms. CryoEM data from Wu et al. 2016 (A), and Walsh et al. 2009 (B). B adopted from Savalli et al. 2016.

The biophysical properties of $Ca_V1.1$ VSD III activation are compatible with voltage dependence and kinetics of skeletal Ca^{2+} release

Results from VCF recordings show that the four VSDs are heterogeneous for voltage dependence, voltage sensitivity and kinetics (Figs. 31, 33). These different biophysical properties suggest that VSDs might be enrolled in diverse channel functions, and thus they can be used to gain some mechanistic insight about $Ca_V1.1$ role in EC coupling. As recently reported for mammal skeletal muscle, the voltage dependence of Ca^{2+} release has a steep voltage-sensitivity and a mid-voltage activation (V_{half}) of ~ -30 mV (Ferreira Gregorio et al., 2017). These characteristics exclude the participation of VSD I and II to RyR gating, mainly for their slow activation kinetics incompatible with the fast time course of the release (Fig. 37, black line vs blu/red). In the case of VSD I, another exclusion criterium is provided by the existence of a charge-neutralizing mutation in VSD I, that preserve a normal EC coupling, when the mutant channel is expressed in dysgenic myotubes (Eltit et al., 2012).

On the contrary, VSD III and IV possess a fast kinetics and a half activation potential around ~ -30 mV (Figs. 31, 33, 37 and Table II). However, the voltage sensitivity of VSD IV is not compatible with the steepness reported for Ca^{2+} release, making VSD III the most qualified candidate as the sensing "particle" for skeletal EC coupling. This hypothesis may find support from previous works reporting

that the intracellular loop between VSD II and III is a key structural element for skeletal EC coupling (Nakai et al., 1998; Kugler et al., 2004; Takekura et al., 2004; Benedetti et al., 2015).

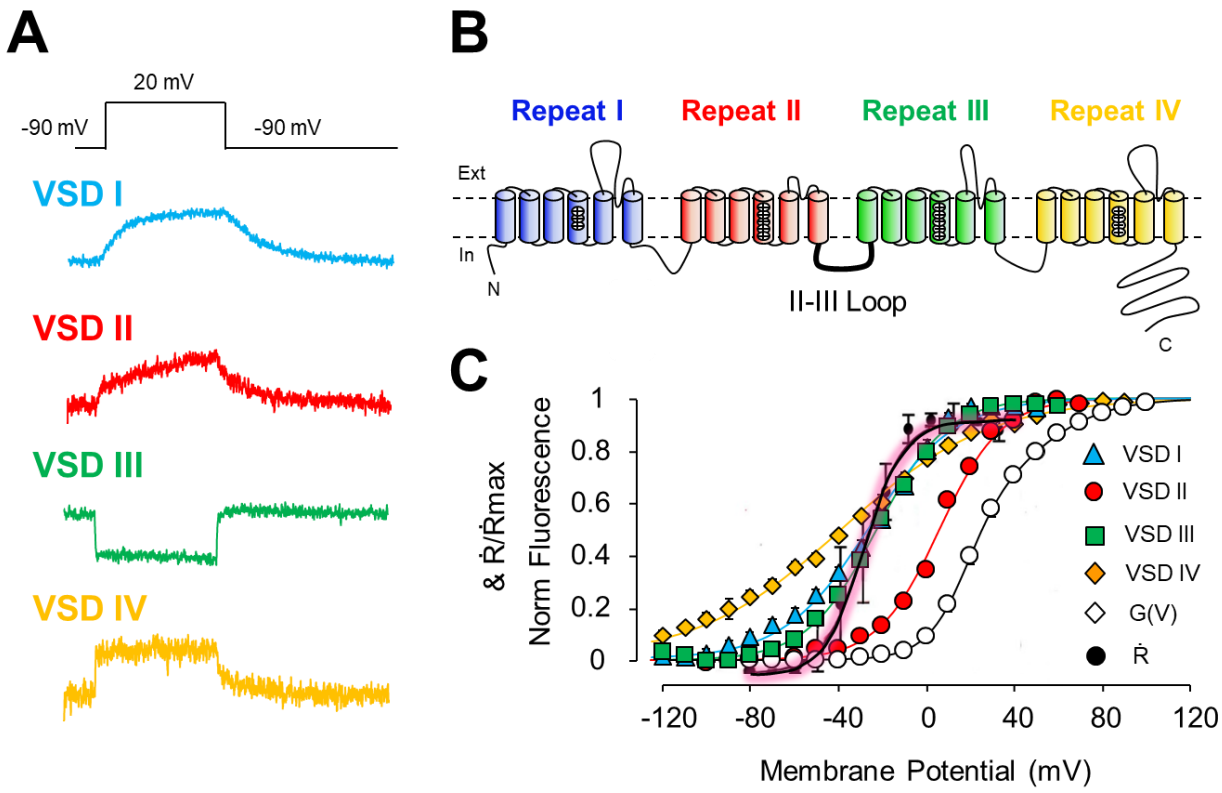

Figure 37 - VSD III of $Ca_V1.1$ channels has biophysical properties that are potentially compatible with those of skeletal Ca^{2+} release. A) Fluorescence traces recorded at 20 mV from each Cys mutant expressing α_{1S}, $\alpha_2\delta$-1, β_{1a} and Stac3 proteins. The four VSDs possess different kinetic features. **B**) $Ca_V1.1$ topology highlighting the intracellular II-III loop, generally recognized to be important for skeletal EC coupling. **C**) The voltage dependent activation curve of all VSDs from Fig. 31 are superimposed to the Ca^{2+} release voltage dependence (black line), calculated from BALB/c mouse myofiber (Ferreira Gregorio et al., 2017). Fast kinetic and voltage dependent activation of VSD III are compatible with the properties of Ca_{2+} release.

In summary, we used VCF to track the movement of the four voltage sensing domains (VSDs) in $Ca_V1.1$ channel and shed light on the mechanisms by which $\alpha_2\delta$ subunit modulates the properties of L type Ca_V1 channels. We found that the four VSDs display a staggering heterogeneity, each with specific kinetics and voltage dependence (Fig.30). The co-expression of the $\alpha_2\delta$ subunit causes a change only in VSD I, while the same subunit modifies VSD I, II and III in $Ca_V1.2$ channels.

A neutralization of R174 in $Ca_V1.1$ VSD I caused a depolarizing shift of ~ 30 mV in the voltage dependence of activation (G(V) curve), which also became shallower, suggesting that this residue contribute to $Ca_V1.1$. voltage sensing. This hypothesis was confirmed by direct measurement of the voltage-dependent activation of VSD I which was found deeply affected by this mutation: its effective charge was reduced, and the voltage dependence shifted to the left on the voltage axis. These data allow us to reinforce the view that VSD I drives the activation of the $Ca_V1.1$ pore.

However, because of its slow kinetics, VSD I is unlikely to have a significant role in the opening of RYR1, since the Ca^{2+} release is a very fast event that occurs within an action potential of ~ 5 ms. Our data suggest that VSD III possesses voltage-dependent and time-dependent properties compatible with the one of Ca^{2+} release and we propose that this VSD is the sensor that open RYR during the electrical depolarization of the muscle action potential.

These data are the first demonstration that the mechanism by which $\alpha_2\delta$ modulates L-type Ca_V1 channels is isoform specific and evolved to maximize Ca^{2+} influx in $Ca_V1.2$, and to minimize it via $Ca_V1.1$, likely because RyR1 activates without Ca^{2+} influx during skeletal muscle action potential.

REFERENCES

1989. Preliminary report: effect of encainide and flecainide on mortality in a randomized trial of arrhythmia suppression after myocardial infarction. *N Engl J Med*. 321:406-412.

Adams, B.A., T. Tanabe, A. Mikami, S. Numa, and K.G. Beam. 1990. Intramembrane charge movement restored in dysgenic skeletal muscle by injection of dihydropyridine receptor cDNAs. *Nature*. 346:569-572.

Al-Khatib, S.M., W.G. Stevenson, M.J. Ackerman, W.J. Bryant, D.J. Callans, A.B. Curtis, B.J. Deal, T. Dickfeld, M.E. Field, G.C. Fonarow, A.M. Gillis, C.B. Granger, S.C. Hammill, M.A. Hlatky, J.A. Joglar, G.N. Kay, D.D. Matlock, R.J. Myerburg, and R.L. Page. 2018. 2017 AHA/ACC/HRS guideline for management of patients with ventricular arrhythmias and the prevention of sudden cardiac death: Executive summary: A Report of the American College of Cardiology/American Heart Association Task Force on Clinical Practice Guidelines and the Heart Rhythm Society. *Heart Rhythm*. 15:e190-e252.

Antoons, G., A. Oros, V. Bito, K.R. Sipido, and M.A. Vos. 2007. Cellular basis for triggered ventricular arrhythmias that occur in the setting of compensated hypertrophy and heart failure: considerations for diagnosis and treatment. *J Electrocardiol*. 40:S8-14.

Antzelevitch, C., L. Belardinelli, A.C. Zygmunt, A. Burashnikov, J.M. Di Diego, J.M. Fish, J.M. Cordeiro, and G. Thomas. 2004. Electrophysiological effects of ranolazine, a novel antianginal agent with antiarrhythmic properties. *Circulation*. 110:904-910.

Antzelevitch, C., and A. Burashnikov. 2011. Overview of Basic Mechanisms of Cardiac Arrhythmia. *Card Electrophysiol Clin*. 3:23-45.

Antzelevitch, C., and S. Sicouri. 1994. Clinical relevance of cardiac arrhythmias generated by afterdepolarizations. Role of M cells in the generation of U waves, triggered activity and torsade de pointes. *J Am Coll Cardiol*. 23:259-277.

Armstrong, C.M., F.M. Bezanilla, and P. Horowicz. 1972. Twitches in the presence of ethylene glycol bis(-aminoethyl ether)-N,N'-tetracetic acid. *Biochim Biophys Acta*. 267:605-608.

Bangalore, R., G. Mehrke, K. Gingrich, F. Hofmann, and R.S. Kass. 1996. Influence of L-type Ca channel alpha 2/delta-subunit on ionic and gating current in transiently transfected HEK 293 cells. *Am J Physiol*. 270:H1521-1528.

Bannister, R.A. 2016. Bridging the myoplasmic gap II: more recent advances in skeletal muscle excitation-contraction coupling. *J Exp Biol*. 219:175-182.

Bannister, R.A., and K.G. Beam. 2013. Ca(V)1.1: The atypical prototypical voltage-gated Ca(2)(+) channel. *Biochim Biophys Acta*. 1828:1587-1597.

Barish, M.E. 1983. A transient calcium-dependent chloride current in the immature Xenopus oocyte. *J Physiol*. 342:309-325.

Belani, C. 2012. A Phase IIb Randomized Study of Oral Seliciclib in Patients With Previously Treated Non-Small Cell Lung Cancer

Efficacy Study of Oral Seliciclib to Treat Non-Small Cell Lung Cancer. *In*.

Belardinelli, L., G. Liu, C. Smith-Maxwell, W.Q. Wang, N. El-Bizri, R. Hirakawa, S. Karpinski, C.H. Li, L. Hu, X.J. Li, W. Crumb, L. Wu, D. Koltun, J. Zablocki, L. Yao, A.K. Dhalla, S. Rajamani, and J.C. Shryock. 2013. A novel, potent, and selective inhibitor of cardiac late sodium current suppresses experimental arrhythmias. *J Pharmacol Exp Ther*. 344:23-32.

Bell, R.M., M.M. Mocanu, and D.M. Yellon. 2011. Retrograde heart perfusion: the Langendorff technique of isolated heart perfusion. *J Mol Cell Cardiol*. 50:940-950.

Benedetti, B., P. Tuluc, V. Mastrolia, C. Dlaska, and B.E. Flucher. 2015. Physiological and pharmacological modulation of the embryonic skeletal muscle calcium channel splice variant CaV1.1e. *Biophys J*. 108:1072-1080.

Bengel, P., S. Ahmad, and S. Sossalla. 2017. Inhibition of Late Sodium Current as an Innovative Antiarrhythmic Strategy. *Curr Heart Fail Rep*. 14:179-186.

Benson, C., J. White, J. De Bono, A. O'Donnell, F. Raynaud, C. Cruickshank, H. McGrath, M. Walton, P. Workman, S. Kaye, J. Cassidy, A. Gianella-Borradori, I. Judson, and C. Twelves. 2007. A phase I trial of the selective oral cyclin-dependent kinase inhibitor seliciclib (CYC202; R-Roscovitine), administered twice daily for 7 days every 21 days. *Br J Cancer*. 96:29-37.

Bers, D.M. 2002. Cardiac excitation-contraction coupling. *Nature*. 415:198-205.
Bers, D.M., and V.M. Stiffel. 1993. Ratio of ryanodine to dihydropyridine receptors in cardiac and skeletal muscle and implications for E-C coupling. *Am J Physiol*. 264:C1587-1593.
Beuckelmann, D.J., and W.G. Wier. 1988. Mechanism of release of calcium from sarcoplasmic reticulum of guinea-pig cardiac cells. *J Physiol*. 405:233-255.
Bezanilla, F. 2008. How membrane proteins sense voltage. *Nat Rev Mol Cell Biol*. 9:323-332.
Bezanilla, F. 2018. Gating currents. *J Gen Physiol*. 150:911-932.
Block, B.A., T. Imagawa, K.P. Campbell, and C. Franzini-Armstrong. 1988. Structural evidence for direct interaction between the molecular components of the transverse tubule/sarcoplasmic reticulum junction in skeletal muscle. *J Cell Biol*. 107:2587-2600.
Bossu, A., M.J.C. Houtman, V.M.F. Meijborg, R. Varkevisser, H.D.M. Beekman, A. Dunnink, J.M.T. de Bakker, N. Mollova, S. Rajamani, L. Belardinelli, M.A.G. van der Heyden, and M.A. Vos. 2018. Selective late sodium current inhibitor GS-458967 suppresses Torsades de Pointes by mostly affecting perpetuation but not initiation of the arrhythmia. *Br J Pharmacol*.
Buraei, Z., G. Schofield, and K.S. Elmslie. 2007. Roscovitine differentially affects CaV2 and Kv channels by binding to the open state. *Neuropharmacology*. 52:883-894.
Buraei, Z., and J. Yang. 2010. The ss subunit of voltage-gated Ca2+ channels. *Physiol Rev*. 90:1461-1506.
Buraei, Z., and J. Yang. 2013. Structure and function of the beta subunit of voltage-gated Ca(2)(+) channels. *Biochim Biophys Acta*. 1828:1530-1540.
Burashnikov, E., R. Pfeiffer, H. Barajas-Martinez, E. Delpon, D. Hu, M. Desai, M. Borggrefe, M. Haissaguerre, R. Kanter, G.D. Pollevick, A. Guerchicoff, R. Laino, M. Marieb, K. Nademanee, G.B. Nam, R. Robles, R. Schimpf, D.D. Stapleton, S. Viskin, S. Winters, C. Wolpert, S. Zimmern, C. Veltmann, and C. Antzelevitch. 2010. Mutations in the cardiac L-type calcium channel associated with inherited J-wave syndromes and sudden cardiac death. *Heart Rhythm*. 7:1872-1882.
Calderon, J.C., P. Bolanos, and C. Caputo. 2014. The excitation-contraction coupling mechanism in skeletal muscle. *Biophys Rev*. 6:133-160.
Catterall, W.A. 2000. Structure and regulation of voltage-gated Ca2+ channels. *Annu Rev Cell Dev Biol*. 16:521-555.
Catterall, W.A. 2010. Ion channel voltage sensors: structure, function, and pathophysiology. *Neuron*. 67:915-928.
Catterall, W.A. 2011. Voltage-gated calcium channels. *Cold Spring Harb Perspect Biol*. 3:a003947.
Cha, A., and F. Bezanilla. 1997. Characterizing voltage-dependent conformational changes in the Shaker K+ channel with fluorescence. *Neuron*. 19:1127-1140.
Colecraft, H.M., B. Alseikhan, S.X. Takahashi, D. Chaudhuri, S. Mittman, V. Yegnasubramanian, R.S. Alvania, D.C. Johns, E. Marban, and D.T. Yue. 2002. Novel functional properties of Ca(2+) channel beta subunits revealed by their expression in adult rat heart cells. *J Physiol*. 541:435-452.
Cranefield, P.F. 1977. Action potentials, afterpotentials, and arrhythmias. *Circ Res*. 41:415-423.
Cranefield, P.F., and R.S. Aronson. 1974. Initiation of sustained rhythmic activity by single propagated action potentials in canine cardiac Purkinje fibers exposed to sodium-free solution or to ouabain. *Circ Res*. 34:477-481.
Cranefield, P.F., and R.S. Aronson. 1991. Torsades de pointes and early afterdepolarizations. *Cardiovasc Drugs Ther*. 5:531-537.
Curtis, B.M., and W.A. Catterall. 1984. Purification of the calcium antagonist receptor of the voltage-sensitive calcium channel from skeletal muscle transverse tubules. *Biochemistry*. 23:2113-2118.
Damiano, B.P., and M.R. Rosen. 1984. Effects of pacing on triggered activity induced by early afterdepolarizations. *Circulation*. 69:1013-1025.
Davies, A., I. Kadurin, A. Alvarez-Laviada, L. Douglas, M. Nieto-Rostro, C.S. Bauer, W.S. Pratt, and A.C. Dolphin. 2010. The alpha2delta subunits of voltage-gated calcium channels form GPI-anchored proteins, a posttranslational modification essential for function. *Proc Natl Acad Sci U S A*. 107:1654-1659.

Dayal, A., J. Schredelseker, C. Franzini-Armstrong, and M. Grabner. 2010. Skeletal muscle excitation-contraction coupling is independent of a conserved heptad repeat motif in the C-terminus of the DHPRbeta(1a) subunit. *Cell Calcium*. 47:500-506.

Dirksen, R.T., and K.G. Beam. 1999. Role of calcium permeation in dihydropyridine receptor function. Insights into channel gating and excitation-contraction coupling. *J Gen Physiol*. 114:393-403.

Dolphin, A.C. 2013. The alpha2delta subunits of voltage-gated calcium channels. *Biochim Biophys Acta*. 1828:1541-1549.

Dolphin, A.C. 2016. Voltage-gated calcium channels and their auxiliary subunits: physiology and pathophysiology and pharmacology. *J Physiol*. 594:5369-5390.

Dzhura, I., and A. Neely. 2003. Differential modulation of cardiac Ca2+ channel gating by beta-subunits. *Biophys J*. 85:274-289.

Eisner, D.A., J.L. Caldwell, K. Kistamas, and A.W. Trafford. 2017. Calcium and Excitation-Contraction Coupling in the Heart. *Circ Res*. 121:181-195.

El-Hayek, R., and N. Ikemoto. 1998. Identification of the minimum essential region in the II-III loop of the dihydropyridine receptor alpha 1 subunit required for activation of skeletal muscle-type excitation-contraction coupling. *Biochemistry*. 37:7015-7020.

Eltit, J.M., R.A. Bannister, O. Moua, F. Altamirano, P.M. Hopkins, I.N. Pessah, T.F. Molinski, J.R. Lopez, K.G. Beam, and P.D. Allen. 2012. Malignant hyperthermia susceptibility arising from altered resting coupling between the skeletal muscle L-type Ca2+ channel and the type 1 ryanodine receptor. *Proc Natl Acad Sci U S A*. 109:7923-7928.

Fabiato, A., and F. Fabiato. 1978. Calcium-induced release of calcium from the sarcoplasmic reticulum of skinned cells from adult human, dog, cat, rabbit, rat, and frog hearts and from fetal and new-born rat ventricles. *Ann N Y Acad Sci*. 307:491-522.

Fabiato, F., A. Fabiato, and E.H. Sonnenblick. 1972. [Regenerative calcium liberation by the sarcoplasmic reticulum on skeletal and cardiac muscle cells]. *J Physiol (Paris)*. 65:Suppl 1:118A.

Fawcett, D.W., and N.S. McNutt. 1969. The ultrastructure of the cat myocardium. I. Ventricular papillary muscle. *J Cell Biol*. 42:1-45.

Ferreira Gregorio, J., G. Pequera, C. Manno, E. Rios, and G. Brum. 2017. The voltage sensor of excitation-contraction coupling in mammals: Inactivation and interaction with Ca(2). *J Gen Physiol*. 149:1041-1058.

Fischer, P.M., and A. Gianella-Borradori. 2003. CDK inhibitors in clinical development for the treatment of cancer. *Expert Opin Investig Drugs*. 12:955-970.

Flucher, B.E., and P. Tuluc. 2017. How and why are calcium currents curtailed in the skeletal muscle voltage-gated calcium channels? *J Physiol*. 595:1451-1463.

Gach, M.P., G. Cherednichenko, C. Haarmann, J.R. Lopez, K.G. Beam, I.N. Pessah, C. Franzini-Armstrong, and P.D. Allen. 2008. Alpha2delta1 dihydropyridine receptor subunit is a critical element for excitation-coupled calcium entry but not for formation of tetrads in skeletal myotubes. *Biophys J*. 94:3023-3034.

Ganapathi, S.B., M. Kester, and K.S. Elmslie. 2009. State-dependent block of HERG potassium channels by R-roscovitine: implications for cancer therapy. *Am J Physiol Cell Physiol*. 296:C701-710.

Gandhi, C.S., and R. Olcese. 2008. The voltage-clamp fluorometry technique. *Methods Mol Biol*. 491:213-231.

Gao, T., A.J. Chien, and M.M. Hosey. 1999. Complexes of the alpha1C and beta subunits generate the necessary signal for membrane targeting of class C L-type calcium channels. *J Biol Chem*. 274:2137-2144.

Garcia, J., T. Tanabe, and K.G. Beam. 1994. Relationship of calcium transients to calcium currents and charge movements in myotubes expressing skeletal and cardiac dihydropyridine receptors. *J Gen Physiol*. 103:125-147.

George, A.L., Jr. 2013. Molecular and genetic basis of sudden cardiac death. *J Clin Invest*. 123:75-83.

Gong, H.C., J. Hang, W. Kohler, L. Li, and T.Z. Su. 2001. Tissue-specific expression and gabapentin-binding properties of calcium channel alpha2delta subunit subtypes. *J Membr Biol*. 184:35-43.

Grace, A.A., and A.J. Camm. 2000. Voltage-gated calcium-channels and antiarrhythmic drug action. *Cardiovasc Res*. 45:43-51.

Gregg, R.G., A. Messing, C. Strube, M. Beurg, R. Moss, M. Behan, M. Sukhareva, S. Haynes, J.A. Powell, R. Coronado, and P.A. Powers. 1996. Absence of the beta subunit (cchb1) of the skeletal muscle dihydropyridine receptor alters expression of the alpha 1 subunit and eliminates excitation-contraction coupling. *Proc Natl Acad Sci U S A*. 93:13961-13966.

Hensley, J., G.E. Billman, J.D. Johnson, C.M. Hohl, and R.A. Altschuld. 1997. Effects of calcium channel antagonists on Ca2+ transients in rat and canine cardiomyocytes. *J Mol Cell Cardiol*. 29:1037-1043.

Hirano, Y., A. Moscucci, and C.T. January. 1992. Direct measurement of L-type Ca2+ window current in heart cells. *Circ Res*. 70:445-455.

Hoppa, M.B., B. Lana, W. Margas, A.C. Dolphin, and T.A. Ryan. 2012. alpha2delta expression sets presynaptic calcium channel abundance and release probability. *Nature*. 486:122-125.

Horstick, E.J., J.W. Linsley, J.J. Dowling, M.A. Hauser, K.K. McDonald, A. Ashley-Koch, L. Saint-Amant, A. Satish, W.W. Cui, W. Zhou, S.M. Sprague, D.S. Stamm, C.M. Powell, M.C. Speer, C. Franzini-Armstrong, H. Hirata, and J.Y. Kuwada. 2013. Stac3 is a component of the excitation-contraction coupling machinery and mutated in Native American myopathy. *Nat Commun*. 4:1952.

Huelsing, D.J., K.W. Spitzer, and A.E. Pollard. 2000. Electrotonic suppression of early afterdepolarizations in isolated rabbit Purkinje myocytes. *Am J Physiol Heart Circ Physiol*. 279:H250-259.

Huffaker, R., S.T. Lamp, J.N. Weiss, and B. Kogan. 2004. Intracellular calcium cycling, early afterdepolarizations, and reentry in simulated long QT syndrome. *Heart Rhythm*. 1:441-448.

Hullin, R., I.F. Khan, S. Wirtz, P. Mohacsi, G. Varadi, A. Schwartz, and S. Herzig. 2003. Cardiac L-type calcium channel beta-subunits expressed in human heart have differential effects on single channel characteristics. *J Biol Chem*. 278:21623-21630.

Hullin, R., J. Matthes, S. von Vietinghoff, I. Bodi, M. Rubio, K. D'Souza, I. Friedrich Khan, D. Rottlander, U.C. Hoppe, P. Mohacsi, E. Schmitteckert, R. Gilsbach, M. Bunemann, L. Hein, A. Schwartz, and S. Herzig. 2007. Increased expression of the auxiliary beta(2)-subunit of ventricular L-type Ca(2)+ channels leads to single-channel activity characteristic of heart failure. *PLoS One*. 2:e292.

Hullin, R., D. Singer-Lahat, M. Freichel, M. Biel, N. Dascal, F. Hofmann, and V. Flockerzi. 1992. Calcium channel beta subunit heterogeneity: functional expression of cloned cDNA from heart, aorta and brain. *EMBO J*. 11:885-890.

Jalife, J. 2000. Ventricular fibrillation: mechanisms of initiation and maintenance. *Annu Rev Physiol*. 62:25-50.

January, C.T., and A. Moscucci. 1992. Cellular mechanisms of early afterdepolarizations. *Ann N Y Acad Sci*. 644:23-32.

January, C.T., and J.M. Riddle. 1989. Early afterdepolarizations: mechanism of induction and block. A role for L-type Ca2+ current. *Circ Res*. 64:977-990.

January, C.T., J.M. Riddle, and J.J. Salata. 1988. A model for early afterdepolarizations: induction with the Ca2+ channel agonist Bay K 8644. *Circ. Res*. 62:563-571.

Jay, S.D., A.H. Sharp, S.D. Kahl, T.S. Vedvick, M.M. Harpold, and K.P. Campbell. 1991. Structural characterization of the dihydropyridine-sensitive calcium channel alpha 2-subunit and the associated delta peptides. *J Biol Chem*. 266:3287-3293.

Karagueuzian, H.S., T.P. Nguyen, Z. Qu, and J.N. Weiss. 2013. Oxidative stress, fibrosis, and early afterdepolarization-mediated cardiac arrhythmias. *Front Physiol*. 4:19.

Karagueuzian, H.S., A. Pezhouman, M. Angelini, and R. Olcese. 2017. Enhanced Late Na and Ca Currents as Effective Antiarrhythmic Drug Targets. *Front Pharmacol*. 8:36.

Kasielke, N., G.J. Obermair, G. Kugler, M. Grabner, and B.E. Flucher. 2003. Cardiac-type EC-coupling in dysgenic myotubes restored with Ca2+ channel subunit isoforms alpha1C and alpha1D does not correlate with current density. *Biophys J*. 84:3816-3828.

Kugler, G., R.G. Weiss, B.E. Flucher, and M. Grabner. 2004. Structural requirements of the dihydropyridine receptor alpha1S II-III loop for skeletal-type excitation-contraction coupling. *J Biol Chem*. 279:4721-4728.

Lakowicz, J.R. 2006. Principles of Fluorescence Spectroscopy 3rd.ed. Springer, Boston, MA.

Lamb, G.D., R. El-Hayek, N. Ikemoto, and D.G. Stephenson. 2000. Effects of dihydropyridine receptor II-III loop peptides on Ca(2+) release in skinned skeletal muscle fibers. *Am J Physiol Cell Physiol*. 279:C891-905.

Lamb, G.D., and T. Walsh. 1987. Calcium currents, charge movement and dihydropyridine binding in fast- and slow-twitch muscles of rat and rabbit. *J Physiol*. 393:595-617.

Li, Y., and D.M. Bers. 2001. A cardiac dihydropyridine receptor II-III loop peptide inhibits resting Ca(2+) sparks in ferret ventricular myocytes. *The Journal of physiology*. 537:17-26.

Liang, M., T.B. Tarr, K. Bravo-Altamirano, G. Valdomir, G. Rensch, L. Swanson, N.R. DeStefino, C.M. Mazzarisi, R.A. Olszewski, G.M. Wilson, S.D. Meriney, and P. Wipf. 2012. Synthesis and biological evaluation of a selective N- and p/q-type calcium channel agonist. *ACS Med Chem Lett*. 3:985-990.

Linsley, J.W., I.U. Hsu, L. Groom, V. Yarotskyy, M. Lavorato, E.J. Horstick, D. Linsley, W. Wang, C. Franzini-Armstrong, R.T. Dirksen, and J.Y. Kuwada. 2017. Congenital myopathy results from misregulation of a muscle Ca2+ channel by mutant Stac3. *Proc Natl Acad Sci U S A*. 114:E228-E236.

London, B., and J.W. Krueger. 1986. Contraction in voltage-clamped, internally perfused single heart cells. *J Gen Physiol*. 88:475-505.

Madhvani, R.V., M. Angelini, Y. Xie, A. Pantazis, S. Suriany, N.P. Borgstrom, A. Garfinkel, Z. Qu, J.N. Weiss, and R. Olcese. 2015. Targeting the late component of the cardiac L-type Ca2+ current to suppress early afterdepolarizations. *J Gen Physiol*. 145:395-404.

Madhvani, R.V., Y. Xie, A. Pantazis, A. Garfinkel, Z. Qu, J.N. Weiss, and R. Olcese. 2011. Shaping a new Ca(2)(+) conductance to suppress early afterdepolarizations in cardiac myocytes. *J Physiol*. 589:6081-6092.

Maltsev, V.A., H.N. Sabbah, R.S. Higgins, N. Silverman, M. Lesch, and A.I. Undrovinas. 1998. Novel, ultraslow inactivating sodium current in human ventricular cardiomyocytes. *Circulation*. 98:2545-2552.

Mannuzzu, L.M., M.M. Moronne, and E.Y. Isacoff. 1996. Direct physical measure of conformational rearrangement underlying potassium channel gating. *Science*. 271:213-216.

Marban, E., S.W. Robinson, and W.G. Wier. 1986. Mechanisms of arrhythmogenic delayed and early afterdepolarizations in ferret ventricular muscle. *J Clin Invest*. 78:1185-1192.

Meijer, L., and E. Raymond. 2003. Roscovitine and other purines as kinase inhibitors. From starfish oocytes to clinical trials. *Acc Chem Res*. 36:417-425.

Meissner, G. 2017. The structural basis of ryanodine receptor ion channel function. *J Gen Physiol*. 149:1065-1089.

Meissner, M., P. Weissgerber, J.E. Londono, J. Prenen, S. Link, S. Ruppenthal, J.D. Molkentin, P. Lipp, B. Nilius, M. Freichel, and V. Flockerzi. 2011. Moderate calcium channel dysfunction in adult mice with inducible cardiomyocyte-specific excision of the cacnb2 gene. *J Biol Chem*. 286:15875-15882.

Mikami, A., K. Imoto, T. Tanabe, T. Niidome, Y. Mori, H. Takeshima, S. Narumiya, and S. Numa. 1989. Primary structure and functional expression of the cardiac dihydropyridine-sensitive calcium channel. *Nature*. 340:230-233.

Morita, N., A.A. Sovari, Y. Xie, M.C. Fishbein, W.J. Mandel, A. Garfinkel, S.F. Lin, P.S. Chen, L.H. Xie, F. Chen, Z. Qu, J.N. Weiss, and H.S. Karagueuzian. 2009. Increased susceptibility of aged hearts to ventricular fibrillation during oxidative stress. *Am J Physiol Heart Circ Physiol*. 297:H1594-1605.

Nakai, J., B.A. Adams, K. Imoto, and K.G. Beam. 1994. Critical roles of the S3 segment and S3-S4 linker of repeat I in activation of L-type calcium channels. *Proc Natl Acad Sci U S A*. 91:1014-1018.

Nakai, J., T. Tanabe, T. Konno, B. Adams, and K.G. Beam. 1998. Localization in the II-III loop of the dihydropyridine receptor of a sequence critical for excitation-contraction coupling. *J Biol Chem*. 273:24983-24986.

Neely, A., X. Wei, R. Olcese, L. Birnbaumer, and E. Stefani. 1993. Potentiation by the beta subunit of the ratio of the ionic current to the charge movement in the cardiac calcium channel. *Science*. 262:575-578.

Nelson, B.R., F. Wu, Y. Liu, D.M. Anderson, J. McAnally, W. Lin, S.C. Cannon, R. Bassel-Duby, and E.N. Olson. 2013. Skeletal muscle-specific T-tubule protein STAC3 mediates voltage-induced Ca2+ release and contractility. *Proc Natl Acad Sci U S A*. 110:11881-11886.

Obermair, G.J., G. Kugler, S. Baumgartner, P. Tuluc, M. Grabner, and B.E. Flucher. 2005. The Ca2+ channel alpha2delta-1 subunit determines Ca2+ current kinetics in skeletal muscle but not targeting of alpha1S or excitation-contraction coupling. *J Biol Chem*. 280:2229-2237.

Olcese, R., N. Qin, T. Schneider, A. Neely, X. Wei, E. Stefani, and L. Birnbaumer. 1994. The amino terminus of a calcium channel beta subunit sets rates of channel inactivation independently of the subunit's effect on activation. *Neuron*. 13:1433-1438.

Pantazis, A., and R. Olcese. 2013. Cut-Open Oocyte Voltage-Clamp Technique. *In* Encyclopedia of Biophysics. G.C.K. Roberts, editor. Springer Berlin Heidelberg, Berlin, Heidelberg. 406-413.

Pantazis, A., N. Savalli, D. Sigg, A. Neely, and R. Olcese. 2014. Functional heterogeneity of the four voltage sensors of a human L-type calcium channel. *Proc Natl Acad Sci U S A*. 111:18381-18386.

Patel, R., and A.H. Dickenson. 2016. Mechanisms of the gabapentinoids and alpha 2 delta-1 calcium channel subunit in neuropathic pain. *Pharmacol Res Perspect*. 4:e00205.

Peterson, B.Z., C.D. DeMaria, J.P. Adelman, and D.T. Yue. 1999. Calmodulin is the Ca2+ sensor for Ca2+ -dependent inactivation of L-type calcium channels. *Neuron*. 22:549-558.

Pezhouman, A., H. Cao, M.C. Fishbein, L. Belardinelli, J.N. Weiss, and H.S. Karagueuzian. 2018. Atrial Fibrillation Initiated by Early Afterdepolarization-Mediated Triggered Activity during Acute Oxidative Stress: Efficacy of Late Sodium Current Blockade. *J Heart Health*. 4.

Pezhouman, A., S. Madahian, H. Stepanyan, H. Ghukasyan, Z. Qu, L. Belardinelli, and H.S. Karagueuzian. 2014. Selective inhibition of late sodium current suppresses ventricular tachycardia and fibrillation in intact rat hearts. *Heart Rhythm*. 11:492-501.

Pezhouman, A., N. Singh, Z. Song, M. Nivala, A. Eskandari, H. Cao, A. Bapat, C.Y. Ko, T. Nguyen, Z. Qu, H.S. Karagueuzian, and J.N. Weiss. 2015. Molecular Basis of Hypokalemia-Induced Ventricular Fibrillation. *Circulation*. 132:1528-1537.

Platano, D., N. Qin, F. Noceti, L. Birnbaumer, E. Stefani, and R. Olcese. 2000. Expression of the alpha(2)delta subunit interferes with prepulse facilitation in cardiac L-type calcium channels. *Biophys J*. 78:2959-2972.

Polster, A., B.R. Nelson, E.N. Olson, and K.G. Beam. 2016. Stac3 has a direct role in skeletal muscle-type excitation-contraction coupling that is disrupted by a myopathy-causing mutation. *Proc Natl Acad Sci U S A*. 113:10986-10991.

Polster, A., S. Perni, H. Bichraoui, and K.G. Beam. 2015. Stac adaptor proteins regulate trafficking and function of muscle and neuronal L-type Ca2+ channels. *Proc Natl Acad Sci U S A*. 112:602-606.

Pragnell, M., M. De Waard, Y. Mori, T. Tanabe, T.P. Snutch, and K.P. Campbell. 1994. Calcium channel beta-subunit binds to a conserved motif in the I-II cytoplasmic linker of the alpha 1-subunit. *Nature*. 368:67-70.

Priori, S.G., C. Blomstrom-Lundqvist, A. Mazzanti, N. Blom, M. Borggrefe, J. Camm, P.M. Elliott, D. Fitzsimons, R. Hatala, G. Hindricks, P. Kirchhof, K. Kjeldsen, K.H. Kuck, A. Hernandez-Madrid, N. Nikolaou, T.M. Norekval, C. Spaulding, and D.J. Van Veldhuisen. 2015. 2015 ESC Guidelines for the management of patients with ventricular arrhythmias and the prevention of sudden cardiac death: The Task Force for the Management of Patients with Ventricular Arrhythmias and the Prevention of Sudden Cardiac Death of the European Society of Cardiology (ESC)Endorsed by: Association for European Paediatric and Congenital Cardiology (AEPC). *Europace*. 17:1601-1687.

Priori, S.G., and P.B. Corr. 1990. Mechanisms underlying early and delayed afterdepolarizations induced by catecholamines. *Am J Physiol*. 258:H1796-1805.

Puglisi, J.L., W. Yuan, J.W. Bassani, and D.M. Bers. 1999. Ca(2+) influx through Ca(2+) channels in rabbit ventricular myocytes during action potential clamp: influence of temperature. *Circ Res*. 85:e7-e16.

Qu, Z., and D. Chung. 2012. Mechanisms and determinants of ultralong action potential duration and slow rate-dependence in cardiac myocytes. *PLoS. One*. 7:e43587.

Qu, Z., L.H. Xie, R. Olcese, H.S. Karagueuzian, P.S. Chen, A. Garfinkel, and J.N. Weiss. 2013. Early afterdepolarizations in cardiac myocytes: beyond reduced repolarization reserve. *Cardiovasc. Res*. 99:6-15.

Rebbeck, R.T., Y. Karunasekara, E.M. Gallant, P.G. Board, N.A. Beard, M.G. Casarotto, and A.F. Dulhunty. 2011. The beta(1a) subunit of the skeletal DHPR binds to skeletal RyR1 and activates the channel via its 35-residue C-terminal tail. *Biophys J*. 100:922-930.

Ringer, S. 1883. A further Contribution regarding the influence of the different Constituents of the Blood on the Contraction of the Heart. *J Physiol*. 4:29-42 23.

Rios, E. 2018. Calcium-induced release of calcium in muscle: 50 years of work and the emerging consensus. *J Gen Physiol*. 150:521-537.

Rios, E., and G. Pizarro. 1988. Voltage Sensors and Calcium Channels of Excitation-Contraction Coupling. *Physiology*. 3:223-227.

Rios, E., and G. Pizarro. 1991. Voltage sensor of excitation-contraction coupling in skeletal muscle. *Physiol Rev*. 71:849-908.

Robin, G., and B. Allard. 2015. Voltage-gated Ca(2+) influx through L-type channels contributes to sarcoplasmic reticulum Ca(2+) loading in skeletal muscle. *J Physiol*. 593:4781-4797.

Rosen, M.R. 2009. A short, biased history of triggered activity. *Hellenic J Cardiol*. 50:170-178.

Rosen, M.R., H. Gelband, C. Merker, and B.F. Hoffman. 1973. Mechanisms of digitalis toxicity. Effects of ouabain on phase four of canine Purkinje fiber transmembrane potentials. *Circulation*. 47:681-689.

Rosen, M.R., A.L. Wit, and B.F. Hoffman. 1975. Electrophysiology and pharmacology of cardiac arrhythmias. VI. Cardiac effects of verapamil. *Am Heart J*. 89:665-673.

Sanchez, J.A., and E. Stefani. 1978. Inward calcium current in twitch muscle fibres of the frog. *J Physiol*. 283:197-209.

Sanguinetti, M.C., and M. Tristani-Firouzi. 2006. hERG potassium channels and cardiac arrhythmia. *Nature*. 440:463-469.

Sato, D., C.E. Clancy, and D.M. Bers. 2017. Dynamics of sodium current mediated early afterdepolarizations. *Heliyon*. 3:e00388.

Sato, D., L.H. Xie, T.P. Nguyen, J.N. Weiss, and Z. Qu. 2010. Irregularly appearing early afterdepolarizations in cardiac myocytes: random fluctuations or dynamical chaos? *Biophys J*. 99:765-773.

Sato, D., L.H. Xie, A.A. Sovari, D.X. Tran, N. Morita, F. Xie, H. Karagueuzian, A. Garfinkel, J.N. Weiss, and Z. Qu. 2009. Synchronization of chaotic early afterdepolarizations in the genesis of cardiac arrhythmias. *Proc Natl Acad Sci U S A*. 106:2983-2988.

Savalli, N., A. Pantazis, D. Sigg, J.N. Weiss, A. Neely, and R. Olcese. 2016. The alpha2delta-1 subunit remodels CaV1.2 voltage sensors and allows Ca2+ influx at physiological membrane potentials. *J Gen Physiol*. 148:147-159.

Savalli, N., F. Wu, M. Quinonez, S.C. Cannon, and R. Olcese. 2019. A Mutation Linked to Malignant Hyperthermia in the Skeletal CaV1.1 Channel Stabilizes the Resting State of Voltage Sensor I and Impairs Channel Activation. *Byophysical Journal*. 116.

Schneider, M.F., and W.K. Chandler. 1973. Voltage dependent charge movement of skeletal muscle: a possible step in excitation-contraction coupling. *Nature*. 242:244-246.

Schredelseker, J., V. Di Biase, G.J. Obermair, E.T. Felder, B.E. Flucher, C. Franzini-Armstrong, and M. Grabner. 2005. The beta 1a subunit is essential for the assembly of dihydropyridine-receptor arrays in skeletal muscle. *Proc Natl Acad Sci U S A*. 102:17219-17224.

Sham, J.S., L.S. Song, Y. Chen, L.H. Deng, M.D. Stern, E.G. Lakatta, and H. Cheng. 1998. Termination of Ca2+ release by a local inactivation of ryanodine receptors in cardiac myocytes. *Proc Natl Acad Sci U S A*. 95:15096-15101.

Shaw, R.M., and H.M. Colecraft. 2013. L-type calcium channel targeting and local signalling in cardiac myocytes. *Cardiovasc Res*. 98:177-186.

Shimizu, W., T. Ohe, T. Kurita, M. Kawade, Y. Arakaki, N. Aihara, S. Kamakura, T. Kamiya, and K. Shimomura. 1995. Effects of verapamil and propranolol on early afterdepolarizations and ventricular arrhythmias induced by epinephrine in congenital long QT syndrome. *J Am Coll Cardiol*. 26:1299-1309.

Shirokov, R., G. Ferreira, J. Yi, and E. Rios. 1998. Inactivation of gating currents of L-type calcium channels. Specific role of the alpha 2 delta subunit. *J Gen Physiol*. 111:807-823.

Shistik, E., T. Ivanina, T. Puri, M. Hosey, and N. Dascal. 1995. Ca2+ current enhancement by alpha 2/delta and beta subunits in Xenopus oocytes: contribution of changes in channel gating and alpha 1 protein level. *J Physiol*. 489 (Pt 1):55-62.

Singer, D., M. Biel, I. Lotan, V. Flockerzi, F. Hofmann, and N. Dascal. 1991. The roles of the subunits in the function of the calcium channel. *Science*. 253:1553-1557.

Sipido, K.R., G. Callewaert, and E. Carmeliet. 1995. Inhibition and rapid recovery of Ca2+ current during Ca2+ release from sarcoplasmic reticulum in guinea pig ventricular myocytes. *Circ Res*. 76:102-109.

Skogestad, J., and J.M. Aronsen. 2018. Hypokalemia-Induced Arrhythmias and Heart Failure: New Insights and Implications for Therapy. *Front Physiol*. 9:1500.

Song, L., D.W. Awari, E.Y. Han, E. Uche-Anya, S.H. Park, Y.A. Yabe, W.K. Chung, and M. Yazawa. 2015. Dual optical recordings for action potentials and calcium handling in induced pluripotent stem cell models of cardiac arrhythmias using genetically encoded fluorescent indicators. *Stem Cells Transl Med*. 4:468-475.

Splawski, I., K.W. Timothy, L.M. Sharpe, N. Decher, P. Kumar, R. Bloise, C. Napolitano, P.J. Schwartz, R.M. Joseph, K. Condouris, H. Tager-Flusberg, S.G. Priori, M.C. Sanguinetti, and M.T. Keating. 2004. Ca(V)1.2 calcium channel dysfunction causes a multisystem disorder including arrhythmia and autism. *Cell*. 119:19-31.

Steccanella, F., N. Savalli, T. Yusifov, G.B. Battista, A. Neely, and R. Olcese. 2019. How Does the α2δ-1 Subunit Modulate Skeletal CaV1.1 Channels? *Biophysical Journal*. 116.

Stefani, E., and F. Bezanilla. 1998. Cut-open oocyte voltage-clamp technique. *Methods Enzymol*. 293:300-318.

Striessnig, J., A. Pinggera, G. Kaur, G. Bock, and P. Tuluc. 2014. L-type Ca(2+) channels in heart and brain. *Wiley Interdiscip Rev Membr Transp Signal*. 3:15-38.

Strube, C., M. Beurg, P.A. Powers, R.G. Gregg, and R. Coronado. 1996. Reduced Ca2+ current, charge movement, and absence of Ca2+ transients in skeletal muscle deficient in dihydropyridine receptor beta 1 subunit. *Biophys J*. 71:2531-2543.

Szabo, B., R. Sweidan, C.V. Rajagopalan, and R. Lazzara. 1994. Role of Na+:Ca2+ exchange current in Cs(+)-induced early afterdepolarizations in Purkinje fibers. *J Cardiovasc Electrophysiol*. 5:933-944.

Szentandrassy, N., D. Nagy, B. Hegyi, J. Magyar, T. Banyasz, and P.N. P. 2015. Class IV antiarrhythmic agents: new compounds using an old strategy. *Curr Pharm Des*. 21:977-1010.

Takekura, H., C. Paolini, C. Franzini-Armstrong, G. Kugler, M. Grabner, and B.E. Flucher. 2004. Differential contribution of skeletal and cardiac II-III loop sequences to the assembly of dihydropyridine-receptor arrays in skeletal muscle. *Mol Biol Cell*. 15:5408-5419.

Tanabe, T., K.G. Beam, J.A. Powell, and S. Numa. 1988. Restoration of excitation-contraction coupling and slow calcium current in dysgenic muscle by dihydropyridine receptor complementary DNA. *Nature*. 336:134-139.

Tanabe, T., A. Mikami, S. Numa, and K.G. Beam. 1990. Cardiac-type excitation-contraction coupling in dysgenic skeletal muscle injected with cardiac dihydropyridine receptor cDNA. *Nature*. 344:451-453.

Tanabe, T., H. Takeshima, A. Mikami, V. Flockerzi, H. Takahashi, K. Kangawa, M. Kojima, H. Matsuo, T. Hirose, and S. Numa. 1987. Primary structure of the receptor for calcium channel blockers from skeletal muscle. *Nature*. 328:313-318.

Tareilus, E., M. Roux, N. Qin, R. Olcese, J. Zhou, E. Stefani, and L. Birnbaumer. 1997. A Xenopus oocyte beta subunit: evidence for a role in the assembly/expression of voltage-gated calcium channels that is separate from its role as a regulatory subunit. *Proc Natl Acad Sci U S A*. 94:1703-1708.

Tarr, T.B., W. Malick, M. Liang, G. Valdomir, M. Frasso, D. Lacomis, S.W. Reddel, A. Garcia-Ocano, P. Wipf, and S.D. Meriney. 2013. Evaluation of a novel calcium channel agonist for therapeutic potential in Lambert-Eaton myasthenic syndrome. *J Neurosci*. 33:10559-10567.

Templin, C., J.R. Ghadri, J.S. Rougier, A. Baumer, V. Kaplan, M. Albesa, H. Sticht, A. Rauch, C. Puleo, D. Hu, H. Barajas-Martinez, C. Antzelevitch, T.F. Luscher, H. Abriel, and F. Duru. 2011. Identification of a novel loss-of-function calcium channel gene mutation in short QT syndrome (SQTS6). *Eur Heart J*. 32:1077-1088.

Trenor, B., K. Cardona, L. Romero, J.F. Gomez, J. Saiz, S. Rajamani, L. Belardinelli, and W. Giles. 2018. Pro-arrhythmic effects of low plasma [K(+)] in human ventricle: An illustrated review. *Trends Cardiovasc Med*. 28:233-242.

Tse, G. 2016. Mechanisms of cardiac arrhythmias. *J Arrhythm*. 32:75-81.

Tuluc, P., B. Benedetti, P. Coste de Bagneaux, M. Grabner, and B.E. Flucher. 2016. Two distinct voltage-sensing domains control voltage sensitivity and kinetics of current activation in CaV1.1 calcium channels. *J Gen Physiol*. 147:437-449.

Tuluc, P., G. Kern, G.J. Obermair, and B.E. Flucher. 2007. Computer modeling of siRNA knockdown effects indicates an essential role of the Ca2+ channel alpha2delta-1 subunit in cardiac excitation-contraction coupling. *Proc Natl Acad Sci U S A*. 104:11091-11096.

Tuluc, P., N. Molenda, B. Schlick, G.J. Obermair, B.E. Flucher, and K. Jurkat-Rott. 2009. A CaV1.1 Ca2+ channel splice variant with high conductance and voltage-sensitivity alters EC coupling in developing skeletal muscle. *Biophys J*. 96:35-44.

van Weerd, J.H., and V.M. Christoffels. 2016. The formation and function of the cardiac conduction system. *Development*. 143:197-210.

Varadi, G., P. Lory, D. Schultz, M. Varadi, and A. Schwartz. 1991. Acceleration of activation and inactivation by the beta subunit of the skeletal muscle calcium channel. *Nature*. 352:159-162.

Waldo, A.L., A.J. Camm, H. deRuyter, P.L. Friedman, D.J. MacNeil, J.F. Pauls, B. Pitt, C.M. Pratt, P.J. Schwartz, and E.P. Veltri. 1996. Effect of d-sotalol on mortality in patients with left ventricular dysfunction after recent and remote myocardial infarction. The SWORD Investigators. Survival With Oral d-Sotalol. *Lancet*. 348:7-12.

Walsh, C.P., A. Davies, A.J. Butcher, A.C. Dolphin, and A. Kitmitto. 2009. Three-dimensional structure of CaV3.1: comparison with the cardiac L-type voltage-gated calcium channel monomer architecture. *J Biol Chem*. 284:22310-22321.

Ward, C.A., and W.R. Giles. 1997. Ionic mechanism of the effects of hydrogen peroxide in rat ventricular myocytes. *J Physiol*. 500 (Pt 3):631-642.

Weiss, J.N., A. Garfinkel, H.S. Karagueuzian, P.S. Chen, and Z. Qu. 2010. Early afterdepolarizations and cardiac arrhythmias. *Heart Rhythm*. 7:1891-1899.

Weiss, J.N., A. Garfinkel, H.S. Karagueuzian, T.P. Nguyen, R. Olcese, P.S. Chen, and Z. Qu. 2015. Perspective: a dynamics-based classification of ventricular arrhythmias. *J Mol Cell Cardiol*. 82:136-152.

Weiss, J.N., Z. Qu, and K. Shivkumar. 2017. Electrophysiology of Hypokalemia and Hyperkalemia. *Circ Arrhythm Electrophysiol*. 10.

Weissgerber, P., B. Held, W. Bloch, L. Kaestner, K.R. Chien, B.K. Fleischmann, P. Lipp, V. Flockerzi, and M. Freichel. 2006. Reduced cardiac L-type Ca2+ current in Ca(V)beta2-/- embryos impairs cardiac development and contraction with secondary defects in vascular maturation. *Circ Res*. 99:749-757.

Wit, A.L. 2018. Afterdepolarizations and triggered activity as a mechanism for clinical arrhythmias. *Pacing Clin Electrophysiol*.

Wong King Yuen, S.M., M. Campiglio, C.C. Tung, B.E. Flucher, and F. Van Petegem. 2017. Structural insights into binding of STAC proteins to voltage-gated calcium channels. *Proc Natl Acad Sci U S A*. 114:E9520-E9528.

Wu, J., Z. Yan, Z. Li, X. Qian, S. Lu, M. Dong, Q. Zhou, and N. Yan. 2016. Structure of the voltage-gated calcium channel Ca(v)1.1 at 3.6 A resolution. *Nature*. 537:191-196.

Xie, L.H., F. Chen, H.S. Karagueuzian, and J.N. Weiss. 2009. Oxidative-stress-induced afterdepolarizations and calmodulin kinase II signaling. *Circ. Res*. 104:79-86.

Xie, Y., D. Sato, A. Garfinkel, Z. Qu, and J.N. Weiss. 2010. So little source, so much sink: requirements for afterdepolarizations to propagate in tissue. *Biophys J*. 99:1408-1415.

Yang, L., A. Katchman, J. Kushner, A. Kushnir, S.I. Zakharov, B.X. Chen, Z. Shuja, P. Subramanyam, G. Liu, A. Papa, D. Roybal, G.S. Pitt, H.M. Colecraft, and S.O. Marx. 2019. Cardiac CaV1.2 channels require beta subunits for beta-adrenergic-mediated modulation but not trafficking. *J Clin Invest*. 129:647-658.

Yang, L., A. Katchman, J.P. Morrow, D. Doshi, and S.O. Marx. 2011. Cardiac L-type calcium channel (Cav1.2) associates with gamma subunits. *FASEB J*. 25:928-936.

Yarotskyy, V., and K.S. Elmslie. 2007. Roscovitine, a cyclin-dependent kinase inhibitor, affects several gating mechanisms to inhibit cardiac L-type (Ca(V)1.2) calcium channels. *Br J Pharmacol*. 152:386-395.

Yarotskyy, V., G. Gao, L. Du, S.B. Ganapathi, B.Z. Peterson, and K.S. Elmslie. 2010. Roscovitine binds to novel L-channel (CaV1.2) sites that separately affect activation and inactivation. *J Biol Chem*. 285:43-53.

Yarotskyy, V., G. Gao, B.Z. Peterson, and K.S. Elmslie. 2009. The Timothy syndrome mutation of cardiac CaV1.2 (L-type) channels: multiple altered gating mechanisms and pharmacological restoration of inactivation. *J Physiol*. 587:551-565.

Yazawa, M., B. Hsueh, X. Jia, A.M. Pasca, J.A. Bernstein, J. Hallmayer, and R.E. Dolmetsch. 2011. Using induced pluripotent stem cells to investigate cardiac phenotypes in Timothy syndrome. *Nature*. 471:230-234.

Zhao, Z., Y. Xie, H. Wen, D. Xiao, C. Allen, N. Fefelova, W. Dun, P.A. Boyden, Z. Qu, and L.H. Xie. 2012. Role of the transient outward potassium current in the genesis of early afterdepolarizations in cardiac cells. *Cardiovasc Res*. 95:308-316.

Zuhlke, R.D., G.S. Pitt, K. Deisseroth, R.W. Tsien, and H. Reuter. 1999. Calmodulin supports both inactivation and facilitation of L-type calcium channels. *Nature*. 399:159-162.